Self-assembled thin films of thiocyanate and selenocyanate bithiophenes

A Thesis

Presented to the

Department of Chemistry

Of

Lakehead University

By

Kaitlyn T. Kelly

In partial fulfillment of requirements for the degree of

Master of Chemistry

February 5th, 2015

Official Signature of Supervisor Page

Abstract

Presented herein is the organic synthesis and thin film (TF) assembly of six alkyl-substituted thiocyante and selenocyante bithiophene molecules: NCSe-T_2-Hx, NCS-T_2-Hx, NCS-Hx-T_2-Hx, NCSe-Hx-T_2-Hx, NCS-Hx-T_2-Hx-SCN and NCSe-Hx-T_2-Hx-SeCN. TFs assembled from these thio and selenocyanates were characterized by six different techniques: electrochemical capacitance (C_p) measurements, scanning electron microscopy (SEM), energy dispersive x-ray spectroscopy (EDX), atomic force microscopy (AFM), x-ray photoelectron spectroscopy (XPS) and time-of-flight secondary ion mass spectrometry (ToF-SIMS). C_p experiments were used to confirm the development of TFs on an amorphous Au surface using ethanol or hexanes as a reaction solvent. A sputtered Au surface was observed by SEM/EDX to be an inappropriate surface for TF assembly. TFs assembled onto epitaxially grown Au were characterized by multiple techniques. Large crystallites were observed on TFs assembled from NCSe-T_2-Hx and NCSe-Hx-T_2-Hx-SeCN. Chemical maps of these crystallites were obtained through SEM/EDX. The presence of a covalent Au-S or Au-Se bond on the surface was confirmed by XPS signals from the S $2p^{3/2}$ and Se $3d^{5/2}/3d^{3/2}$ regions respectively. XPS signals of ~ 399 eV in the N 1s region were observed in all assemblies characterized by this technique, indicating the presence of residual gold-bound cyanide ($Au(CN)_{ads}$) on the surface. ToF-SIMs chemical intensity maps confirmed the presence of expected TF fragments on the surface of all TFs characterized by this technique. ToF-SIMS results suggested that TFs connected to the Au surface through an aromatically bound S or Se atom produced TFs with higher surface coverage.

Acknowledgements

I would like to thank my supervisor Dr. Craig MacKinnon for teaching me to be a synthetic chemist and allowing me to call the MacKinnon Lab home for three years. I would also like to extend appreciation to my committee members Dr. Aicheng Chen, Dr. Christine Gottardo and Dr. Kai Ylijoki for their input and guidance in the research and writing of this thesis.

I would like to thank Dr. Mark Gallagher for fabricating our epitaxially grown gold substrates, as well as for his surface science expertise and guidance.

I would like to thank the Lakehead University Chemistry Tech Team, Debbie Puumala, Brad Miller, Christina Richard, and Jarrett Sylvestre for fixing *everything* I broke and answering *all* of my questions

As organic chemists, we are grateful the Chen Lab for their electrochemical and surface science knowledge. I would like to extend many thanks to Dr. Guosheng Wu for fabricating our sputtered Au substrates and running our SEM/EDX experiments. As well, to Dr. Sapanbir Thind who conducted our electrochemical capacitance experiments and Jali Wen for running our AFM samples.

Lastly, we were lucky to find Dr. Mark Biesinger and Dr. Heng-Yong Nie at Surface Science Western. Their advice and expertise in the characterization of organic thin films was invaluable and much needed.

Table of Contents

List of Abbreviations

A	absorbance
AFM	atomic force microscopy
Bu	butyl group
C_p	capacitance
˚C	degrees Celsius
cm^{-1}	wavenumber
d	doublet (NMR descriptor)
EDS	energy dispersive spectrscopy
DMF	*N, N*-dimethylformamide
dppp	1,3-bis(diphenylphosphino)propane
E	energy
Et_2O	diethyl ether
EtOH	ethanol
g	gram
Hx	hexyl group
Hz	Hertz
IR	infrared spectroscopy
J	NMR coupling constant
M	molarity
MeOH	methanol
m/z	mass to charge ratio
mL	millilitre
mmol	millimole
mp	melting point
LUIL	Lakehead University Instrumentation Laboratory

NBS	N-bromosuccinimide
nBuli	n-butyl lithium
nm	nanometre
PPh_3	triphenyl phosphine
Pn	pentyl group
ppm	parts per million
R	alkyl group
s	singlet (NMR descriptor)
SAM	self-assembled monolayer
SEM	scanning electron microscopy
S_N2	bimolecular nucleophilic substitution
STM	scanning tunneling microscopy
T	2,5-thienyl
t	triplet
tBuLi	tertiary butyllithium
THF	tetrahydrofuran
TF	thin film
TMEDA	tetramethylethylenediamine
ToF-SIMS	time-of-flight Secondary Ion Mass Spectrometry
XPS	x-ray photoelectron spectroscopy
δ	NMR chemical shift

List of Schemes

List of Figures

List of Tables

Chapter 1 - Introduction to thiolate organic thin films

Thin films (TFs) of organic molecules on metal or semiconductor surfaces can broadly be viewed as an interface between two domains of differing chemical and physical properties. One extensively studied set of organic TFs is that of organothiolates on Au surfaces. The most common method of fabrication of these structures is a self-assembly reaction of organic thiols onto an oxide-free Au surface. Thiol precursors generally self-assemble to form well-defined monolayers, called self-assembled monolayers (SAMs). In this thesis, the more general umbrella term thin film (TF) will be used for the products of the thiocyanate surface attachment, which could be SAMs, thicker self-assembled films, or amorphous films. The overarching goal of this study is to further develop an alternative method of fabrication for thiolate TFs via an assembly reaction of organic thiocyanates. The purpose of this chapter is twofold. Firstly, this chapter serves as an overview of the system this study seeks to emulate, thiolate TFs assembled from thiols. Secondly, this chapter reviews the development of the alternative system, thiolate TFs from thiocyanate precursors.

1.1 Organic TFs of thiolates

Thiolate TFs from thiol precursors on Au substrates have been exhaustively developed and investigated for three decades after being first reported by Nuzzo and Allard in the early 1980s.[1] Since this time, thousands of papers and multiple reviews have been published detailing the structure, chemistry, and self-assembly process of many different organic thiolate TFs, as well as demonstrating a wide array of applications. The purpose of this section is to serve as a broad review of organic thiolate TFs of thiol precursors. Specifically, it will describe how the identity of each constituent part of the precursor imparts chemical and physical qualities to the resulting TF, detail theoretical and practical aspects of the self-assembly process, as well as illustrate a number of applications.

1.1.1 Anatomy of thiolate TFs

One unit of an organic TF is composed of four constituent parts: a terminal functional group, an organic backbone, a heteroatom linker, and a metal substrate. A schematic diagram of one assembled TF molecule is shown in Figure 1. The identity of each imparts unique physical and chemical qualities to the assembled TF. It is a goal of this area of materials science to maximize the number of different chemical combinations that can be used to form a well-defined TF in order to increase the number of potential applications.

Figure 1. Schematic diagram of one assembled TF molecule. Each of the 4 TF components is labelled and displayed.

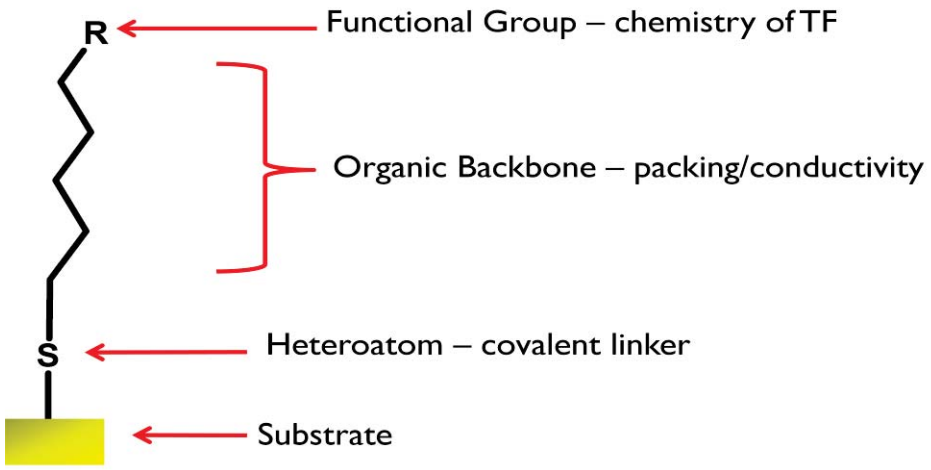

Organic synthesis has allowed many different groups to be substituted into the three organic parts: the terminal functional group, the organic backbone and the heteroatom linker (in the form of a precursor functional group). The terminal functional group primarily determines the overall chemical properties of the TF. For example, $-CH_3$ or $-CF_3$ groups impart hydrophobic and highly anti-adherent properties, while the substitution of -COOH, $-NH_2$ or -OH groups produce a hydrophilic thin film that may bind proteins and metal ions.[1] The organic backbone dictates the packing and conductivity of the thin film. Next, the heteroatom linker serves to join the organic and metal domains through a strong

covalent bond between the two. In this study, the heteroatom linker is a sulfur or selenium atom assembled from a thiocyanate or selenocyante precursor. Silicon is also another common linker.[1] Thiols, (and to a lesser extent thiocyanates,) have been assembled onto a number of different metal surfaces. In the case of thiol precursors, this array includes Au, Ag, Cu, Pd, Pt, Ni, and Fe, as well as a number of semiconductors, such as GaAs and InP.[1] TFs of thiocyanate precursors have also been successfully assembled onto Ag and Pt surfaces grown through e-beam evaporation.[2] However, Au with a (111) reconstruction remains the most successful and well studied substrate for both precursors. This reconstruction of Au forms preferentially through a thermal annealing process used in substrate fabrication.[2] Lastly and importantly, the surface must always be oxide free for the self-assembly process to occur.[1]

1.1.2 The self-assembly process of thiols into thiolate TFs

The metal substrate and individual organic precursors undergo the self-assembly process to form a TF. The most fundamental part of this process is a chemical reaction between the precursor group of the organic molecule, for example the thiol or thiocyanate group, and the metal substrate. The product of this reaction is a strong covalent bond between the heteroatom of the organic domain and the metal substrate. Intermolecular interactions between the organic moieties, as well as between organic moieties and the metal surface, have also been shown to play a role in self-assembly.[1]

Practically speaking, the self-assembly reaction is straightforward to conduct. In the case of thiols, typically, a suitable substrate is immersed in a 10-1000 μM solution of a chosen precursor. This solution is usually ethanolic, however, other solvents such as chloroform and hexanes have been shown to facilitate the reaction.[1] As well, the thiol solution can be in a liquid or gaseous phase, but predominantly a liquid phase is used. Reaction times required for the formation of a well-developed TF vary depending on the organic substrate. For example, long chain alkanethiols require 2-12 hours, while shorter chain

alkanethiols or alkanethiols with terminal functional groups may require 24 hours.[1] As discussed in Section 1.2, reaction conditions for thiocyanates are similar. However, thiol and thiocyanate assembly proceed by different chemical reactions which differ in kinetics and mechanism. [2]

1.1.3 Applications of thiolate TFs

Thiolate TFs have been utilized in a myriad of different nano- and microscopic applications. These applications include chemical and biomolecule sensing, molecular and organic electronics, chemical templating, lithography, and the wetting of surfaces.[1] While thiolate TFs have not yet been developed into practical devices, they have been incorporated into experimental set-ups as functional components. Thiolate TFs are usually highly chemically and structurally tailored for a specific application and are incorporated into experimental designs due to their ability to link organic and metal domains physically and electronically. This section illustrates numerous examples of successful thiolate TF applications in the areas of lithography and biosensing.

1.1.3.1 Lithography

Thiolate TFs are used in lithographic applications primarily because clever manipulation of the self-assembly process allows for the design of nano- and micropatterns on the metal substrate. In addition, the chemistry of the TF can be specifically designed for the ultimate application of the lithographic surface.

For example, B.M. Lambe and group demonstrated the fabrication of patterned thiolate TFs via microfluidic lithography.[3] In this process, a spiral polydimethylsiloxane (PDMS) microfluidic cassette was placed on an Au substrate and a solution of hexanethiol was flowed through its microfluidic channel. The cassette was removed to reveal a spiral alkane TF feature on the Au substrate. An SEM image of the patterned features is shown in Figure 2:

Figure 2. SEM image of hexadecanethiol (HDT) patterned onto a gold substrate through microfluidic lithography. Patterned features resulted from flowing a solution of the alkanethiol through the channels of a polydimethylsiloxane (PDMS) microfluidic cassette that was reversibly sealed onto the Au.[3]

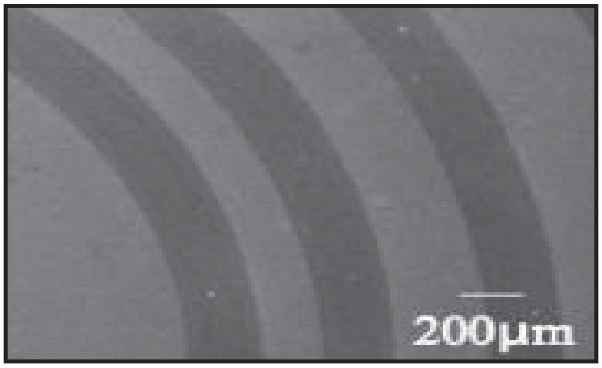

Next, a second self-assembly reaction was conducted to back-fill the rest of the Au substrate with a tetra(ethylene glycol) (TEG) terminated alkane TF. The resulting patterned TF was then used to conduct studies of cell motility and cell-to-cell communication.

Another method of writing lithographic patterns on organic thiolate TFs is with computer-programmed AFM lithography. In this method, demonstrated in 2011, by Treva T. Brown and co-workers, a prepared self-assembled monolayer of dodecanethiol on Au(111) was immersed in a solution of mercaptohexadecanoic acid (MHDA).[4] While immersed in the solution, an AFM cantilever tip was then used to scratch away the TF, 'nanoshaving' a computer-programmed pattern into the TF. As the AFM tip nanoshaved assembled molecules from the surface, MHDA in solution underwent an assembly reaction with the freshly bare Au surface, resulting in two different substrates patterned on the surface.

1.1.3.2 Biosensing

TFs of organic thiolates have found particularly successful use in the area of biosensing. The principal role of a biosensor is to selectively bind to analyte biomolecules or other analyte species and initiate a clear signal of this event, when and only when, a desired species binds. Biosensors are typically used to study the nature of the interaction between a biomolecule and another analyte species, or to detect and quantify the presence of a specific biomolecule.

When incorporated into biosensors, thiolate TFs usually serve two purposes: to create a barrier between a metal substrate and the biomolecule, and to effectively and selectively bind the biomolecule. Firstly, often in biosensing applications, a biomolecule must be linked to a conductive metal substrate, however, close contact can denature the biomolecule. An appropriate organic backbone between the metal substrate and biomolecule can create a buffer, while also preserving conductivity between the two if necessary. A related issue is the need to link a biomolecule to a metal substrate with a specific orientation. Linking a specific site on a biomolecule to the metal with a strong covalent S-Au bond can effectively orient the biomolecule for experimentation.

Illustratively, B. Bonanni and group demonstrated in 2006 that a sulfhydryl-terminated alkane thiolate TF could effectively immobilize the protein azurin (AZ) on a Au(111) surface during an AFM experiment studying the interaction between AZ and its redox partner Cytochrome 551 (c551).[5] When AZ was immobilized directly onto the Au, it was observed to become denatured and interaction events with c551 were affected. Incorporation of the thiolate TF allowed for preservation of AZ's structural integrity. In addition, terminally substituted sulfhydryl groups did bind to two specific cysteine residues on AZ. This caused the hydrophobic section, which interacts with c551, to be oriented up toward the AFM tip to which c551 was bound via a polyethylene glygol linker.

1.2 Development of Thiocyanate precursors

While the use of thiols in self-assembly has been very successful, the use of this precursor and other alternatives has several drawbacks. In this section, these issues will be outlined and the advantages of thiocyanate precursors will be detailed in addition to the progress in the development of this new precursor.

1.2.1 Thiol oxidation and the need for a new thiolate TF precursor

A key drawback of thiol precursors has been their propensity for oxidation to form disulfide bonds.[6] This side reaction, which is especially problematic with aromatic thiols, results in the presence of extraneous material in the assembly reaction solution. A corollary to this problem is the phenomenon of dithiol polymerization, where the oxidation of each thiol group with that of another dithiol results in the formation of reactant polymers in the assembly solution or on the substrate surface. Polymerization on the surface can result in the formation of a multilayer on the substrate surface, as shown in Figure 3.

Figure 3. Schematic diagram of the formation of a multilayer on substrate surface by α,ω-dithiols. Multilayers are formed via the formation of thiolate bonds with Au and disulfide bonds between precursor molecules.

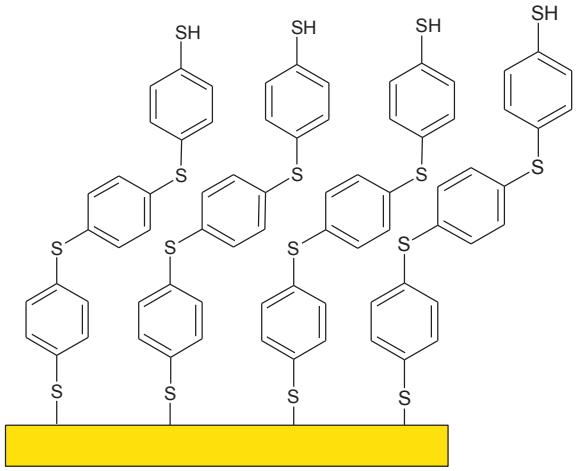

This is the result of one thiol group on a dithiol successfully reacting with the substrate surface while the remaining thiol group reacts with that of another dithiol or polymer.

In addition to thiocyanates, a number of other functional groups have been investigated as precursors for thiolate thin films including organic thiosulfates and acetyl-protected thiols.[6] Often thin films that result from these precursors are poorly developed and reaction conditions must be carefully managed. Change in the chemistry of the organic backbone has been observed to be a consequence of insufficient control of reaction conditions.[6]

1.2.2 Introduction of thiocyanate precursors by Ciszek and group in 2005

In an attempt to overcome these issues in the assembly of thiolate thin films, Ciszek and coworkers investigated the assembly of organic thiocyanates onto Au, Pt, and Ag.[2] The overarching goal of this investigation was to determine if thiocyanates could assemble into well-defined thiolate TFs that were air, light, and moisture stable, while also overcoming the issues encountered with other precursors. TFs of aromatic and alkyl substituted thiocyanates were compared with those synthesized from analogous thiols. Assembly reaction conditions used with thiocyanate precursors were identical to those used for thiols: a gold substrate was immersed in a 1 mM solution of the thiocyanate in methanol or methanol/THF solvent at room temperature for 24-36 h. Overall, the resulting thin films were determined by XPS to be well-defined and stable under ambient conditions. It was found that the aromatic thiocyanates produced TFs that had comparable structure, thickness, and surface coverage to their thiol counterparts, while alkane thiocyanates produced TFs with 10 % lower surface coverage than thiol counterparts. Thiocyanate self-assembly was also successfully conducted on Pt and Ag surfaces. No disulfide formation was observed, however, residual Au-bound cyanide $(CN)_{ads}$ was observed in most assemblies.

1.2.3 Further extension development of thiocyanate precursors

Ciszek's work has been further developed by numerous groups including the MacKinnon group with areas of focus being comparison of TFs produced from thiol and thiocyanate precursors and the optimization of assembly reaction conditions.

In 2006, Dreesen et al. complemented Ciszek's work by using IRRAS, STM, and SFG to compare the TFs prepared on Au(111) substrates by decylthiocyanate and decanethiol.[7] It was observed that thiocyante precursors produced a thiolate monolayer that had a lower packing density and poorer organization than thiol precursors.

In 2008, Choi and group replicated this finding, demonstrating that octylthiocyanate produced a TF that was significantly different than that produced by octanethiol.[8] It was also observed that vapor deposition of thiocyanates at 50˚C produced a TF with long-range ordered domains, whereas liquid solution deposition at this temperature only resulted in small ordered domains in the TF.

In 2008, Schen et al. also demonstrated the effect of increased temperature.[9] Assembly reactions heated for 24 h at 70 ˚C showed increased order as compared with those prepared at room temperature. Importantly, the effect of repeated use of a reaction solution was also reported. As a thiocyanate solution was used repeatedly for assembly reactions, or 'aged', the TFs assembled possessed an increased number of ordered domains. It is thought that contaminants that preferentially adsorb to the substrate are successively removed from the solution. Thiols, in comparison do not show this sensitivity to contamination.

In 2013, Yee et al. replicated the order enhancing effects of increased temperature and demonstrated solvent effects on TF quality.[10] Firstly, it was observed that TFs assembled from thiocyanates at room temperature showed no order, whereas ordered domains were observed for those assembled for 24 h at 50 ˚C. As well, STM and XPS were used to determine that octanethiocyanate had much slower growth kinetics than octanethiol on Au(111). With respect to solvent effects on the assembly reaction, it was observed that for heated samples at 50 ˚C for 24 h, the use of hexanes as a solvent produced the most order, followed by DMF, toluene, and ethanol. Schen et al. demonstrated that higher quality thiolate thin films may be obtained through purification of the thiocyanate solution.

1.2.4 The MacKinnon Group and thiocyanate oligothiophene precursors

In 2009, the MacKinnon group demonstrated that thiocyanates of a variety of oligothiophenes could also undergo an assembly reaction to form thiolate TFs.[11] Our group investigated TFs of oligothiophenes for several reasons. Firstly, this type of oligomer is easily modified through organic

synthesis, especially through transition metal-catalyzed cross-coupling reactions. As well, oligothiophenes possess good charge transport properties due to the polarizability of constituent S heteroatoms.[12] In the 2009 study, the array of thiocyanates included bi- and terthiophenes with no terminal functional groups, as well as those with thiocyano, ethyl and bromine substituents. A schematic diagram of this oligothiophene array is shown in Figure 4.

Figure 4. Structure of six oligothiophene TFs reported by MacKinnon Group in 2009. All TFs were synthesized from thiocyanate precursors. Electrochemical capacitance experiments (C_p) were used to confirm successful TF formation.[11]

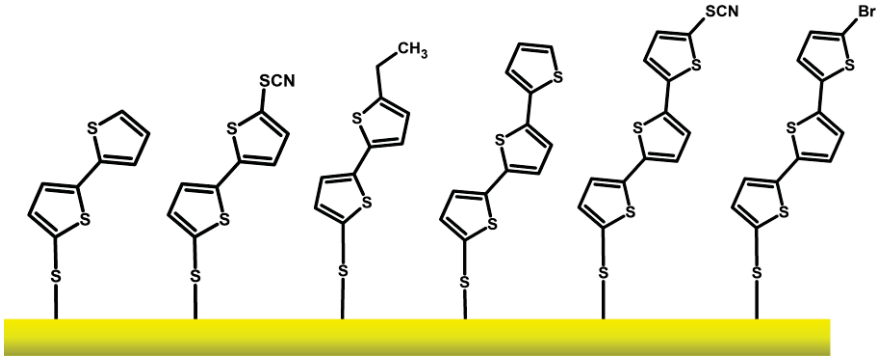

In all assembly reactions, the Au substrate was immersed in a saturated ethanolic solution of a particular precursor at room temperature for 20 minutes, removed, rinsed with pure EtOH, and characterized with electrochemical capacitance experiments or AFM. First, the assembly reaction for each was conducted on an amorphous Au electrode. After the assembly reaction, the electrochemical capacitance of the electrode was re-measured and compared with that of the electrode prior to the assembly reaction. A significant reduction in measured capacitance in each case indicated that an insulating organic TF had formed on the surface of the Au. An assembly reaction was also conducted with NCS-T_2-SCN on an epitaxially grown Au substrate using the same assembly conditions as the capacitance experiments. This process was also repeated using Br-T_2-SCN. AFM images, (shown in Figure 5,) were obtained of both the resulting Au-T_2-SCN TF and the resulting Au-T_2-Br TF.

Figure 5. AFM images of oligothiophene TFs synthesized from thiocyanate precursors on epitaxially grown Au. Left: Au-S-T_2-SCN. Right: Au-S-T_2-Br.[11]

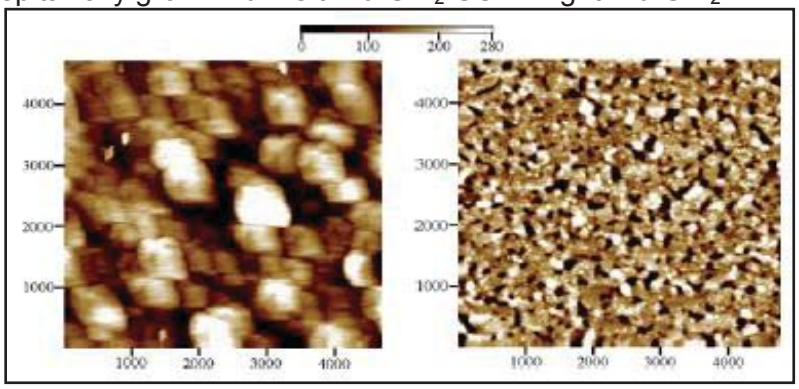

AFM results indicated successful formation of a TF in both cases and showed the formation of crystallites in the Au-S-T_2-SCN TF (Figure 5 (Left)). These crystallites are attributed to intermolecular interactions between the hydrogen atoms bonded to the bithiophene core and the remaining nitrile substituents.

Chapter 2 - Surface Analysis Techniques

Thiolate TFs of organic molecules have been investigated and characterized by a myriad of different surface analysis techniques to gain a full spectrum of information, including structural characteristics of the surface (periodic and non-periodic), surface topography and coverage, elemental composition, valence band structure, bonding states present, and molecular tilt of TF constituent molecules.[1] When characterizing organic TFs, it is important to note that regions of the sample whose physical and chemical properties are of interest may vary from 1 atomic layer (0.1-0.3 nm) to many hundreds of atomic layers (100 nm or more).[13] On a micro or nanoscopic scale, this represents enormous variation. Consequentially, surface analysis techniques must be carefully chosen for sensitivity as well as depth and precision of signal generation. In addition, the type of information gained from the technique must be carefully weighed with its destructive effect on the sample. Thiolate TFs assembled from thiol precursors are easily characterized because they are generally homogeneous and composed of a single monolayer. In addition, over 30 years of thorough investigation of thiols has allowed for an exhaustive list of techniques to be tested, including common scanning probe techniques, like atomic force microscopy (AFM) and scanning tunnelling microscopy (STM); electron and ion spectroscopies, such as Auger electron spectroscopy (AES), X-ray absorption near edge spectroscopy (XANES) and x-ray photoelectron spectroscopy (XPS), and a number of diffraction techniques and vibrational spectroscopies.

The characterization of thiolate thin films assembled from thiocyanate precursors has been observed to be a greater challenge due to their more heterogeneous nature.[6] Currently, STM and XPS have been the primary techniques used in the characterization of these thiolate TFs. Other techniques employed include near edge x-ray absorption fine structure (NEXAFS) absorption spectroscopy, infrared reflection absorption spectroscopy (IRRAS), thermal desorption spectroscopy (TDS), AFM and sum-frequency generation (SFG) spectroscopy, in addition to electrochemical techniques.[7,8,9,10]

In order to complement the heterogeneous nature of the TFs assembled in this study, five different surface analysis techniques were used: AFM, scanning electron microscopy (SEM), energy dispersive x-ray (EDX) spectroscopy, XPS, and time-of-flight secondary ion mass spectrometry (ToF-SIMS). In this section, the theory of signal generation, information gained and limitations of each technique are discussed.[2,7-11]

2.1 Atomic Force Microscopy (AFM)

Atomic force microscopy (AFM) is a technique commonly used to characterize the surface topography of organic thin films. Along with scanning tunneling microscopy (STM), this scanning probe technique has been extensively used in the surface analysis of thiolate TFs synthesized from thiol precursors.

AFM generates topographical information through the use of an apex tip, usually attached to a piezotube. The apex tip measures forces generated as a result of interaction with the surface, such as attractive, magnetic, or electrostatic forces. For example, in contact AFM, the apex tip is rastered across the sample surface and a topographical map is produced from the measured deflections of the tip as a result of interaction with surface features.[14]

AFM is attractive for the surface analysis of organic TFs because it can be performed with little sample preparation and under ambient conditions. It is not limited by sample conductivity, however, a major limitation of this technique is the size of the surface feature it can characterize. AFM imaging of samples containing features taller than 100nm has been observed to be problematic.[15] As well, the nature of the information produced from AFM imaging is very local, ideally it should be supplemented with averaged information, like that obtained from diffraction techniques.

2.2 Scanning electron microscopy and energy dispersive x-ray spectroscopy (SEM and EDX)

Scanning electron microscopy (SEM) and energy dispersive x-ray spectroscopy (EDX) were also employed in the characterization of the organic TFs synthesised in this study. These techniques were used alone and in conjunction to produce chemical mapping images. Although these techniques are often combined in one instrument, both SEM and EDX are discussed separately in this section. Theory of signal production, information provided, and limitations in the characterization of organic thin films are reviewed for each technique.

2.2.1 Scanning-electron microscopy

SEM is a well-developed imaging technique used in the characterization of nanoscopic and microscopic surface structures. This technique is employed extensively in the analysis of geological and biological materials, as well as inorganic semiconductors.[16] As compared with light microscopy, SEM produces higher lateral resolution and depth of focus and can be used to facilitate x-ray spectroscopies such as EDX.[16] To produce an image, SEM employs a highly focused beam of electrons in the place of the focused beam of light used in light microscopy.

The electron beam, called the primary ion beam, is first generated by an electron gun and then progressively focused by a series of electromagnetic lenses into a fine spot on the sample. The type of electron gun used in this study was a Field emission Schottky gun. This electron gun is well-suited for use with the low accelerating voltages required when imaging organic samples. As well, compared with the other principal type of source, thermoionic electron guns, FE Schottky produces much smaller spot sizes and greatly improved resolution (1.5nm vs. 3.5nm).[17] To achieve these improvements, the FE Schottky gun requires high vacuum conditions, which may create practical difficulties in the analysis of organic samples, which may produce volatile particles.

As a result of interaction with the focused primary electron beam spot, the sample generates a number of detectable signals: backscattered electrons, secondary electrons, and x-rays. Emitted x-rays are the detected signal in EDX and are discussed in the EDX section.

Backscattered electrons (BSE) are produced when primary electrons undergo elastic collisions with sample nuclei and are resultantly ejected out of the sample. BSE are not viable in the analysis of organic thin films since the elastic collisions between the primary electron beams and sample nuclei are not well facilitated by the smaller nuclei of the elements of organic materials.[16]

Secondary electrons (SE) are the primary type of signal used in SEM topographic imaging. SE are generated when inelastic collisions between primary electrons and valence electrons results in the ejection of electrons from the conduction band. The SE generated are low energy electrons, (~ 0.4 keV), thus limiting the depth from which they can escape from the sample.[17] This means that energy from the primary electron beam may cause the generation of SE too deep into the sample to escape and be detected. As well, since SE come from the conduction band, sample conductivity limits the types of samples that can be effectively imaged with SEM.[16] Accordingly, inorganic or organic materials are not necessarily good candidates for SEM since they do not have many free electrons with which to produce signals. SE generated are collected by a positively biased electrode, sent to a scintillator and photomultiplier and a topographical image is produced.

Charging is characterized by bright white areas or streaks on the SEM image. This effect occurs when the charge imparted to the sample by the primary electron beam is greater than the charge released by SE and back-scattered electrons. For insulating samples, like organic materials, a primary electron beam accelerating voltage of between 5 to 25 keV, (normal range for SEM,) will result in charging.[16] Three principal solutions to sample charging exist: the use of an accelerating voltage from several hundred to 2000 eV, the use of carbon glue to ground the sample, and carbon-coating the sample. While these procedures may eliminate charging, they may not be appropriate for all samples.

As a result of these limitations, SEM is not commonly used for organic thin films. A further difficulty arises because thiolate TFs often form monolayers, and the inherent sensitivity of SEM is not high enough to detect monolayers. However, larger conducting organic features on top of an organic monolayer have been successfully imaged with SEM, as shown in Figure 6.[18]

Figure 6. SEM images of phencyphos crystals on top of a phencyphos thiolate monolayer. SEM images were successfully obtained using an accelerating voltage of 10 kV and high vacuum conditions.[18]

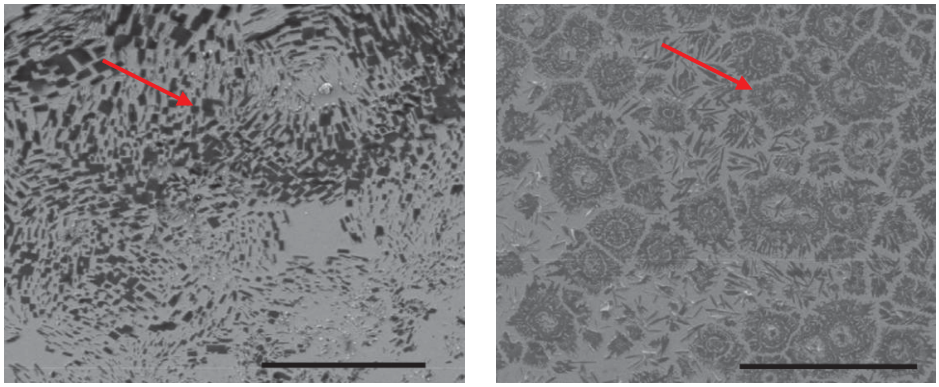

2.2.2 Energy dispersive x-ray spectroscopy

The topographical information provided by SEM can be complemented with chemical information supplied by energy dispersive x-ray spectroscopy (EDX) by interfacing the two techniques to produce chemical maps of the surface.

Energy dispersive x-ray spectroscopy (EDX) is used to determine qualitative and quantitative elemental composition of a sample. This is accomplished by recording the spectrum of the energies of x-ray photons emitted by a sample while scanning with the electron beam. The x-ray signal is generated when the primary electron beam undergoes inelastic collisions with inner shell electrons. The energy imparted causes these electrons to be ejected from the atom. When a higher energy outer shell electron fills the lower energy electron hole created, energy is released in the form of an x-ray photon. [16] The energy difference between the inner and outer shell electron will be the energy of the x-ray photon and is characteristic of the element. [16]

It is important to note that EDX is less sensitive and precise than other techniques such as XPS and STM. For an element to be detected with EDX its concentration must be at least 0.1 wt %, in the case of elements with low atomic number this threshold shifts to at least 1 wt %.[16] As well, any quantitative information gained from EDX is an average concentration calculated from signals than can originate from a depth up to ~1μm into the sample, where as true surface analysis techniques only detect signals from a depth of up to tens of nanometres. [13]

2.3 X-ray photoelectron spectroscopy (XPS)

X-ray photoelectron spectroscopy (XPS) is a widely used electron spectroscopy that is a powerful tool for determining elemental composition and chemical environment. Since the information gained is specific to approximately the outermost 10 nm, XPS is considered a true surface analysis technique. Attractive features of XPS include minimal sample preparation and destruction, as well as qualitative and quantitative detection of elements present in concentrations as low as 0.05 at.%. [13] The measured signals in XPS are the binding energies of photoelectrons ejected from the sample through the photoelectric effect.

In order to generate this signal, first, the sample surface is irradiated with an x-ray beam of photons. When a photon interacts with an electron in the sample, a complete transfer of energy from the photon to the electron occurs, and the photon is annihilated. If enough energy is transferred, the electron will be ejected from the sample surface. It is the kinetic energy (E_k) of these ejected electrons that is then detected. The E_k of these electrons is of a discrete nature and a function of the electron's binding energy (E_b).[13] Since the work function of the XPS analyzer (Φ_A) can also be determined, the E_b can be calculated by

$$E_b = h\nu - E_k - \Phi_A \qquad (1)\ [13]$$

E_b of an electron is a useful measurement because it is indicative of the elemental identity and electronic environment of its atom of origin. [13] Interpretation of spectra produced from the measured binding

energies of detected photoelectrons is primarily done by comparison with literature values and databases as well as values from related or similar samples.

Two important factors that affect the accuracy of qualitative and quantitative XPS results are the specificity of the depth from which electrons can be detected and the limitations of sensitivity. First, the signals detected by XPS originate from a highly specific region of the surface. While the x-ray beam penetrates and causes the production of photoelectrons up to microns deep into the sample, only those produced up to approximately 10 nm below the surface have enough kinetic energy to be ejected from the sample. [13] As a consequence of the higher energy required for photoelectrons to be ejected from greater depths in the sample, the photoelectrons detected will only be from about the topmost 10 nm of the surface. A potential consequence of high specificity is that a layer of contaminant over the surface, such as an oxide layer, may occupy most of this range, causing the region of interest to be undetected. [12] XPS sensitivity is primarily affected by the cross section of photoelectrons for a given element and background activity.[13] The photoelectron cross section refers to the yield of photoelectrons produced by the x-ray beam. For H and He, the yield simply is not high enough to be detected, and thus these elements cannot be characterized in a sample by XPS.[13] Lastly, background activity factors, such as those caused by poor vacuum, can affect the flight path of photoelectrons from the sample surface to the detector, and therefore affect the signal detected.[13]

2.4 Time-of-flight secondary ion mass spectrometry

Time-of-flight secondary ion mass spectrometry (ToF-SIMS) is a surface imaging technique that has been developed and used mostly for the characterization of semiconductors [19] ToF-SIMS is used for three main purposes: to obtain a mass spectrum of a known point on the surface, to produce a chemical map of the surface (lateral imaging) or to produce a depth profile (dynamic SIMS). This technique allows gas phase fragment ions to be extracted from a sample surface, thus allowing mass

spectrometry to be conducted on a solid without any sample dissolution or appreciable destruction. Compared with other surface imaging techniques, ToF-SIMS provides a number of advantages including increased surface sensitivity, trace component detection, and the ability to examine molecular structure.[17] While ToF-SIMs is not readily used in the characterization of organic thin films, its ability to produce mapping images of ions with up to sub-micrometre resolution makes it a very attractive surface analysis technique. In this section, both the secondary ion source (SIMS) and the analyzer (ToF) are discussed.

In secondary ion mass spectrometry, mass spectra are obtained of secondary ions that have been ejected, or sputtered from the surface of the sample by the energetic interactions with a primary ion beam. The primary ion beam is produced by the primary ion column in which many different species of ions have been utilized, including C_{60}^+, Ga^+, In^+, Cs^+, O_2^+, Au_n^+, and Bi_n^+.[17] Currently, cluster beams, such as Bi_n^+ and Au_n^+ have received favourable attention. This is due to their higher yields compared with monoatomic ion beams, lower surface damage, and good beam width. [19] Once the primary ions are impacted into the sample, it is thought that a cascade of collisions between primary ions and sample atoms occurs. [19]

As a result of energetic collisions, atoms near the surface gain enough energy to be ejected, or sputtered from the surface. Sputtered atoms occur in the form of neutral species, molecular ions, or most commonly, fragment ions.[19] Fragment ions, termed secondary ions, are then entrained by the time-of-flight analyzer (ToF) and a mass spectrum is obtained.

Time-of-flight analyzers produce a mass spectrum based on the principle of separation by velocity. For this to occur, two conditions must be met: all ions collected from the same group, or pulse, must enter the field-free flight-tube at as close to the same time as possible and have as close to the same kinetic energy as possible.[19] If these conditions are accomplished, flight time through a field free flight tube can be used to determine the mass separation of each fragment

$$E_{kin} = \frac{mv^2}{2} \qquad (2)$$ [19]

where E_{kin}, v, and m are the kinetic energy, velocity and mass of a secondary ion, respectively. In order to achieve both conditions, after secondary ions are sputtered and the entire group is entrained in the high vacuum conditions, it is accelerated at a constant voltage so as to give all secondary ions the same kinetic energy as they enter the field-free flight tube.

A reflection can also be incorporated into a ToF analyzer to improve mass resolution. Its effect is to correct any dispersion in the kinetic energy that occurs between fragments of the same m/z. A reflection accomplishes this with an electric field that retards fragments with higher E_{kin} so that they reach the detector at the same time as slower fragments with the same m/z.[19] The resulting improved resolution is accomplished at the expense of decreased sensitivity and decreased mass range.[19]

Overall, for the ToF-SIMs system, a high vacuum is required and both the primary ion column and the ToF analyzers be pulsed.[19] The pulse-analyze pattern is repeated as the ion beam is rastered across an area of the sample. The result is a full mass spectrum that is obtained for each pixel scanned. Once completed, surface images are produced showing the intensity of detection of a particular fragment across the imaged area.

Chapter 3 - Scope of Thesis

Whereas thiolate and selenolate TFs are almost universally synthesized via a self-assembly reaction of thiols and selenols, this study investigated the assembly of thiocyanate and selenocyanates into thiolate and selenolate TFs. Since the assembly of thiocyanates was first reported by Ciszek and group in 2004, numerous groups have built upon this by comparing TFs assembled from thiols and thiocyanates, optimizing assembly conditions, and increasing the number of organic thiocyanates for which TF assembly has been reported. This study aimed to extend this list to alkyl-substituted bithiophenes, to replicate the effects of optimized reaction conditions, and also to explore the assembly of selenocyanates. The assembly of selenocyanates is being attempted for two main reasons. Firstly, SeCN assembly into selenolate TFs has not yet been reported in the literature. Secondly, the use of a Se linker may mitigate any complicating effects of using both an S linker and S atoms in the organic moiety.

First, the organic synthesis of the target substituted bithiophenes **1-3** was undertaken. All syntheses were accomplished using Kumada Grignard reactions, organolithium reactions, and S_N2 and light sensitive thiocyanation and selenocyanation reactions. Once synthesized, assembly reactions were conducted in attempt to fabricate the TFs shown in Figure 7.

Figure 7. Alkyl-substituted thiocyanate and selenocyanate thin films synthesized in this study. For a, x = S and for b, x = Se.

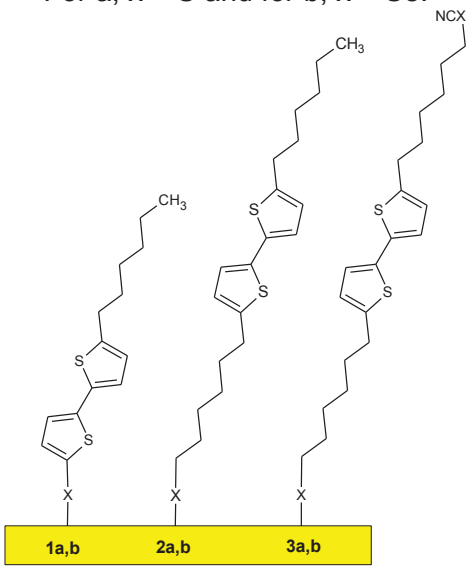

The assembly reaction was first tested on both amorphous and sputtered Au surfaces. Epitaxially grown Au surfaces have been most widely used in the thiocyanate assembly reaction. Therefore TFs assembled onto this substrate were most thoroughly characterized. This included the use of AFM and SEM to evaluate structural characteristics. XPS was used to identify elements present on the surface of each TF and determine if Au-S and Au-Se covalent bonds were formed. SEM/EDX and ToF-SIMs were also used to produce chemical maps of each TF.

Chapter 4 - Results and discussion of synthesis of organic precursors

The synthesis of six target organic thio- and selenocyanates was undertaken prior to thin film assembly. The organic targets, shown in Figure 8, were designed to examine the effect of four different variables in resulting thin film assemblies.

Figure 8. Target thio- and selenocyante precursors (For a, x = S; for b, x = Se).

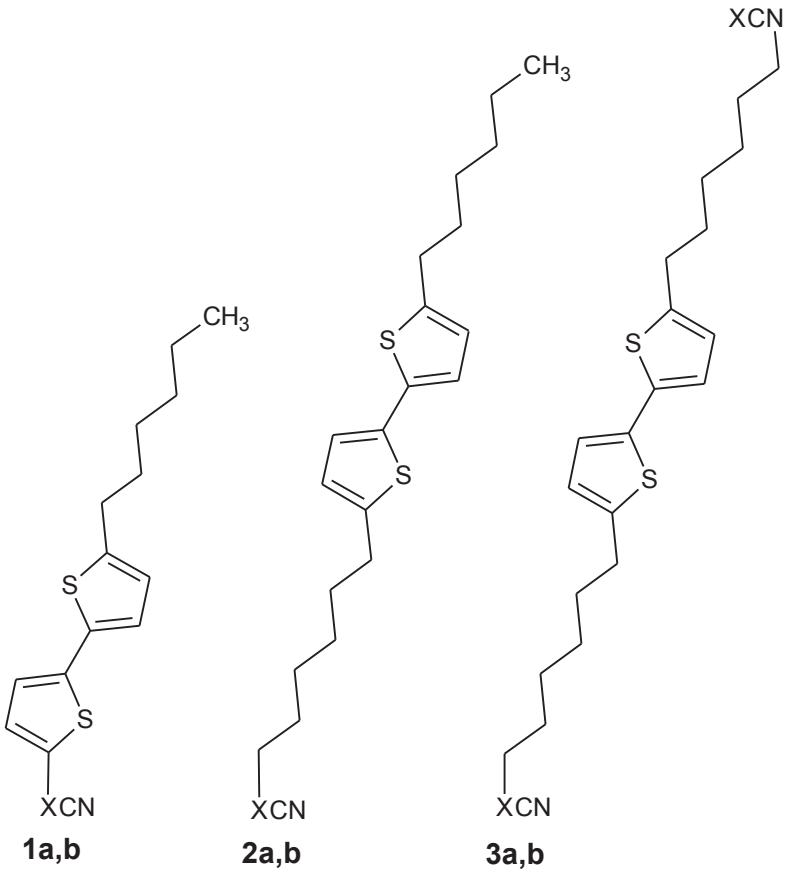

These four variables were mono- verses dialkyl substitution of the bithiophene core, thiocyanation of an aromatic position verses an alkyl position, mono verses di thiocyanation, and the effect of thiocyanation verses selenocyanation on each of the preceding variables. Targets were synthesized from a common precursor, 2,2'-bithiophene (T_2), using two main pathways: the synthesis and subsequent functionalization of 5-hexyl-2,2'-bithiophene (T_2Hx) and the di-lithiation of T_2.

4.1 Synthesis of 2,2'-bithiophene, $\mathbf{T_2}$

The first step in the synthesis of all organic targets was the synthesis of 2,2'-bithiophene ,T_2. This compound was obtained via the Kumada synthesis in good yields (60.6%).[20] Experimental details of this Grignard reaction are shown in Scheme 1:

Scheme 1. Synthesis of 2,2'-bithiophene, $\mathbf{T_2}$

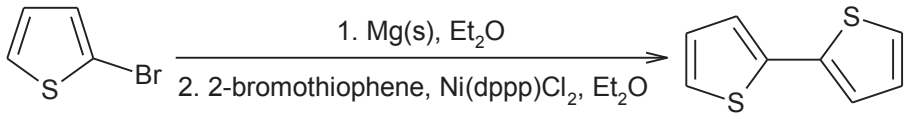

4.2 Synthesis of 5-hexyl-2,2'-bithiophene, $\mathbf{T_2Hx}$

The second step in the synthetic pathway to four of the six organic targets was the synthesis of 5-hexyl-2,2'-bithiophene, T_2Hx. The attachment of a hexyl group at this location proved unexpectedly difficult and required the exploration of multiple reactions (Scheme 2).

Scheme 2. Synthesis of 1a,b and 2a,b first required the synthesis of T_2Hx.

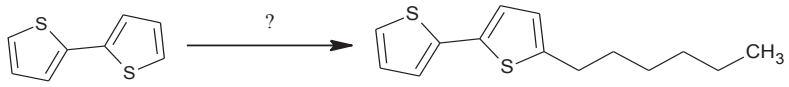

First, a simple lithiation of the α-carbon was attempted using nBuLi, shown in Scheme 3. This reaction was conducted in accordance with the literature procedure[21] repeatedly and only resulted in low yields.

Scheme 3. Attempted synthesis of T_2Hx via lithiation with nBuLi.

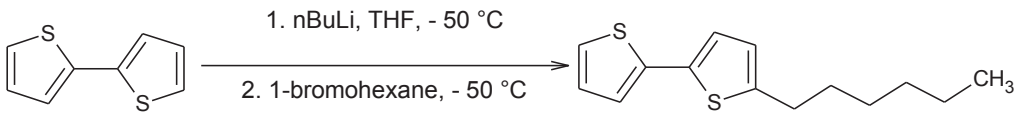

Multiple variations on this procedure were attempted in order to improve the outcome. These included maintaining a reaction temperature of - 78 °C, the addition of multiple equivalents of nBuLi and the use of the stronger tertiary-butyllithium reagent (Scheme 4). However, these did not improve yields.

Scheme 4. Attempted synthesis of T_2Hx via the lithiation of the 5-position of T_2 with tBuLi.

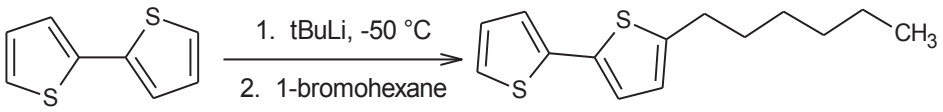

Next, a Grignard coupling of 2-thienylmagnesium bromide and 5-bromo-2-hexylthiophene was attempted using Kumada conditions that had previously yielded good results in our laboratory (Scheme 5).[22]

Scheme 5. Kumada Grignard coupling of 2-bromo-5-hexylthiophene and 2-thiophene magnesium bromide. Two different reaction conditions employed: 1) Dry Et_2O only; 2) Et_2O:Toluene (50:50) solvent mixture.

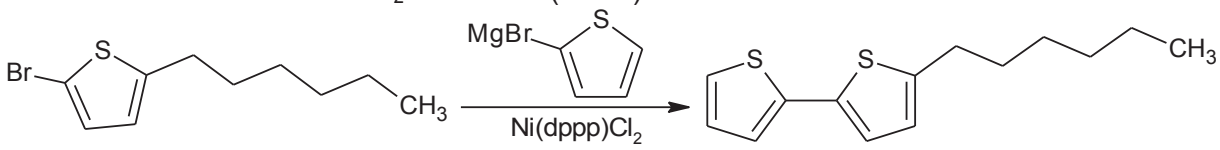

This reaction was attempted using two different solvent conditions. First, it was conducted using only ether, which was used in previous successful attempts. However, the reaction produced low yields. A solvent mixture of Et_2O and toluene (50:50) also produced low yields. Careful attention was given to ensure that air and water sensitive conditions were observed and that previously successful procedures were repeated identically. When the results did not improve, it was concluded that there was an abnormality or quality control issue with the $Ni(dppp)Cl_2$ catalyst. This reagent was suspected since the Grignard reagent appeared to form each time the reaction was attempted. As well, yields from the T_2 synthesis decreased from approximately 80%, which is normally observed in our lab for this reaction.

Finally, an acylation reaction with $SnCl_4$ and hexanoyl chloride and hexanoyl chloride and subsequent Huang-Minlon reduction was utilized (Scheme 6). First, a ketone group was attached to T_2 via a reaction with $SnCl_4$ and hexanoyl chloride. [23]

Scheme 6. Synthesis of T_2OHx via acylation.

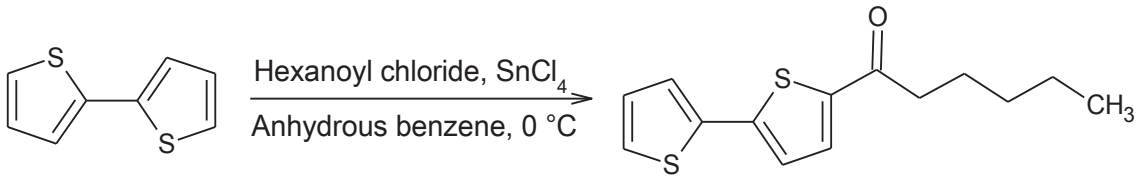

This reaction produced consistent yields of approximately 60%. Degradation of the $SnCl_4$ and hexanoyl chloride were important factors in the obtained yields for this reaction. Yields depreciated dramatically as the age of these reagents increased. This intermediate was isolated and its identity confirmed by IR spectroscopy (as a nujol mull), with a C=O stretching frequency of 1654cm^{-1}. This ketone was reduced to 5-hexyl-2,2'-bithiophene, **T_2Hx**, via the Huang-Minlong reaction, a modification of the Wolff-Kishner reduction (Scheme 7).[24]

Scheme 7. Synthesis of T_2Hx via Huang-Minlon reduction.

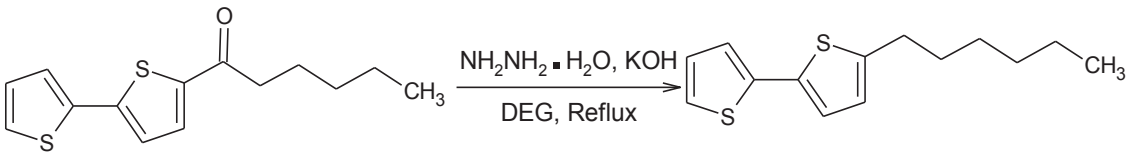

Careful attention to the amount of hydrazine monohydrate allowed for consistent yields of approximately 75% to be achieved.

4.3 Synthesis of SCN-T_2-Hx and SeCN-T_2-Hx, **1a,b**

The aromatic thio- and selenocyanation of T_2Hx was accomplished through the use of a light-sensitive reaction. The thiocyanation of T_2 utilized KSCN and 'dark' reaction conditions and resulted in the formation of multiple oil products (Scheme 8). [11] The mechanism of this reaction is not known, but it is suspected that it proceeds via a radical pathway after the initial *in situ* formation of thiocyanogen or selenocyanogen.

Scheme 8. Synthesis of SCN-T_2Hx, **1a**.

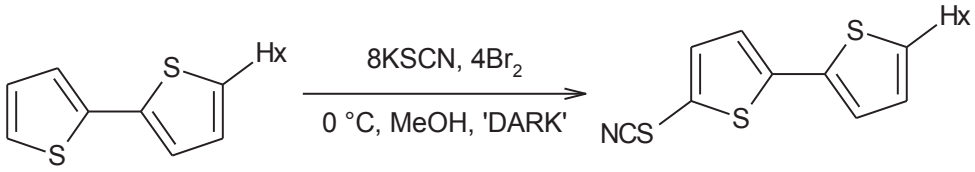

SiO_2 gel chromatography allowed for isolation of the target product, SCN-T_2Hx, although only a low yield was observed for this reaction. Further optimization of the workup of this reaction would likely improve the isolated yields of the brown oil product. From IR spectroscopy, the presence of a thiocyanate group was confirmed from nitrile stretches at 2157 cm^{-1}.

The selenocyanation of T_2Hx was performed under identical reaction conditions using KSeCN in place of KSCN. After SiO_2 gel chromatography, the target product was mostly isolated in low yields, but from IR may have contained a side product. Large amounts of KSeCN appeared to be left over after the reaction, indicating that the reaction does not proceed as well as the KSCN equivalent.[11]

Scheme 9. Synthesis of NCSe-T_2HX, **1b.**

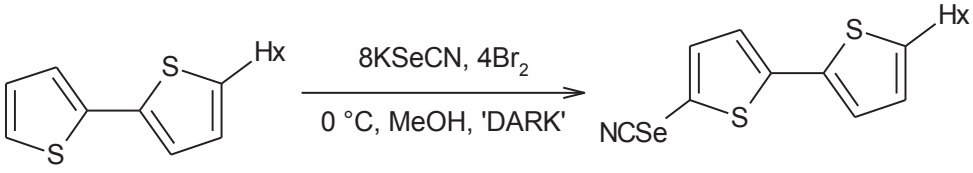

4.4 Synthesis of NCS-Hx-T_2-Hx and NCSe-Hx-T_2-Hx, **2a,b**

The synthesis of **2a** and **2b,** the target precursors with one thio- or selenocyanated group at a terminal alkyl position, was accomplished by a two step transformation of T_2Hx, shown in Scheme 10.

Scheme 10. Synthetic pathway to **2a,b**. For **2a**, x=S and for **2b**, x = Se.

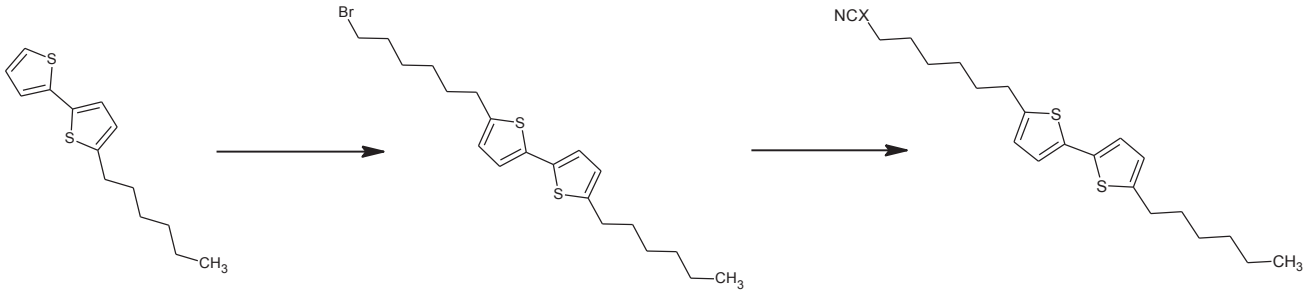

Br-Hx-T_2-Hx was synthesized from T_2Hx through lithiation with tBuLi and reaction with 1,6-dibromohexane (Scheme 11).

Scheme 11. Synthesis of Br-Hx-T_2-Hx

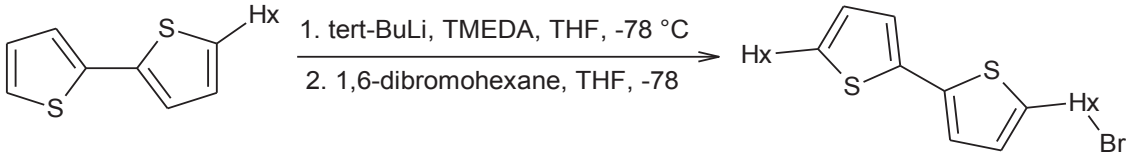

Through this reaction, Br-Hx-T_2-Hx was successfully synthesized in sufficient yields of approximately 13%. Possible changes to improve yield include the use of a different base such as lithium diisopropylamide (LDA) and the use of a more extensively dried solvent.

Synthesis of the thiocyanate target molecule **2a** and the selenocyante counterpart **2b** was accomplished through an S_N2 reaction, (Scheme 12). [25]

Scheme 12. Synthesis of Hx-T_2-Hx-XCN (**2a,b**) via S_N2 reaction with KXCN. X=S or Se. For **2a**, x= S and for **2b** X=Se

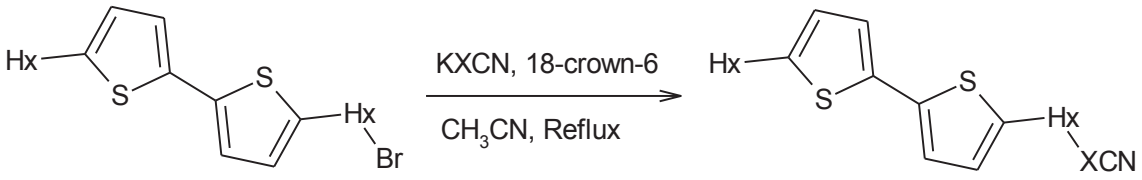

Consistent yields of 67% were achieved for **2a** and 80% for **2b**. From IR spectroscopy, the presence of a thiocyanate and selenocyanate groups were confirmed from nitrile stretches at 2151.02cm^{-1} and 2149.90cm^{-1}, respectively. Both products were stable under ambient conditions for one year.

4.5 Synthesis of NCS-Hx-T_2-Hx-SCN and NCSe-Hx-T_2-Hx-SeCN, **3a,b**

The synthetic pathways to **3a** and **3b** required two transformations of T_2, (Scheme 13).

Scheme 13. Synthetic pathway to **3a,b**, For a, x= S and for b, x= Se.

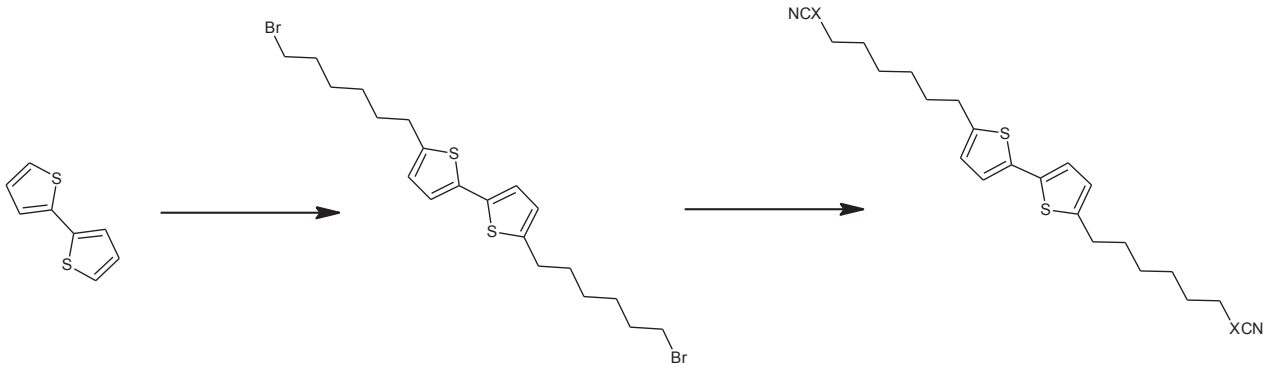

First, a bromo-terminated alkyl substituent was attached at the 5 and 5' positions of T_2. This transformation was first attempted using tBuLi and TMEDA, as shown in Scheme 14.

Scheme 14. Synthesis of bis(bromohexyl)-2,2'-bithiophene

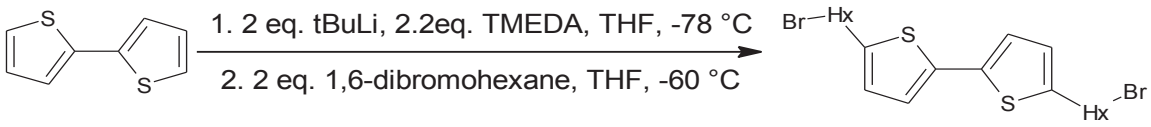

This synthesis produced low yields of the desired product. A second preparation was investigated in attempt to better facilitate the dianion intermediate (Scheme 15).

Scheme 15. Synthesis of Br-Hx-T_2-Hx-Br via nBuLi/TMEDA reflux.

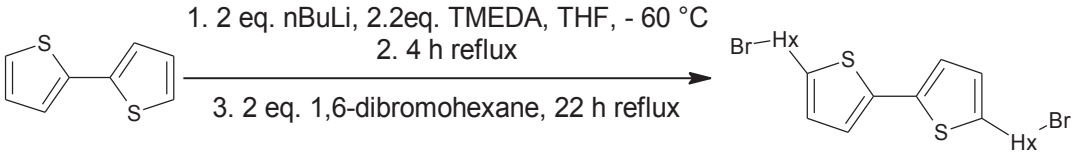

In this reaction, nBuLi was added at – 60 ˚C to avoid initial degradation of the organolithium reagent. Next, the solution of nBuLi, TMEDA and T_2 was refluxed for 4 h and subsequently for another 22 h after the addition of 1,6-dibromohexane. This procedure was adapted from a literature synthesis which demonstrated that the dilithiated dianion of bicyclic molecules was favoured at higher temperatures.[26] This reaction produced yields of 5.5%, which was higher than the attempted dialkylation with tBuLi.

Finally, the synthesis of **3a** and **3b** was accomplished with the same S_N2 reaction used in the synthesis of **2a** and **2b**.

Scheme 16. Synthesis of NCX-Hx-T_2-Hx-XCN

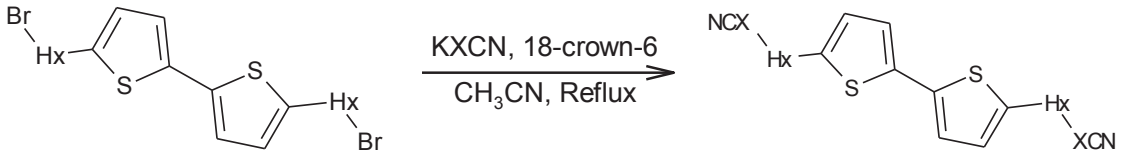

Yields over 90 % were achieved for **3a** and around 60 % for **3b**. Both products were stable under. ambient conditions for over one year. From IR spectroscopy, the presence of a thiocyanate and a selenocyanate group was confirmed from nitrile stretches at 2150 cm^{-1} and 2151 cm^{-1}, respectively.

Chapter 5 - Results and discussion of TF assembly and characterization

5.1 TF assembly on amorphous Au and C_p measurements

Prior to any thin film fabrication or surface analysis, capacitance measurement experiments were conducted to determine if each alkyl-substituted thiocyanate or selenocyanate could assemble onto a gold surface. In these experiments, an amorphous gold electrode was electropolished and flame-annealed. The gold electrode was then assembled into an electrochemical cell as the working electrode, which also employed a platinum coil as a counter electrode and a Ag/AgCl (3M KCl) electrode as the reference electrode. Using a 0.05 M $KClO_4$ electrolyte as the medium, a potential (E/V vs. SCE) was applied from a bias of -0.5 to +0.5 V and the measured capacitance of the bare amorphous Au electrode (Figure 5) was recorded. Next, the electrode was immersed in a 1 mM solution of a thio- or selenocyanate substrate for 24 hours at room temperature. The solution solvent was either dry hexanes or distilled ethanol. After 24 hours, the electrode was removed from the solution, rinsed with the pure solvent, and re-assembled into the same electrochemical cell. The capacitance of the electrode was then re-measured using identical parameters. This process was completed for **2a,b** and **3a,b**. In each instance the measured capacity is shown below (Figure 9).

Figure 9. Graph of applied potential (E/V vs. Ag/AgCl) vs measured capacitance ($\mu F/cm^2$) for amorphous Au electrode before and after 24h immersion in a saturated solution of **2a,b** or **3a,b** in ethanol or hexanes.

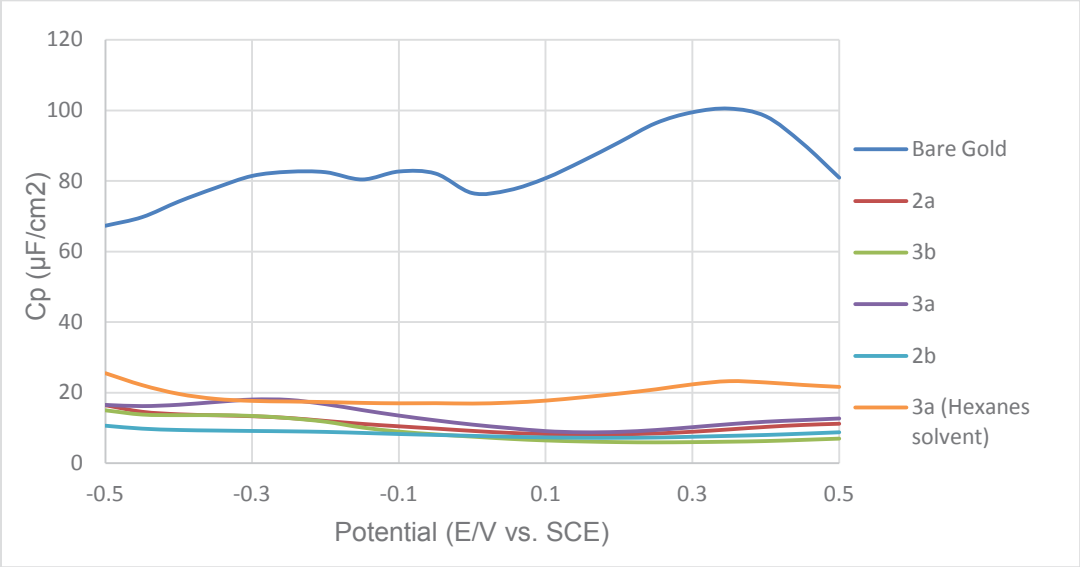

If a thin film formed on the surface of the electrode, the measured capacitance of the electrode should be significantly lower due to the organic layer insulating the electrode from the solution. As observed from Figure 9, the capacitance of the electrode is observed to be significantly lowered after immersion in one of the thiocyanates or selenocyanates. This is assumed to indicate successful formation of a thin film on the surface with each of the substrates. It is also noted that thin film assembly was successfully conducted in dry hexanes as well as ethanol. Substrates **1a** and **1b** were tested using identical experimental parameters to those used for **2ab** and **3ab**, but at a different time, and are therefore shown in a separate graph (Figure 10).

Figure 10. Graph of applied potential (E/V vs. Ag/AgCl) vs. measured capacitance ($\mu F/cm^2$) for amorphous Au electrode before and after 24h immersion in an ethanol solution of **1a** or **1b**

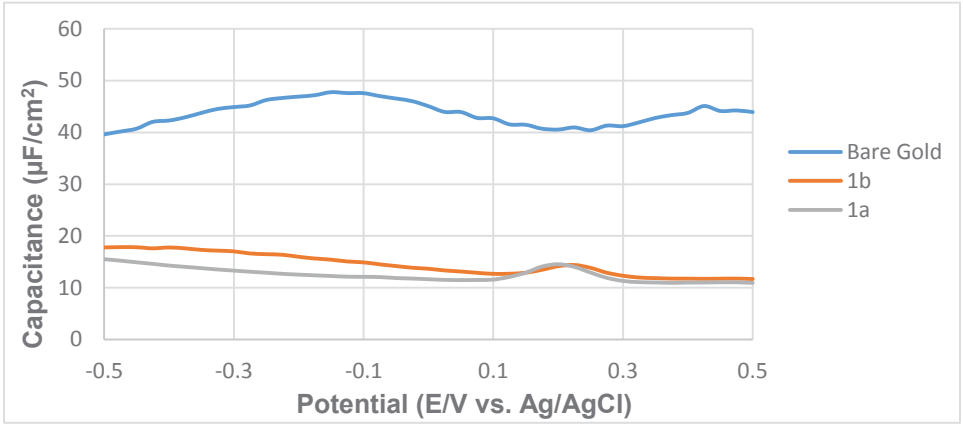

Trends observed from Figure 10 are identical to those observed from Figure 9. After 24 h immersion in an ethanolic solution of the thio- or selenocyanate, the measured capacitance of the electrode is significantly lower than that of the bare Au electrode. It should be noted that the curve of the bare Au electrode appears slightly different in Figures 9 and 10. Since these measurements were conducted at a different time the values are slightly different due to changes in the surface of the amorphous Au electrode; however, the effect of the TF formation follows the same trend even if the absolute values of the capacitance are different. Overall, since substrates **1ab, 2ab** and **3ab** successfully assembled into thin films on amorphous gold, the investigation of other suitable gold substrates was undertaken.

5.2 TF assembly on sputtered Au substrates and SEM/EDX characterization

Since it is known that thiocyanate thin films will form on an amorphous Au surface, on epitaxially grown substrates, and on emplate stripped Au, the possibility of thio- and selenocyanate self-assembly onto a sputtered Au surface was investigated. To synthesize these substrates, Ti plates used for electrochemical electrodes were etched in HCl (18 %) and Au was sputtered on using a sputter coater with a pure Au target. Sputtered substrates were immersed in a 1mM solution of a thiocyanate or selenocyanate substrate for 24 h. After 24 h, sputtered substrates were removed, rinsed with pure solvent, and dried under a stream of $N_{2(g)}$. Organic thiocyante and selenocyanate and solvent combinations used in each sample are shown in Table 1.

Table 1. Substrate and solvent combinations in the attempted self-assembly of thio- and selenocyanates on to sputtered Au substrates.

Sample	Substrate	Solvent used in assembly reaction
A	Hx-T_2-Hx-SCN	Ethanol
B	NCSe-Hx-T_2-Hx-SeCN	Ethanol
C	NCS-Hx-T_2-Hx-SCN	Ethanol
D	Hx-T_2-Hx-SecN	Ethanol
E	NCS-Hx-T_2-Hx-SCN	Hexanes
F	NCS-Hx-T_2-Hx-SCN	Ethanol

From SEM/EDS imaging, no evidence of organic matter on the surface of any of the substrates could be found. It should be noted that SEM/EDX would not be sensitive enough to detect a lone monolayer if it was present on the surface, however, it is expected that some evidence of organic matter would be found if a self-assembly reaction did occur. Ciszek noted that template stripped Au, which is assumed to be smoother than sputtered Au, did facilitate self-assembly, however the TFs produced had a lower surface coverage. [2] While organic matter could not be detected, it was observed that inorganic particles adhered to the sputtered Au surface (Figure 11). From EDX, these particles were observed to contain Sn, Cu, and I, among other elements, all of which constitute contaminants in the reaction solution.

Figure 11. SEM image of sputtered Au substrate after immersion in ethanolic solution of organic substrate. A) Highly heterogeneous surface. B) Inorganic particles absorbed onto surface.

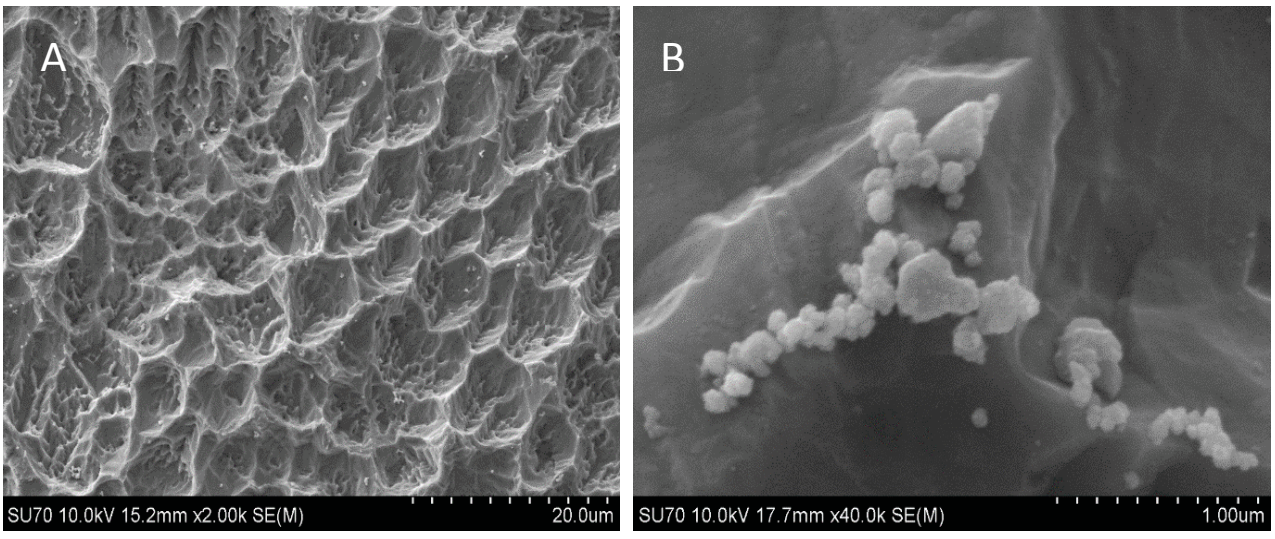

Shen and group demonstrated in 2008 that solution purity was very important in producing a well-developed thin film from thiocyanates.[9] It was found that thiocyanate solutions that were 'aged', ie. a thiocyanate solution used previously for self-assembly reaction produced higher quality thin films than one which had been freshly pepared. Following this, it was postulated that, while sputtered Au substrates were not suitable for organic TF assembly, they could be used as passive anodes to 'clean' the thiocyanate/selenocyanate solution of any impurities prior to self-assembly reaction.

5.3 TF assembly on epitaxially grown Au substrates

To prepare these substrates, Au was epitaxially deposited on a mica wafer in a vacuum chamber. The wafer was cut into 8 individual substrates (~1cm×1cm) and each was annealed with a butane flame. A TF was synthesized on each of these substrates using one of **1a,b**; **2,ab**; or **3a,b** in either ethanol or hexanes. To fabricate each thin film, an Au substrate was immersed in an 'aged'1 mM solution of the precursor in a sealed vial. Vials were heated in a drying oven at 50 °C for 24 h. After this immersion time, Au substrates were removed from the solution, rinsed with the reaction solvent and dried under a stream of $N_{2(g)}$ for several hours. Thin films were stored under an $N_{2(g)}$ atmosphere. Organic precursors and solvents used for each thin film are found in Table 2.

Table 2. Description of each thin film assembled onto epitaxially grown Au including structure, assembly reaction solvent, order in which assembled, and characterization techniques used on each sample.

Sample	Projected structure of single unit of TF	Reaction Solvent	Date	Tests
TF-G	Au-Se-Hx-T_2-Hx-SeCN	EtOH	17/7/2014	SEM/EDX, AFM
TF-H	Au-Se-Hx-T_2-Hx-SeCN	Hexanes	24/7/2014	SEM/EDX, Carbon glue therefore no for XPS
TF-I	Au-S-Hx-T_2-Hx-SCN	EtOH	2/8/2014	SEM/EDX (Not conductive enough) XPS, ToF-SIMS
TF-J	Au-S-Hx-T_2-Hx	EtOH	2/8/2014	XPS, ToF-SIMS
TF-K	Au-Se-Hx-T_2-Hx	EtOH	2/8/2014	XPS, ToF-SIMS
TF-L	Au-Se-T_2-Hx	EtOH	2/8/2014	XPS, ToF-SIMS, SEM/EDX
TF-M	Au-S-T_2-Hx	EtOH	5/8/2014	XPS, ToF-SIMS
TF-N	Au-S-T_2-Hx	Hexanes	5/8/2014	XPS, ToF-SIMS

5.4 SEM/EDX characterization of TFs on epitaxially grown substrates

Scanning electron microscopy with energy dispersive spectroscopy (SEM/EDX) were the first techniques used to conduct surface analyses. SEM/EDX was conducted on four samples: TF-G, TF-H, TF-I and TF-L.

TF-G contained a number of large areas of organic crystallites, as shown in Figure 12. Organic crystallites were found exclusively in clusters of islands on very smooth areas of the Au substrate. Charging is also evident from the bright areas on the images (Figure 12A). This is primarily attributed to the insulating nature of the mica layer onto which the Au was epitaxially deposited. It is also thought that

perhaps the presence of an insulating organic monolayer that the SEM/EDX was not sensitive enough to detect could also be contributing to the charging.

Figure 12. SEM images of organic crystallite islands found on TF-G (Au-Se-Hx-T_2-Hx-SeCN from ethanol) on crystallites were confirmed to be organic via EDX. A) and B) depict different areas on the sample with crystallite islands. A) Cluster of islands on smooth Au surface. B) Another cluster of islands with bright charging in the lower half of the image.

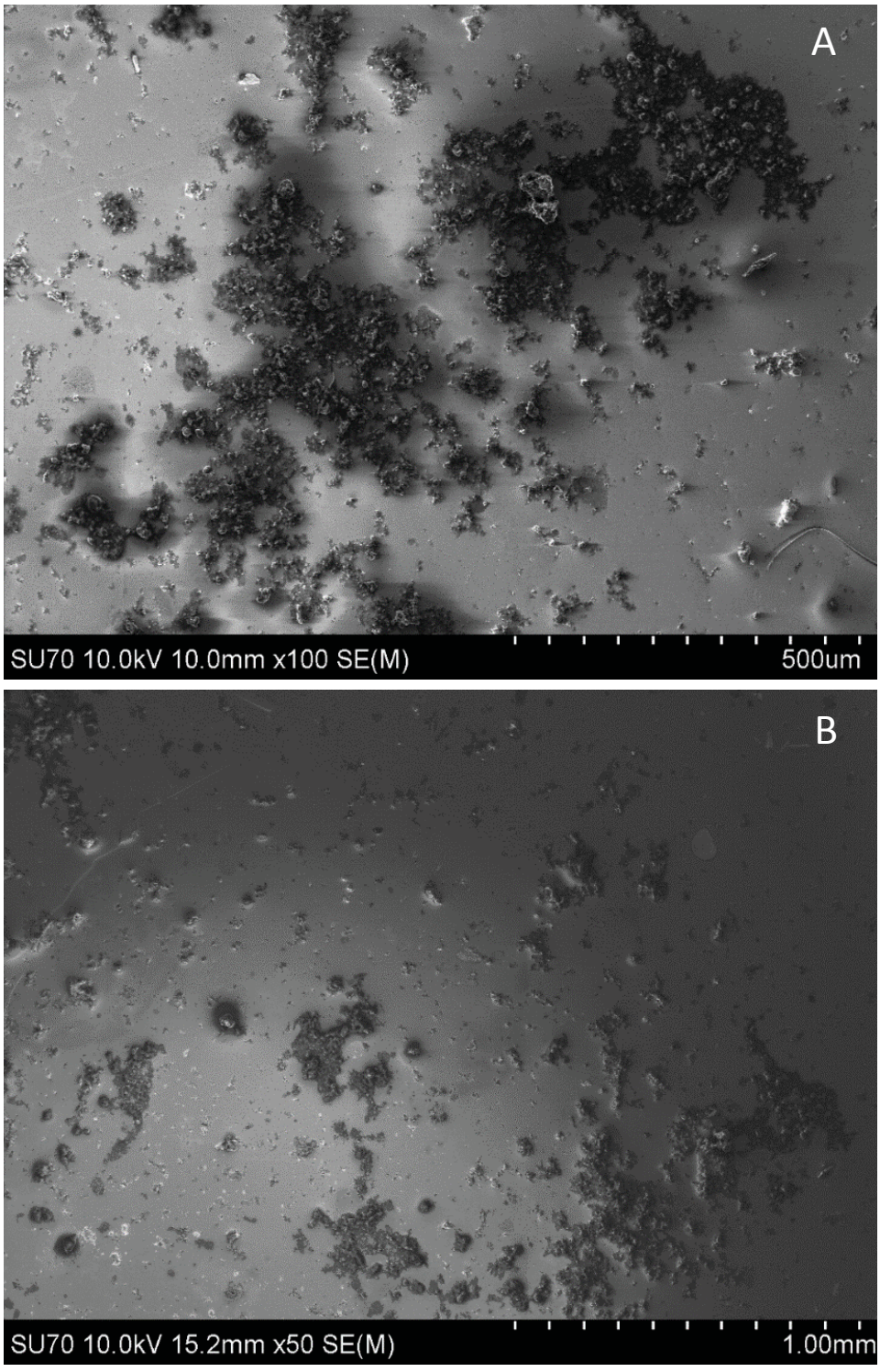

SEM/EDX maps of three different smaller crystallite areas were also obtained for TF-G, as shown in Figure 13, Figure 14, and Figure 15. A map sum spectrum for each of these three SEM/EDX mapping images can be found in Appendix 3. For visual simplification, each element mapped by EDX is displayed separately.

Figure 13 displays an area with several islands. The location of the islands in the SEM image corresponds with the EDX intensity patterns of C, S and Se. Therefore, it is assumed that the islands are crystallites of **3b**. From the EDX map, nitrogen appears to be diffusely spread out across the surface. TF-G should have the structure Au-Se-Hx-T_2-Hx-SeCN, therefore the organic crystallites should contribute to the nitrogen signals. It is known that there will always be trace nitrogen contamination in EDX. As well, residual nitrogen on the surface could account for the nitrogen signals. Lastly, the organic crystallite islands could likely not be picked up by SEM/EDX if they were monolayers, thus the crystallites are assumed to be multilayers of **3b**. The formation of such multilayers could be a result of interactions between remaining selenocyanate substituents.

Figure 13. EDX image of organic crystallites on TF-G. A) SEM image of organic crystallite. B) Carbon map (Kα1). C) Sulfur map (Kα1). D) Selenium map (Lα1). E) Nitrogen map (Kα1). A map sum spectrum for this image can be found in Appendix 3.

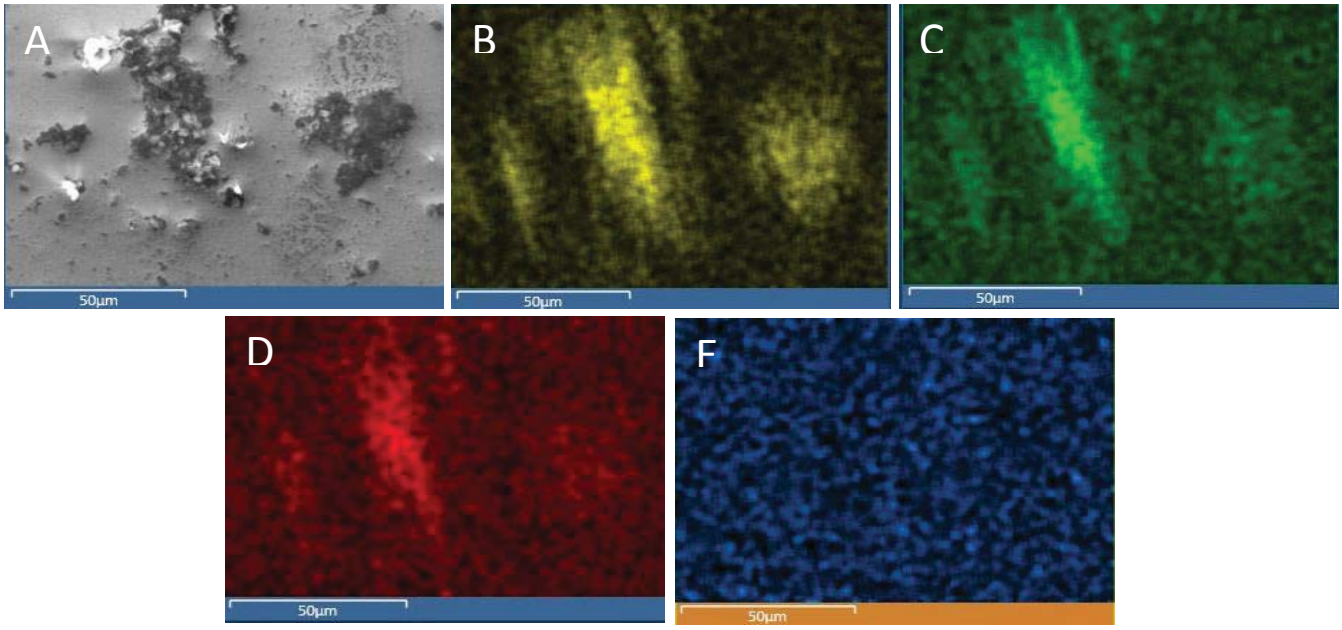

Figure 14 shows SEM and EDX mapping images of a second organic crystallite. Patterns of intensity on EDX maps of carbon (Figure 14B), sulfur (Figure 14C), and selenium (Figure 14E) all match the locations of the crystallites on the SEM image. As well, from Figure 14D, areas that produce no Au signal correspond to the area where the organic crystallites are found in the SEM image. Since the EDX signal penetrates about 1 μm into the sample, it is assumed that these crystallites are fairly thick features.

Figure 14. SEM/EDX mapping images of second organic crystallite found on TF-G. A) SEM image of organic crystallite. Panels B) to E) display EDX mapping images of A). B) Carbon map (C Kα1). C) Sulfur (S Kα1). D) Gold (Au Mα1). E) Selenium map (Se Lα1). A map sum spectrum for this image can be found in Appendix 3.

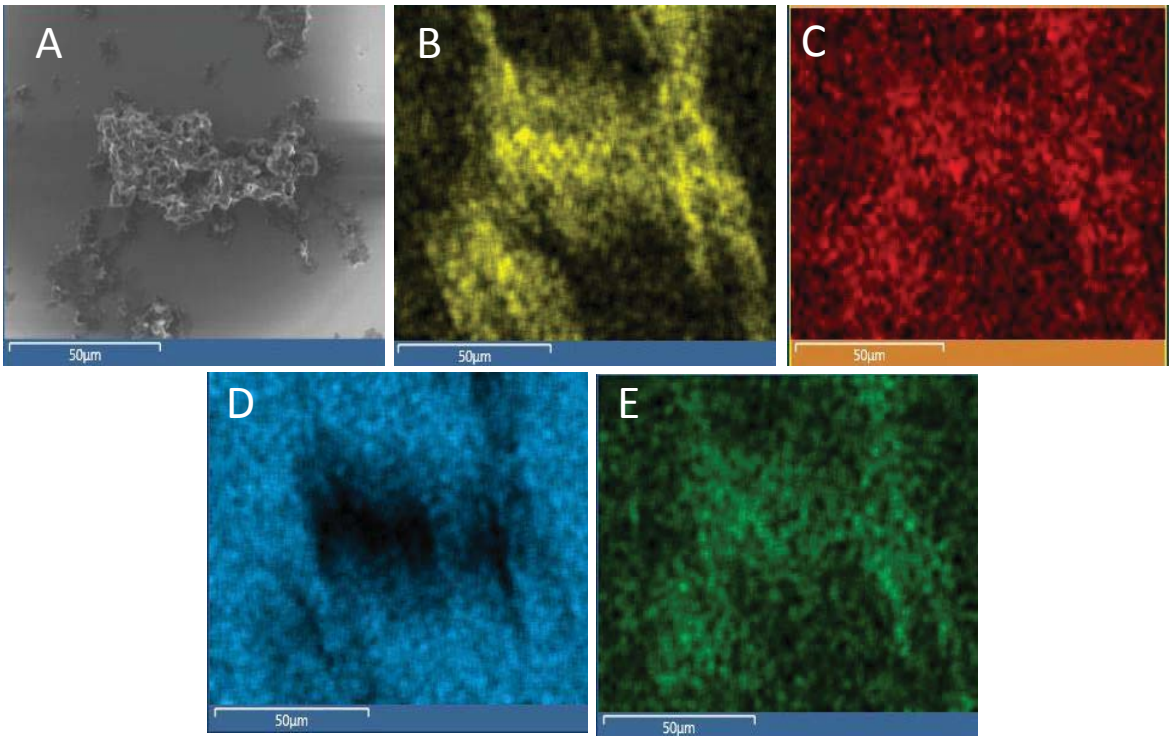

Figure 15 shows SEM/EDX images of a third organic crystallite found on TF-G. Element intensities from EDX maps of sulfur (Figure 15B), carbon (Figure 15C), selenium (Figure 15D) all match the locations of organic crystallites in the SEM image (Figure 15A).

Figure 15. Crystallite map A) SEM image of organic crystallite. Panels B) to D) display EDX images of the same crystallite. B) Sulfur map (S Kα1). C) Carbon map (C Kα1). D) Selenium map (Se Lα1). A map sum spectrum for this image can be found in Appendix 3.

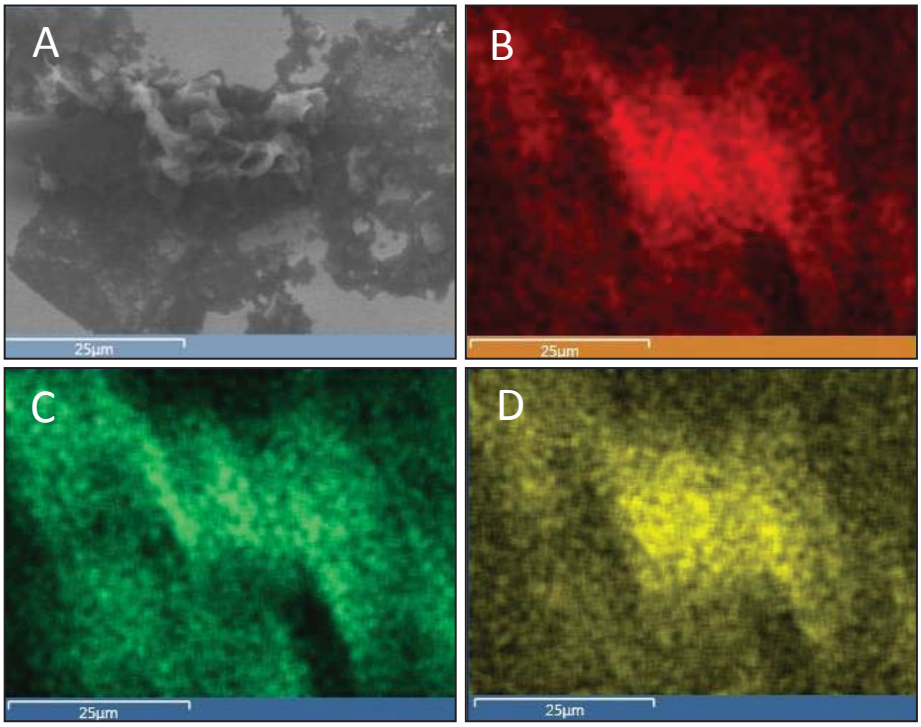

Surface analysis with SEM/EDX was also used on TF-H and TF-I. Organic features could not be found on either sample. A high amount of sample charging was encountered during the analysis of TF-I. Therefore, carbon glue was used to ground sample TF-I, however, despite the better facilitation of the electrical charge, no organic matter could be found on the sample surface. Again, it must be noted that SEM/EDX should not be sensitive enough to detect a monolayer. Since the addition of carbon glue made further surface analysis difficult, TF-I was not further characterized and carbon glue was not used again.

Lastly, to determine if precursors with only one alkyl substituent could form large organic crystallites, SEM/EDX analysis was used on TF-L (Au-Se-T_2-Hx from ethanol). As shown in Figure 16, two large organic features were found on the surface.

Figure 16. SEM images of two organic crystallites found on TF-L (Au-Se-T_2-Hx).

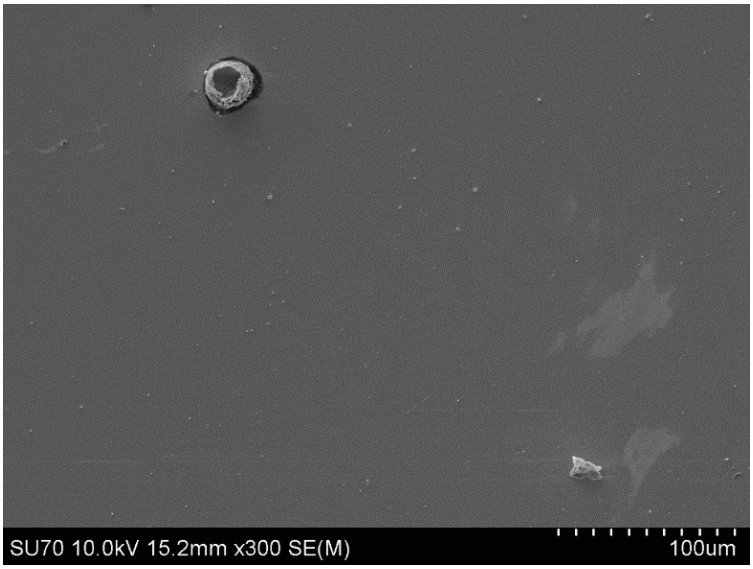

EDX mapping images of each of the crystallites shown in Figure 16 are found in Figure 17 and Figure 18.

Figure 17. SEM/EDX images of round organic crystallite on TF-L. A) SEM image of organic crystallite. Panels B) to E) display EDX mapping images of the crystallite. B) Carbon map (C Kα1). C) Sulfur map (S Kα1). D) Gold map (Mα1). E) Selenium map (Lα1).

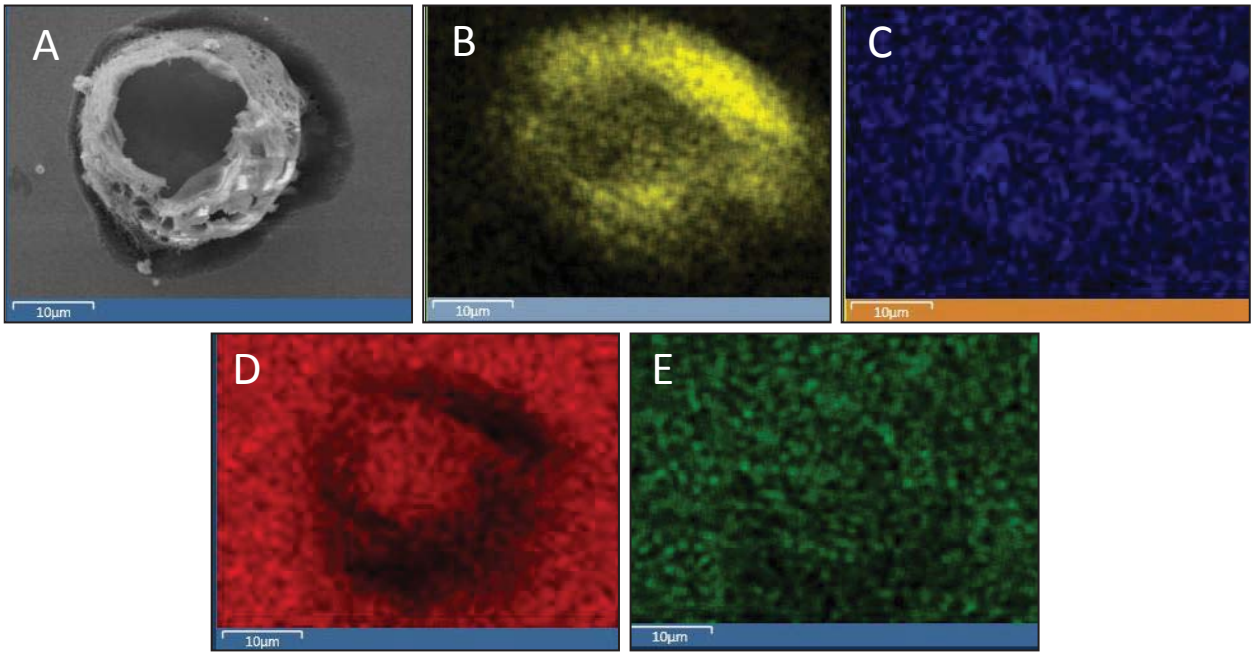

From Figure 17, the intensity pattern of carbon (Figure 17B) matches the location of the crystallite on the SEM images, while that of gold (Figure 17D) shows an absence of signal. The elemental maps of sulfur (Figure 17C) and selenium (Figure 17E) indicate that the each element is present, however, significant patterns are not evident. Lack of pattern in the nitrogen map may be attributed to the presence of contaminant nitrogen, residual $(CN)_{ads}$ or difficulty in mapping nitrogen. Similar to the crystallite shown in Figure 9, it is assumed that the feature height and size of the round organic crystallite is quite large since x-ray photons from Au were not detected.

Figure 18. SEM/EDX on Au-Se-T_2-Hx. A) SEM image of organic crystallite. Panels B) to E) display EDX mapping images of the crystallite. B) Carbon map (C Kα1). C) Sulfur map (S Kα1). D) Gold map (Mα1). E) Selenium map (Lα1).

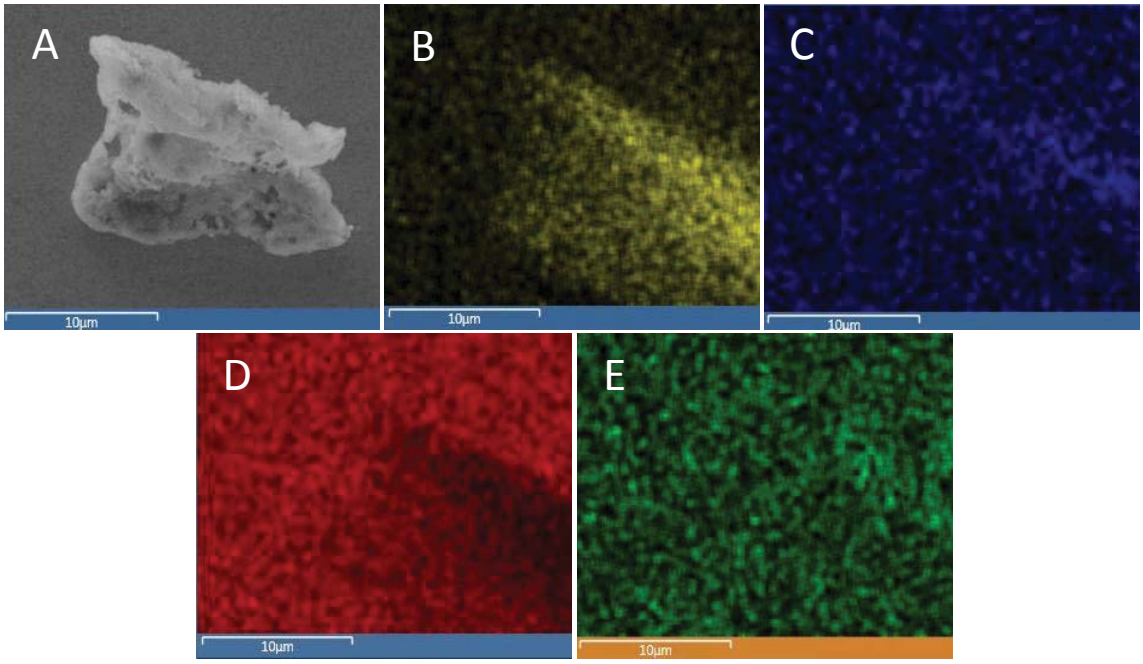

The SEM/EDX images of the other organic crystallite found on TF-L are shown in Figure 18. From the maps of C (Figure 18B) and Au (Figure 18D), the same patterns that were shown in Figure 17 are observed. However, no clear patterns are evident from the elemental maps of S (Figure 18C) and Se (Figure 18D).

Overall, EDX/SEM imaging of the four samples demonstrated that while organic crystallites do form from the self-assembly of thiocyanates and selenocyanates on epitaxially grown Au, occurrences are limited. As well, surface analysis of TFs assembled from these precursors would likely be better facilitated by techniques traditionally used in the analysis of thiolate thin films such as AFM, XPS, and STM.

5.5 AFM characterization of TFs on epitaxially grown substrates

Atomic force microscopy (AFM) was previously used by the MacKinnon Lab to successfully characterize two TFs assembled from thiocyanate precursors. However, in his original publication on thiocyanate precursors, Ciszek noted that AFM was unsuitable for this type of thiolate TF.[27] In the present study, the use of contact AFM was also attempted in the surface analysis of TF-G (Figure 19).

Figure 19. AFM image of TF-G (Au-Se-Hx-T_2-Hx-SeCN from ethanol). Large white spots toward center of image indicating features too large to topographically imaged.

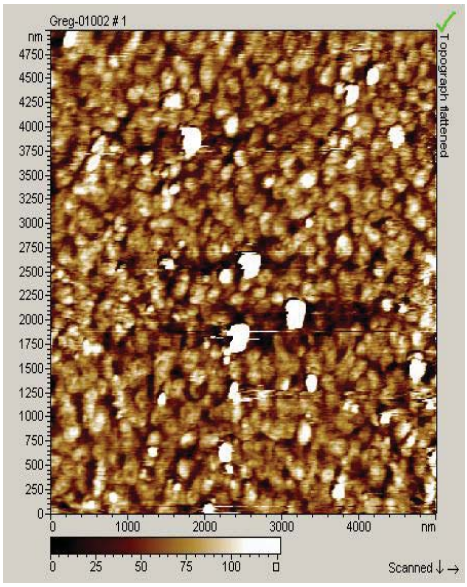

These results show consistency with Ciszek's observations. Large white spots toward the center of the image are indicative of features that are too tall to be effectively characterized by the apex tip. Based on the image in Figure 19, it is assumed that contact AFM is an inappropriate surface analysis technique for the TFs in this study and the use of AFM was not again attempted.

5.6 XPS characterization of TFs on epitaxially grown Au substrates

Surface analysis with XPS was greatly important since this technique allowed for the investigation of the elemental composition of the surface and the chemical nature of the bond between the organic and metal moiety. XPS was conducted on six of the eight thin films assembled on epitaxially grown Au substrates. Survey spectra were obtained for six thin films to determine major elements present in the sample. Further high resolution spectra were obtained of the XPS regions of nitrogen (N 1s), sulfur (S 2p), carbon (C 1s), gold (Au 4f) and selenium (Se 3d). In this section, high resolution peaks are discussed and compared with literature values. Full high resolution spectra can be found in Appendix 3.

The N 1s XPS region was characterized to investigate the presence of nitrogen residue on the surface as well as the chemical state of the second thiocyanate substituent on TF-I. A typical high resolution scan of this peak is shown in Figure 20:

Figure 20. XPS high resolution spectra of 1Ns peak typical of residual gold-bound cyanide.

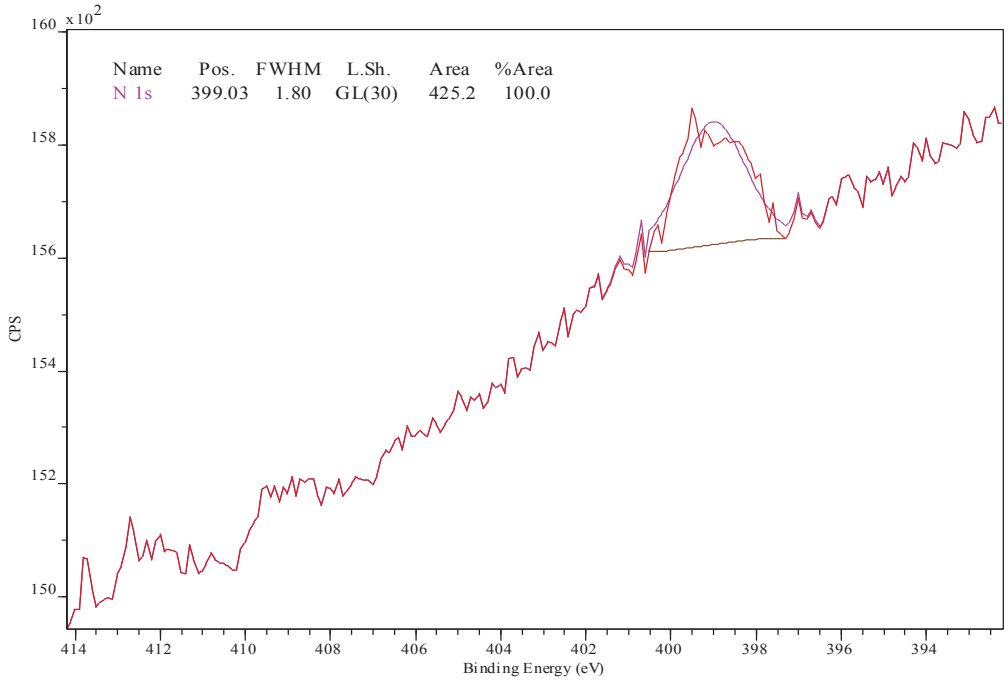

Ciszek observed two different N 1s signals from residual nitrogen on the metal surface.[24] The first was that of adsorbed cyanide, or $(CN)_{ads}$, at 397.7 eV. The second signal was that of gold-bonded

cyanide, or $Au(CN)_{ads}$ at 399.5 eV. The $Au(CN)_{ads}$ peak reported by Ciszek is identical to that observed when cyanide is used to etch a metal surface. Based on the high occurrence of this signal, Ciszek proposed that thiocyanate TF assembly occurs through a surface mediated reduction of the thiocyanate, resulting in the $[Au(CN)_2]^-$ leaving the surface as a by-product. Overall, Ciszek observed some form of residual nitrogen in the majority of assemblies.[27] The N 1s signals obtained for each sample analyzed by XPS in this study are shown in Table 3:

Table 3. Binding energies from high resolution XPS characterization of N 1s region of six thin films. Signals are internally referenced against Au 4f at 83.95 eV.

TF #	Thin Film	N 1s (eV)
I	Au-S-Hx-T_2-Hx-SCN	399.56
J	Au-S-Hx-T_2-Hx	399.28
K	Au-Se-Hx-T_2-Hx	399.11
L	Au-Se-T_2-Hx	399.91
M	Au-S-T_2-Hx (in ethanol)	399.03
N	Au-S-T_2-Hx (in hexanes)	398.88

TF-I matches the $Au(CN)_{ads}$ peak most closely at 399.56 eV. However, interestingly a second signal for the remaining thiocyanate group was not observed. It is possible that this peak overlapped with that of $Au(CN)_{ads}$ or simply was not detected. All other signals are close to the $Au(CN)_{ads}$ signal but vary over 1.0 eV. However, all signals vary most from the peak for $(CN)_{ads}$. Therefore, all N 1s signals obtained from TFs I-N are attributed to $Au(CN)_{ads}$.

XP spectroscopy of the S 2p region of each sample was also conducted. Signals for numerous chemical states of sulfur were expected. A typical high resolution spectrum of this reaction is shown in Figure 21:

Figure 21. XPS high resolution spectra of S 2p region

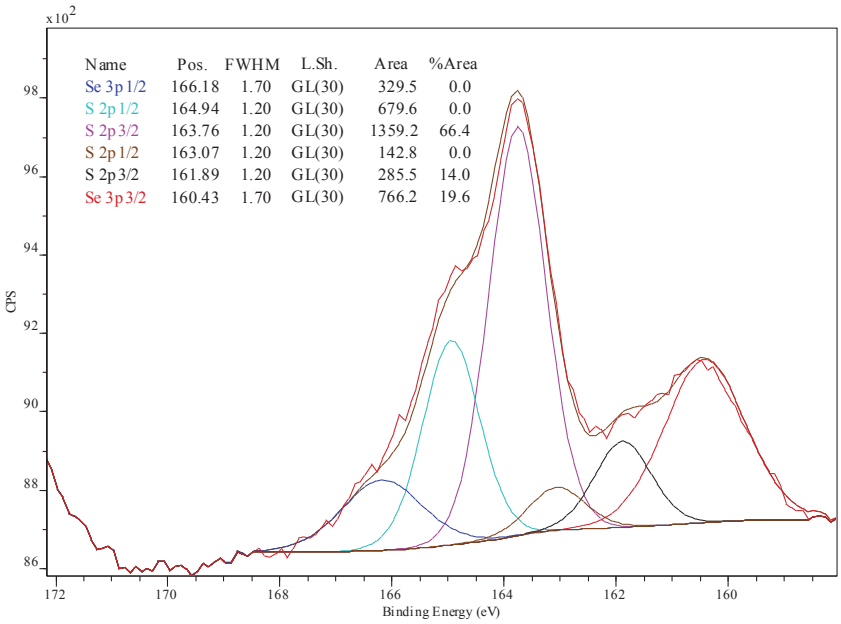

Careful interpretation of the S 2p XPS region of each thin film was required in order to determine the chemical nature of the linkage between the organic and metal domains. Signals obtained for each of the samples are shown in Table 4:

Table 4. Binding energies from high resolution XPS characterization of S 2p region of six thin films. Signals are internally referenced against Au 4f at 83.95 eV.

Sample	Thin Film	1st S $p^{3/2}$	2nd S $p^{3/2}$	3rd S $p^{3/2}$	Se $3p^{3/2}$
TF-I	Au-S-Hx-T_2-Hx-SCN	161.30	162.08	163.60	--
TF-J	Au-S-Hx-T_2-Hx	161.29	162.10	163.53	--
TF- K	Au-Se-Hx-T_2-Hx	--	162.57	163.88	160.69
TF-L	Au-Se-T_2-Hx	161.88	163.67	--	161.08
TF-M	Au-S-T_2-Hx (ethanol)	161.30	161.92	163.74	--
TF-N	Au-S-T_2-Hx	161.89	163.89	--	160.43

Ciszek observed binding energies of 161.8 and 161.9 eV for alkyl thiolates and 162.0 eV for aromatic thiolates. [25] TF-M and TF-N follow these values closely with S 2p signals of 161.92 and 161.89 eV respectively. Signals at 162.10 eV for TF-J and 162.08 eV for TF-I are attributed to alkyl-thiolates. Signals from 163.0 to 164.0 eV are attributed to the sulfur atoms in the core bithiophene.[28] Oxidized sulfur species are associated with peaks in the S 2p region above 166 eV. [27] Since this was not observed for any of the samples, it assumed that there was no detectable oxidization in the tested thin films despite being characterized by XPS roughly one month after the assembly process took place.

High resolution XP spectra of the C 1s region were also obtained. Limited literature values were available for thiolate and selenolate thin films of oligothiophenes, therefore signals from this region were used to evaluate the presence of an organic moiety on the surface rather than to characterize it. A typical spectrum of this region is shown in Figure 22.

Figure 22. XPS high resolution spectra from C 1s region

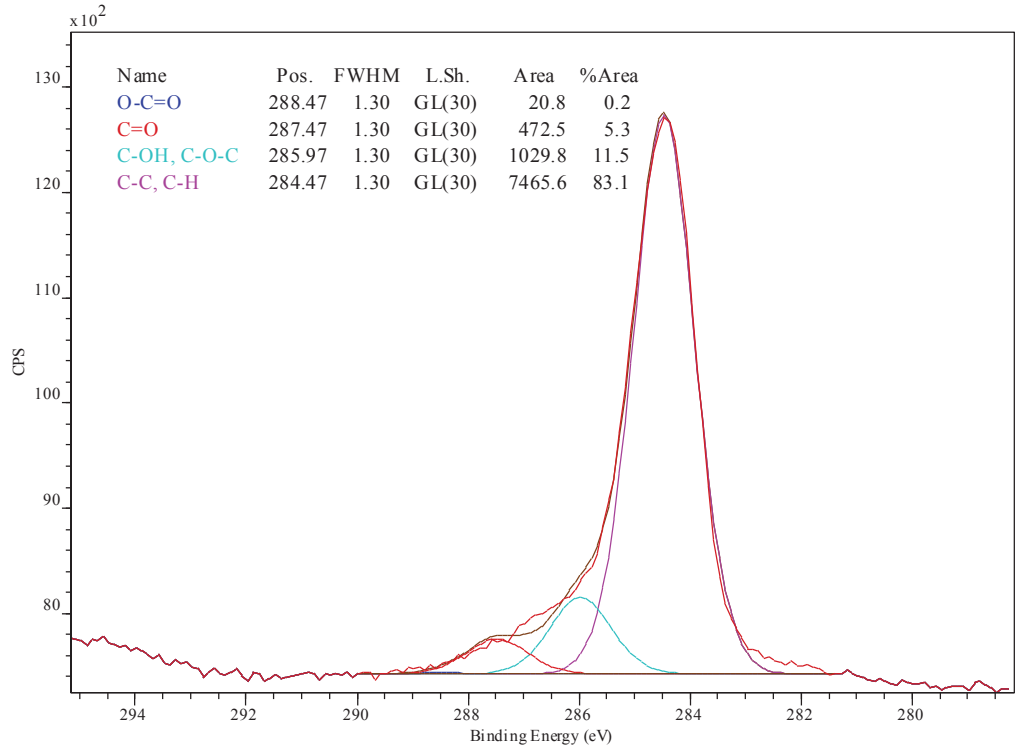

High resolution XP spectroscopy results from the C 1s region confirm the presence of organic carbon on the gold substrates. Each thin film produced a signal between 284.37 - 284.85 eV, which is attributed to organic carbon. [28] Other signals are attributed to species of oxygen-bound carbon that exist as trace contaminants.

Table 5. Binding energies from high resolution XPS characterization of C 1s region of six thin films. Signals are internally referenced against Au 4f at 83.95 eV.

Sample	Thin Film	1st C 1s	2nd C 1s	3rd C 1s	4th C 1s
TF-I	Au-S-Hx-T_2-Hx-SCN	284.39	285.89	287.39	--
TF-J	Au-S-Hx-T_2-Hx	284.37	285.87	287.37	288.37
TF-K	Au-Se-Hx-T_2-Hx	284.55	286.05	287.55	288.55
TF-L	Au-Se-T_2-Hx	284.42	285.92	287.42	288.42
TF-M	Au-S-T_2-Hx	284.85	286.35	287.85	288.85
TF-N	Au-S-T_2-Hx (hexanes)	284.47	285.97	287.47	288.47

ToF-SIMS surface analysis, (discussed in section 5.7,) was used to characterize the nature of the TFs present on the surface both in terms of structure, (from fragments detected,) and surface coverage, (from observed intensity patterns.)

Lastly, high resolution spectra of the Se 3d region for TF-K and TF-L were also obtained to evaluate the presence of a selenolate bond. A typical spectrum of this XPS region is shown in Figure 23:

Figure 23. High resolution XPS spectra of Se 3d

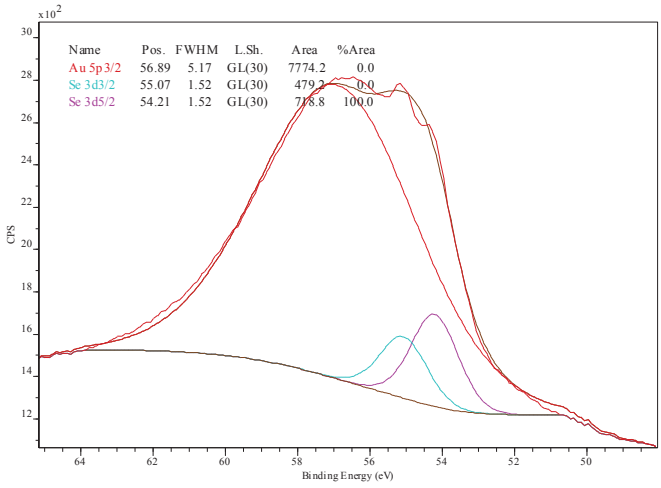

Measured binding energies for both thin films are shown in Table 6. Reported literatures values for the Au-selenolate bond focus heavily on both 3d peaks detected as a result of orbital-splitting.[29]

Table 6. Binding energies from high resolution XPS characterization of Se 3d region of six thin films. Signals are internally referenced against Au 4f at 83.95 eV.

TF #	Thin film	$3d^{5/2}$ (eV)	$3d^{3/2}$ (ev)
TF-K	Au-Se-Hx-T_2-Hx	54.21	55.07
TF-L	Au-Se-T_2-Hx	54.79	55.65

Daniel Kafer reported the selenolate signal as a doublet between 54.0 to 56.6 eV with splitting of 0.86 eV.[29] Both TF-K and TF-L match these criteria, therefore both are assumed to have successfully formed a selenolate-gold bond as an anchor between the organic and metal moiety.

Quantitative XPS results for each of the six samples discussed in this section were also obtained. However, a number of factors contributed to uncertainty in the accuracy of these results. Previously discussed binding signals for carbon and residual nitrogen indicate there is contamination in the samples. Se and Se signals contain a significant amount of spectral overlay. As well, it was observed from SEM/EDX and AFM that the TFs assembled in this study were morphologically very heterogeneous. Due to these complicating factors, the quantitative XPS results are not discussed in this thesis.

5.7 ToF-SIMS characterization of TFs on epitaxially grown substrates

Time-of-flight secondary ion mass spectrometry (ToF-SIMS) was used to obtain intensity maps of specific fragments for the six thin films for which XPS data was obtained. Chemical maps of a total of 6 fragments were collected: HS^-, Se^-, SC_4H^-, Au_3^-, Na^+, K^+, $C_3H_5^-$, and Au_3^+.

Fragment maps for TF-N (Au-S-T_2-Hx from hexanes) are shown in Figure 24. For this sample, surface coverage of all fragments appears mostly homogeneous, with the exception of Na^+ and K^+ contaminants.

Figure 24. ToF-SIMs mapping images for TF-N (Au-S-T_2-Hx from hexanes). Top row contains mapping images of negative ions.Bottom row contains mapping images of positive ions.

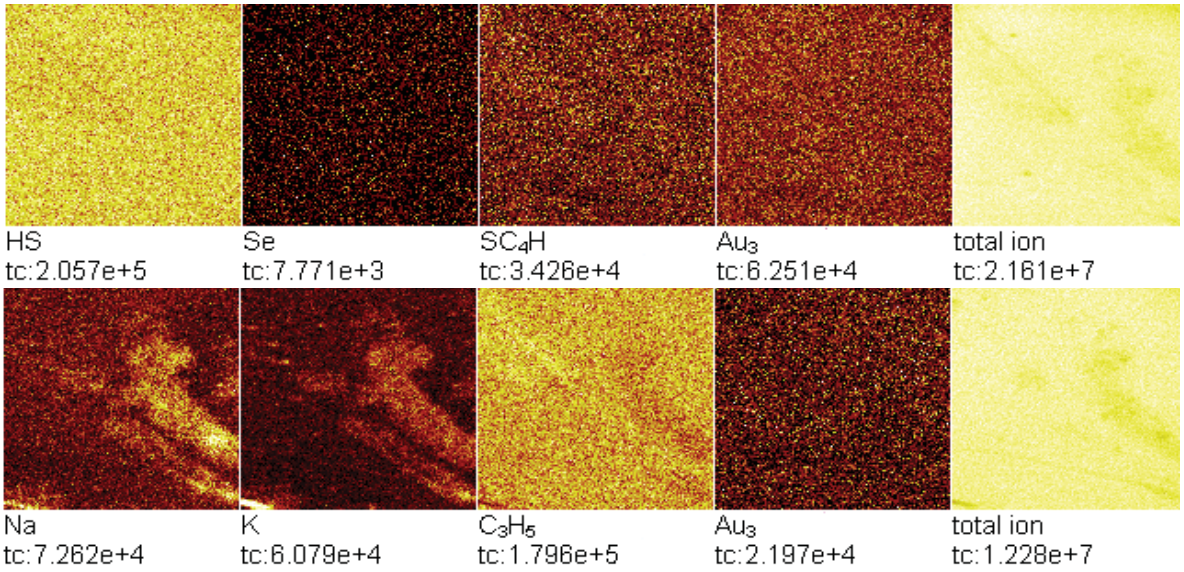

Similar feature patterns are evident for both these contaminants, which can be partially seen in that of $C_3H_5^-$. These high intensity features appear to be crystallites of Na^+ and K^+. As well, from the fragment map of Se^-, homogenous but diffuse selenium contamination is evident.

For TF-M (Au-S-T_2-Hx in ethanol), chemical intensity maps, shown in Figure 25, appear mostly homogeneous for Au, sulfur and organic fragments. Na^+ and K^+ map patterns vary except for one high intensity feature in the upper left corner. This specific feature is assumed to be a large cluster of potassium and sodium contamination, since a mirroring low intensity feature is observed in all other maps. The diffuse selenium signals are attributed to the sample being exposed to an environment where selenium was present.

Figure 25. ToF-SIMs mapping images for TF-M (Au-S-T_2-Hx from ethanol). Top row contains mapping images of negative ions. Bottom row contains mapping images of positive ions.

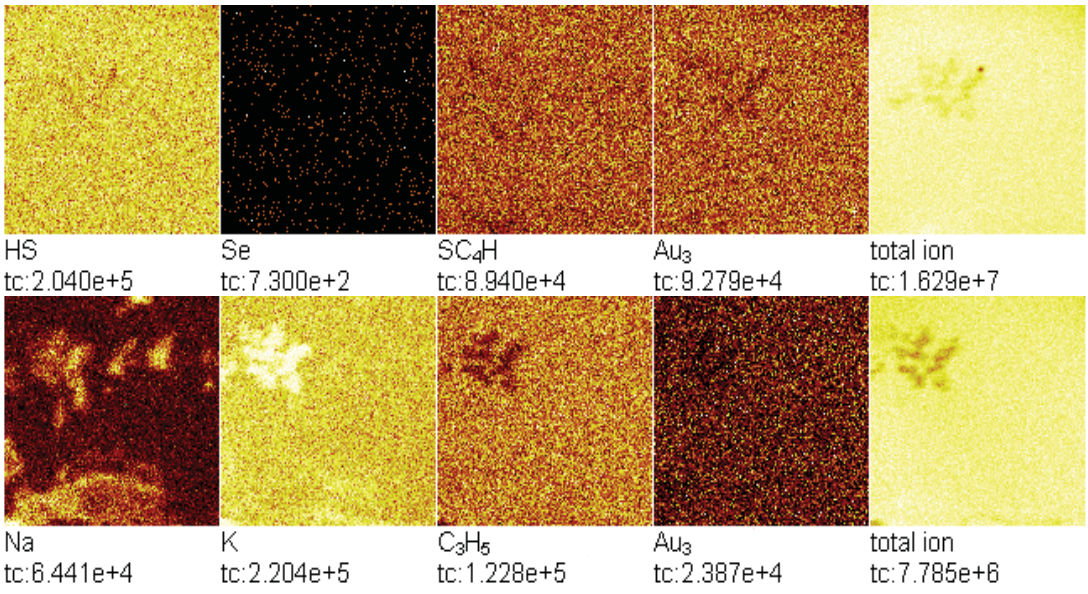

For TF-J (Au-S-Hx-T_2-Hx), shown in Figure 26, all fragment intensity maps were observed to be mostly homogenous. No selenium contamination was observed for this sample and the intensity of Na^+ and K^+ maps is also observed to be low.

Figure 26. ToF-SIMs mapping images for TF-J (Au-S-Hx-T_2-Hx). Top row contains mapping images of negative ions. Bottom row contain mapping images of positive ions.

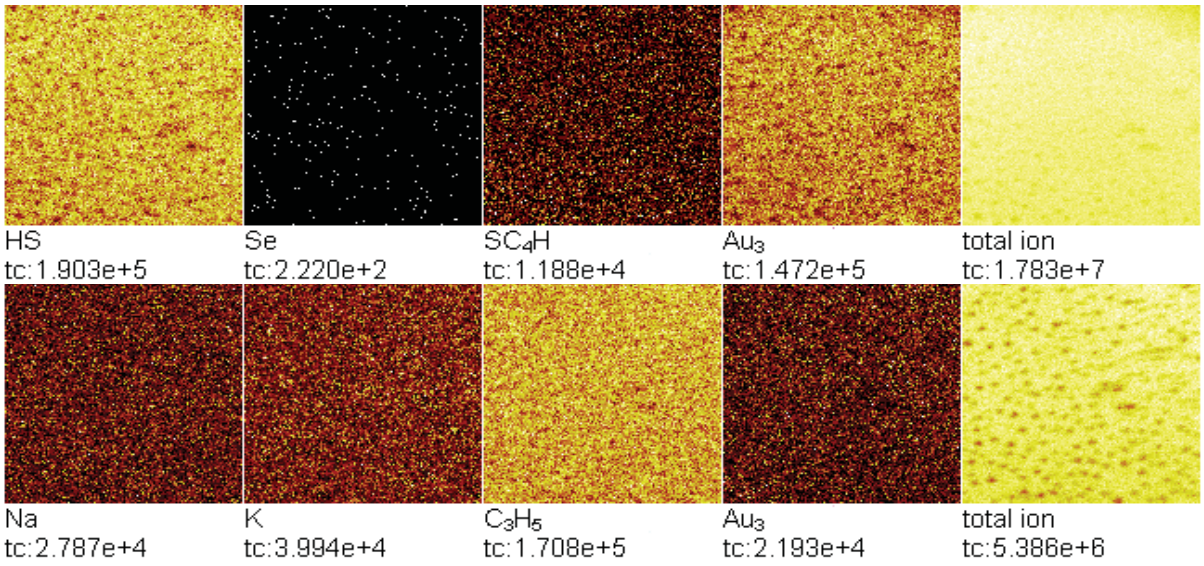

For TF-K (Au-Se-Hx-T_2-Hx), shown in Figure 27, all organic, sulfur, Au, and Se fragment maps are mostly homogeneous. Several patterns of intensity are observed on Na^+ and K^+ fragment maps and largely correlate with each other. These areas of alkali contaminant intensity correlate with the diffuse areas of darkness that are seen in all other fragment maps, indicating that these areas of the sample are covered in contamination.

Figure 27. ToF-SIMs mapping images for TF-K (Au-Se-Hx-T_2-Hx). Top row contains mapping images of negative ions. Bottom row contain mapping images of positive ions.

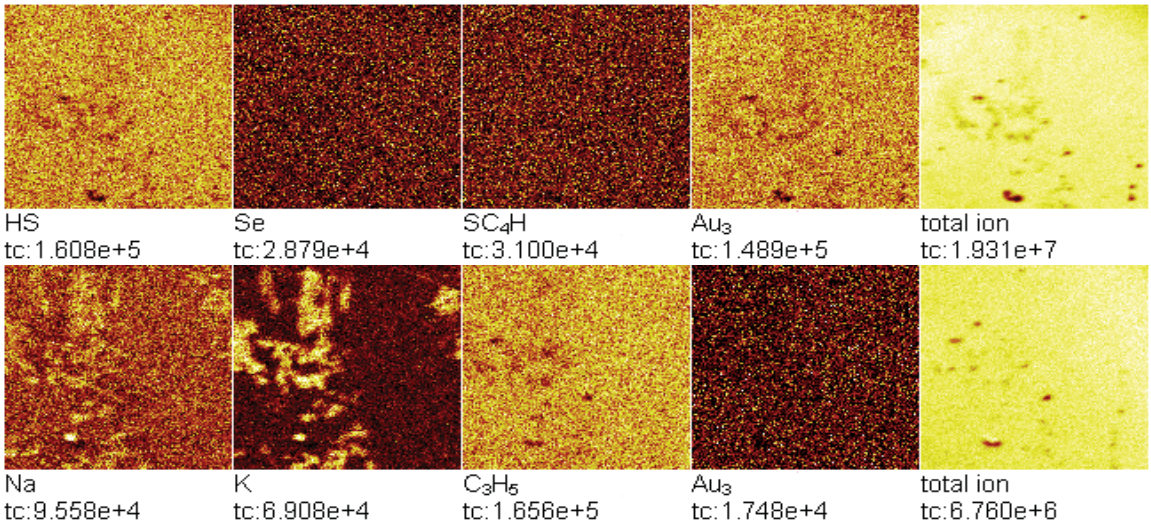

Chemical intensity maps produced from ToF-SIMS of TF-L (Au-Se-T_2-Hx) are shown in Figure 28. While all fragment maps were observed to form large homogenous areas, many large features of fluctuating intensity were observed from the ToF-SIMS images. The locations of intensity features in all fragment maps mostly match, like the other thin films, however, the intensity trends are different. From Figure 20, the maps of Na^+, K^+ and $C_3H_5^+$, Au^+ and Au^- show areas of lower intensity where HS^- and SC_4H^- show areas of high intensity. The low intensity of Na^+, K^+, and Au suggest that these areas may be larger organic features. However only HS^- and SC_4H^- show high increased intensity in these areas, while C_3H_5 is lower intensity and Se appears to be mostly homogeneous over the entire surface area. This sample was subjected to SEM/EDX and XPS prior to ToF-SIMS, it is also possible that irradiation from electron and x-ray energy has damaged the surface.

Figure 28. ToF-SIMs mapping images for Sample L (Au-Se-T_2-Hx). Top row contains mapping images of negative ions. Bottom row contains mapping images of positive ions.

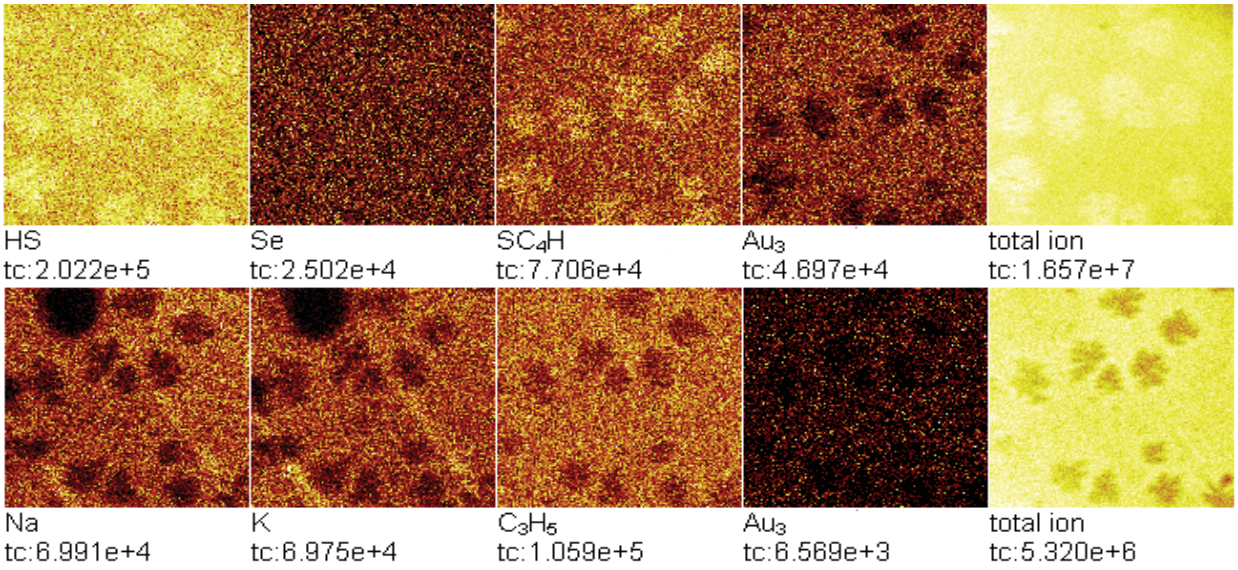

Chemical intensity maps produced from ToF-SIMS of TF-I (Au-S-Hx-T_2-Hx-SCN) are shown in Figure 29. Na^+ and K^+ maps contained similar features of high intensity, where HS^-, SC_4H^-, Au_3^-, and to a lower extent $C_3H_5^+$ and Au_3^+ posses features of lower intensity. It is assumed that these areas are small crystallites of alkai contamination. This sample was also subject to SEM/EDX and XPS prior to ToF-SIMS. Therefore it is possible that some features on fragment maps for this sample could be the result of damage from electron and X-ray irradiation, or simply damage from repeated handling or environmental exposure. This sample contained no selenium contamination.

Figure 29. ToF-SIMs mapping images for Sample I (Au-S-Hx-T_2-Hx-SCN). Top row contains mapping images of negative ions. Bottom row contains mapping images of positive ions.

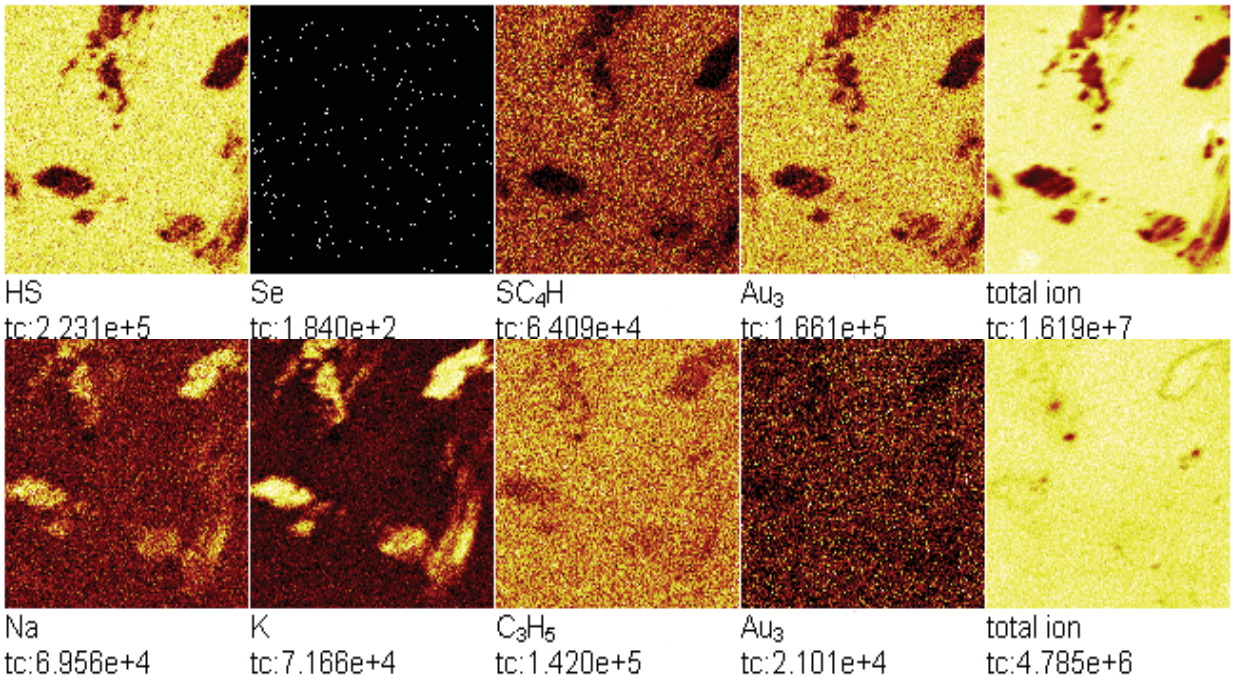

TF-N (Au-S-T_2-Hx in hexanes) and TF-M (Au-S-T_2-Hx in ethanol) are observed to produce very similar thin films. In both, K^+ and Na^+ crystallites were found. Thin film fragments appeared homogeneously located throughout the maps, indicating good surface coverage.

TF J (Au-S-Hx-T_2-Hx) and TF K (Au-Se-Hx-T_2-Hx) are also observed to produce similar thin films. The maps of the thin film fragments are observed to have a greater number of lower intensity features. This is attributed to a lower surface coverage than thin films N and M. Overall, TF L was the only TF analyzed with ToF-SIMs that was observed to contain thin film fragments multiple features of higher intensity, which may indicate larger organic crystallites on the surface.

First, HS^- was observed to be the thin film fragment with the highest intensity for most of the thin film samples, followed by $C_3H_5^-$ and SC_4H^+. This trend is assumed to be due to fragmentation processes that occur during ToF-SIMS. Overall, samples with only one alkyl substituent (N, M and L) produced organic fragments with higher intensities and greater homogeneity than their dialkyl counterparts. The trend extrapolated from this is that TFs bound to the surface through an aromatically substituted S or Se atom produce TFs with higher surface coverage than those bound through an alkyl substituent.

Chapter 6 - Summary and Conclusions

Assembly reactions were conducted using the 6 alkyl-substituted thio and selenocyanate bithiophene precursors, (**1ab**, **2ab**, and **3ab**,) with three different Au substrates. All 6 precursors were successfully assembled onto an amorphous Au electrode. This was confirmed by the observation of a significant decrease in the measured capacitance of the Au electrode after each assembly reaction. Thio and selenocyanate assembly was also observed to occur in hexanes, though no appreciable difference was found between identical precursors assembled in different solvents. Sputtered Au surfaces were found to be unsuitable substrates by SEM/EDX. This is consistent with Ciszek's observations that template stripped Au substrated did not produce as high quality TFs as the smoother Au(111) surface. Eight TFs were successfully synthesized on epitaxially grown Au. AFM was determined to be an inappropriate technique for characterizing thiolate TFs assembled from thio and selenocyanate precursors. This is consistent with Ciszek's observations. Organic crystallites were observed by SEM/EDX of TF-G (Au-Se-Hx-T_2-Hx-SeCN from ethanol) and TF-L (Au-Se-T_2-Hx). Six of the eight TFs assembled on epitaxially grown Au were characterized by XPS. In all, a signal of ~ 399 eV in the N 1s region was indicative of residual $(CN)_{ads}$ on the surface of all assemblies. For thiolate TFs, a signal in the S 2p3/2 region was indicative of an Au-S covalent bond present in the TF. For selenolate TFs, a doublet in the Se 3d region with a splitting of 0.86 eV was indicative of an Au-Se covalent bond.

Overall, this study has demonstrated that SCN and SeCN precursors can act as substitutes for SH and SeH precursors in the assembly of thiolate and selenolate TFs of substituted oligothiophenes. Specifically, taken together surface analysis results suggest that while the few crystallites found were fairly large, the TFs are typically thin and mostly uniform. This is contrasted with the larger crystallites found on AFM images of NCS-T_2-SCN and NCS-T_2-Br.

Chapter 7 - Future Work

Future work that complements this study would include the synthesis of TFs of NCSe-T_2-SeCN and NCS-T_2-SCN on epitaxially grown Au, the assembly of patterned TFs from thiocyanate precursors, and the use of more complex surface analysis techniques. TFs of the structure Au-Se-T_2-SCN and Au-S-T_2-SCN would complement the study and previous work by the MacKinnon group by demonstrating the effect of dithiol- or diselenocyation on the assembly process. ToF-SIMS analysis of thiolate or selenolate TFs without any alkyl groups substituted into the bithiophene core would further elucidate the effect of alkyl substituents on TF assembly. Patterned TFs, TFs containing more type of constituent molecule, assembled from thiocyanates or selenocyanates have not yet been reported and thus remain an area for exploration. It should also be noted that although T_2 is not itself a good semiconductor, it is a good model compound for larger oligothiophenes. The initial success reported in this study provides support for future TF assembly using thio- or selenocyanates of larger oligothiophenes, T_3 to T_8.

Lastly, few characterization techniques have been used in the characterization of TFs from thiocyanate precursors, especially those of oligothiophenes. The extension of this list to include diffraction techniques like XRD and LEEDS would allow for the determination of characteristics like orientation of molecules on the surface and degree of order.

Chapter 8 - Experimental

8.1 General synthetic and instrumental details

Names of chemical suppliers and details of purification of starting materials are described in Appendix 2. Unless otherwise indicated all organic reactions were conducted under an inert nitrogen atmosphere following standard Schlenk techniques using a double manifold vacuum line with a savant VLP200 series rotary vacuum pump. Infrared (IR) absorption spectra were recorded neat or as a nujol mull on a Nicolet 380 FT-IR spectrometer; vibrational frequencies are reported as wavenumbers (cm^{-1}) with an instrumental resolution of 1 cm^{-1}. Magnetic resonance spectra (NMR) were obtained using a Varian Unity Inova 500 spectrometer at the Lakehead University Instrument Laboratory (LUIL). All spectra were collected at room temperature and chemical shifts were internally referenced to tetramethylsilane (TMS) and are reported in parts per million (ppm). Mass spectra were collected in the LUIL through direct injection into a Bruker Amazon Ion Trap mass spectrometer using HPLC grade acetonitrile as a solvent. Melting points were measured on an IA9000 Series Melting Point Apparatus from Electrothermal and are uncorrected.

8.2 Organic syntheses

Preparation of 2,2'-bithiophene, ***T_2***

This compound was prepared following a literature route.[20] Mg turnings (4.86 g, 199.55 mmol) were added to a 500 mL 3-necked round-bottomed flask equipped with a pressure-equalizing dropping funnel, rubber septum, gas nozzle, and stir bar. With the flask under vacuum, Mg turnings and glass walls were heated with a heat gun to drive off water. After the assembled apparatus was cooled to room temperature and back filled with $N_{2\,(g)}$ dry Et_2O (~15 mL) was added via syringe to the 3-necked flask. A mixture of 2-bromothiophene (27.03 g, 162.54 mmol) in dry Et_2O (~75 mL) was added dropwise after first initiating the reaction by quick addition of several millilitres of the solution plus a crystal of I_2. An ice water bath was used to maintain a controlled reflux during the addition. The resulting mixture was stirred for 3

hours under $N_{2\,(g)}$ to generate the Grignard reagent TMgBr. During this time, a second mixture was prepared. Ni(dppp)Cl_2 (0.255 g, 0.487 mmol, 0.33 %) was added to a 500 mL 3-necked flask equipped with a gas nozzle, rubber septum, glass stopper, and stir bar. The oven-dried glassware was evacuated and purged with N_2 (g) over five cycles and allowed to cool to room temperature. To this flask, dry Et_2O (~100 mL) and 2-bromothiophene (25.1 g, 147.2 mmol) were added sequentially via syringe. Both mixtures were cooled on an ice bath for 10 minutes. Next, the Grignard reagent mixture was cannulated into the catalyst mixture keeping both mixtures cooled on ice baths. The opaque, black mixture was stirred overnight at room temperature. After this time, the mixture was added to 150 mL of a saturated NH_4Cl solution and stirred for 30 minutes, followed by extraction into Et_2O. Combined organic fractions were dried over $MgSO_4$. The solvent was removed via rotary evaporation to obtain a brown liquid and brown crystalline solid. The product was further purified via fractional distillation to obtain a clear, colourless, crystalline solid. (15.5 g, 60.6 %). Mp (31-33°C). ^{1}H NMR (500 MHz, $CDCl_3$, δ (ppm), J (Hz)): δ 7.24-7.18 (m, 4H), 7.01 (m, 2H).

Preparation of 1-(2,2'-bithiophen-5-yl)hexan-1-one, ***$T_2C(O)Pn$***

This compound was prepared via a literature route.[23] 2,2'-bithiophene (8.76 g, 52.6 mmol) was added to an oven-dried 250 mL 3-necked round-bottomed flask, which was evacuated and purged with $N_{2\,(g)}$ over five cycles. Dry benzene (~60 mL) and hexanoyl chloride (12.8 mL, 12.3 g, 91.6 mmol) were added via syringe. After the resulting clear, colourless solution was cooled on an ice bath for 10 minutes, $SnCl_4$ (6.6 mL, 14.7 g, 56.4 mmol) was added dropwise via syringe. The resulting black, opaque mixture was stirred on an ice bath for 30 minutes. The mixture was poured onto ice (~200 mL), stirred for 20 minutes, and CH_2Cl_2 (~200 mL) was added. The organic layer was washed with distilled H_2O (3× ~30 mL) and a saturated solution of $NaHCO_3$ (3×~30 mL), and then dried over $MgSO_4$. Solvent was removed via rotary evaporation to yield a chalky, yellow solid. The product was further purified via column chromatography (SiO_2 gel) using a 4:1 solvent system of hexanes:CH_2Cl_2 to yield a bright yellow, chalky solid (8.8059 g, 63.2 %). Mp (76.2-78.5 °C). ^{1}H NMR (500 MHz, $CDCl_3$, δ (ppm), J (Hz)): δ 7.60 (d, *J*=4.0Hz, 1H), 7.32

(d, *J*=2.5Hz, 2H), 7.17 (d, *J* = 4.0Hz, 1H), 7.07 (d, *J* = 8.5Hz, 1H), 2.88 (t, J_{AC} = 15 Hz, J_{AB} = 7.5Hz, 2H), 1.76 (m, 2H), 1.37 (m, 4H), 0.95 (t, J_{AC} = 13.5, J_{AB} = 6.5, 3H). IR: 1654cm^{-1} (C=O stretch). Mass spectrum: m/z 567 ([2M+K]$^+$, 33.6 %), 551.1 ([2M+Na]$^+$, 100 %), 287 ([M+Na]$^+$, 15.9 %), 303 ([M+K]$^+$, 35.4 %), 265.1 ([M+H]$^+$, 5.3 %).

Preparation of 5-hexyl-2,2'-bithiophene, ***T_2Hx***

This compound was synthesized via the Huang-Minlon modification of the Wolff-Kishner reaction.[24] A 250 mL 3-necked round-bottomed flask was equipped with a stir bar, glass stopper, rubber septum and Dean-Stark trap. The Dean-Stark trap was capped with a reflux condenser and a gas nozzle. Diethylene glycol (~70 mL) was added to the flask, followed by $T_2C(O)Pn$ (4.65 g, 17.6 mmol) and powdered KOH (3.8 g, 68 mmol). To this mixture, hydrazine monohydrate (0.9 mL, 0.9 g, 18.1 mmol, 98%) was added via syringe. The resulting mixture was refluxed under $N_{2\,(g)}$ until liquid formation in the trap subsided (~2 h). After this time, the Dean-Stark trap was replaced with a reflux condenser and the clear, orange solution was refluxed for another 4 hours. Once cooled to room temperature, the mixture was diluted in the 3-necked flask with distilled water (~100 mL), poured into HCl (6 N, 300 mL) and stirred for 30 minutes. The aqueous layer was extracted with Et_2O (4×~50 mL). The organic fractions were combined, dried over $MgSO_4$, and residual solvent was removed via rotary evaporation to yield a translucent orange oil. This product was further purified via column chromatography (SiO_2 gel) using hexanes as eluent to yield a clear, yellow liquid (6.64 g, 82.6 %). ^{1}H NMR (500 MHz, $CDCl_3$, δ (ppm), J (Hz)): δ 7.16 (d, *J* = 5.0Hz, 1H), 7.01 (d, *J* = 3.5Hz, 1H), 6.99 (m, 2H), 6.68 (d, *J* = 5.0Hz, 1H), 2.80 (t, *J* = 7.5Hz, 2H), 1.69 (m, 2H), 1.32 (m, 6H), 0.90 (t, J_{AC} = 13.5, J_{AB} = 6.5 Hz, 3H). Mass spectrum: m/z 289.0 ([M+K]$^+$, 79.1 %), 273.1 ([M+Na]$^+$, 100 %) , 251.0 ([M+H]$^+$, 45.8 %).

Preparation of 5,5'-bis(6-bromohexyl)-2,2'-bithiophene, ***Br-Hx-T$_2$-Hx-Br***

This reaction was adapted from a literature procedure.[26] T_2 (2.4618 g, 14.8 mmol) was added to an oven-dried 500 mL 3-necked round-bottomed flask equipped with a gas nozzle, stir bar, thermometer and rubber septum The flask was evacuated and purged with $N_{2(g)}$ over five cycles. Dry hexanes (100 mL) and TMEDA (5.4 mL, 4.2 g, 36.1 mmol) were added sequentially via syringe. The resulting solution was cooled to -60 ˚C with a $N_{2\,(l)}$/acetone bath and nBuLi (30 mL, 30 mmol, 1.0 M) was added dropwise via syringe. The resulting mixture was allowed to warm to room temperature and refluxed for 4 hours. After this time, 1,6-dibromohexane (4.6 mL, 7.3 g, 29.9 mmol) was added to the refluxing solution dropwise via syringe. The resulting solution was refluxed for another 20 hours. After this time, the solution was cooled to room temperature, poured into a saturated solution of $NaHCO_3$ (~200 mL) and stirred for 20 minutes. The mixture was poured into a 1 L separatory funnel and the aqueous layer was extracted with CH_2Cl_2 (5×100 mL). The combined organic layers were washed with a saturated solution of $NaHCO_3$ (4×50 mL) and distilled water (4×50 mL), and dried over $MgSO_4$. Solvent was evaporated via rotary evaporation to yield a yellow, chalky solid. The solid was purified by column chromatography (SiO_2 gel) using an 80:20 solvent mixture of hexanes and CH_2Cl_2. The product containing band was rotovapped to yield a yellow solid. This purified solid was again purified by column chromatography (SiO_2 gel) using a solvent mixture of hexanes:CH_2Cl_2 (9:1) to yield dull yellow solid (0.4246 g, 5.8 %). Mp (86.5-87.1 °C) ^{1}H NMR (500 MHz, $CDCl_3$, δ (ppm), J (Hz)): δ 6.90 (d, J = 3.5 Hz, 2H), 6.65 (d, J = 3.5 Hz, 2H), 3.42 (t, J_{AC} = 13.5 Hz, J_{AB} = 6.5 Hz, 4H), 2.79 (t, J_{AC} = 14.5 Hz, J_{AB} = 7.5 Hz, 4H), 1.88 (m, 4H), 1.70 (m, 4H), 1.49 - 1.40 (m, 8H). ^{13}C NMR (500 MHz, $CDCl_3$, δ (ppm), J (Hz)): 144.26 (C, 2C), 135.4 (C, 2C), 124.7 (C, 2C), 122.7 (CH, 2C), 33.9 (CH, 2C), 32.7 (CH_2, 2C), 31.40 (CH_2, 2C), 30.0 (CH_2, 2C), 28.1 (CH_2, 2C), 27.9 (CH_2, 2C).

Preparation of 5-(6-bromohexyl)-5'-hexyl-2,2'-bithiophene, ***Hx-T$_2$-Hx-Br***

An oven-dried 500 mL 3-necked round-bottomed flask was equipped with a stir bar, gas nozzle, thermometer adapter, and rubber septum. The flask was evacuated and purged with $N_{2\,(g)}$ over five

cycles. To this flask, dry THF (~70 mL), T_2Hx (3.08 g, 12.3 mmol) and TMEDA (1.74 mL, 1.35 g, 11.6 mmol) were added via syringe. The resulting solution was cooled to -78 ˚C with a $N_{2\,(l)}$/acetone bath. tert-BuLi (6.85 mL, 11.6 mmol, 1.7M) was added dropwise via syringe. The opaque, dark purple solution was stirred for 1 hour between -78 ˚C and -50 ˚C. A second oven-dried 500 mL 3-necked round-bottomed flask was evacuated and purged with $N_{2\,(g)}$ over five cycles. To the second flask, dry THF (~60 mL) and 1,6-dibromohexane (2.84 g, 1.79 mL, 11.6 mmol) were added via syringe. Both flasks were cooled to -78 ˚C with an $N_{2(l)}$/acetone bath. At this temperature, the T_2Hx solution was cannulated into the 1,6-dibromohexane solution. The resulting solution was allowed to warm to room temperature and stirred overnight. After this time, the flask was cooled on an ice bath and HCl (2 M, ~100 mL) was added slowly to quench the reaction. The mixture was diluted with Et_2O (~200 mL) and transferred to a 1L separatory funnel. The organic layer was washed with $NaHCO_3$ (3×40 mL) and NaCl solution (3×40 mL). The organic layer was dried over $MgSO_4$ and rotovapped at 30 ˚C to obtain a green oil. The product was purified twice via column chromatography (SiO_2 gel) using 100 % hexanes as eluent; a yellow oil was obtained. The oil was left in the fridge over several days, during which a yellow solid crystallized out of the oil. The mixture was Buchner filtered and washed with ethanol to yield a bright yellow solid (0.5905 g, 12.6 %). Mp (41.2-43.6 °C) ^{1}H NMR (500MHz, $CDCl_3$, δ(ppm), J(Hz)): δ 6.89 (d, J = 2Hz, 2H), 6.45 (d, J = 1Hz, 2H), 3.42 (t, J_{AC}= 12 Hz, J_{AB} = 4.5 Hz, 2H), 2.79 (m, 4H), 1.89 (m, 2H), 1.67 (m, 4H), 1.54 - 1.30 (m, 10H), 0.88 (t, J_{AC} = 14 Hz, J_{AB} = 6.5 Hz, 3H). ^{13}C NMR (500 MHz, $CDCl_3$, δ (ppm), J (Hz)): 144.77 (C, 1C), 144.16 (C, 1C), 135.46 (C, 1C), 135.20 (C, 1C), 124.71 (CH, 1C), 124.57 (CH, 1C), 122.64 (CH, 1C), 122.58 (CH, 1C), 33.92 (CH_2, 1C), 32.66 (CH_2, 1C), 31.58 (CH_2, 2C), 31.35 (CH_2, 1C), 30.15 (CH_2, 1C), 29.98 (CH_2, 1C), 28.76 (CH_2, 1C), 28.12 (CH_2, 1C), 27.88 (CH_2, 1C), 22.58 (CH_2, 1C), 14.10 (CH_3, 1C).

Preparation of 5,5'-bis(6-thiocyanohexyl)-2,2-bithiophene, ***NCS-Hx-T_2-Hx-SCN***

This reaction was adapted from a literature preparation.[25] Br-Hx-T_2-Hx-Br (0.0703 g, 0.1428 mmol), 18-crown-6 (0.0137 g, 0.05183 mmol), KSCN (0.1020 g, 1.95 mmol), and CH_3CN (30 mL) were

combined in a 100mL round-bottomed flask equipped with a reflux condenser and stir bar. The resulting mixture was refluxed for 17 hours under $N_{2\,(g)}$. After this time, the pale yellow solution was cooled to room-temperature. Et_2O (~100 mL) was added to the flask and the mixture was transferred to a separatory funnel. The organic layer was washed with distilled water (4×25 mL) and dried over $MgSO_4$. Solvent was removed via rotary evaporation to yield a yellow solid (0.0597 g, 0.1420 mmol, 99.4 %). Mp (73.7-74.5 °C). IR: 2149.56 cm^{-1} (C≡N stretch). Mass spectrum: m/z 487 ($[M+K]^+$, 14.5 %), 471 ($[M+Na]^+$, 100 %), 449.1 ($[M+H]^+$, 4.3 %). ^1H NMR (500MHz, $CDCl_3$, δ(ppm), J(Hz)): δ 6.98 (d, J = 4Hz, 2H), 6.60 (d, J = 3.5, 2H), 2.96 (t, J_{AC} = 14.5 Hz, J_{AB} = 7.5 4H), 2.81 (m, 4H), 1.87 (m, 4H), 1.73 (m, 4H), 1.52 – 1.34 (m, 8H). ^{13}C NMR (500 MHz, $CDCl_3$, δ (ppm), J (Hz)): 144.04 (C, 2C), 135.39 (C, 2C), 124.82 (CH, 2C), 122.70 (CH, 2C), 112.36 (CH, 2C), 33.96 (CH_2, 2C), 31.25 (CH_2, 2C), 29.77 (CH_2, 2C), 28.20 (CH_2, 2C), 27.68 (CH_2, 2C).

Preparation of 5,5'-bis(6-selenocyanohexyl)-2,2'-bithiophene, ***NCSe-Hx-T$_2$-Hx-SeCN***

This reaction was adapted from a literature preparation.[25] Br-Hx-T_2-Hx-Br (0.1269 g, 0.2577 mmol), 18-crown-6 (0.0168 g, 0.06356 mmol), KSeCN (0.27 g, 1.874 mmol), and CH_3CN (30 mL) were combined in a 100 mL round-bottomed flask with a stir bar. A reflux condenser was attached and the mixture was refluxed for 17 hours under $N_{2\,(g)}$. After this time, the pale yellow solution was cooled to room-temperature. Et_2O (~100 mL) was added to the flask and the mixture was transferred to a separatory funnel. The organic layer was washed with distilled water (4×25 mL) and dried over $MgSO_4$. Solvent was removed via rotary evaporation to yield a yellow solid (0.0850 g, 0.1567 mmol, 60.8 %). Mp (68.8-71.3 °C) IR: 2150.54 cm^{-1} (C≡N stretch). ^1H NMR (500MHz, $CDCl_3$, δ(ppm), J(Hz)): δ 6.90 (d, *J* = 4Hz, 2H), 6.66 (d, *J* = 3.5 Hz, 2H), 3.06 (t, J_{AC} = 14.5, J_{AB} = 7.5 Hz, 4H), 2.81 (t, J_{AC} = 14.5, J_{AB} = 7 Hz, 4H), 1.94 (m, 4H), 1.73 (m, 4H), 1.51 – 1.43 (m, 8H).

^{13}C NMR (500 MHz, $CDCl_3$, δ (ppm), J (Hz)): 144.07 (C, 2C), 135.39 (C, 2C), 124.82 (CH, 2C), 122.70 (CH, 2C), 101.53 (CN, 2C), 31.23 (CH_2, 2C), 30.71 (CH_2, 2C), 29.94 (CH_2, 2C), 29.50 (CH_2, 2C), 29.50 (CH_2, 2C), 28.83 (CH_2, 2C), 28.15 (CH_2, 2C).

Preparation of 5-hexyl-5'-(6-thiocyanohexyl)-2,2'-bithiophene, ***NCS-Hx-T$_2$-Hx***

This reaction was adapted from a literature route.[25] Br-Hx-T_2Hx (0.606 g, 1.465 mmol), 18-crown-6 (0.1376 g, 0.521 mmol), KSCN (0.6408 g, 6059 mmol), and CH_3CN (40 mL) were combined in a 100 mL round bottom flask equipped with a stir bar and reflux condenser. This mixture was refluxed for 16h under $N_{2\,(g)}$. After this time, the mixture was cooled to room temperature and diluted with Et_2O (100 mL). The combined organic layers were washed with distilled water and dried over $MgSO_4$. Solvent was removed via rotary evaporation to yield a pale yellow solid (0.3867 g, 67.4 %). Mp (36.4-37.1 °C) IR: 2151.02 cm^{-1} (C≡N stretch). Mass spectrum: m/z 430.1 ($[M+K]^+$, 31.4 %), 414.1 ($[M+Na]^+$, 100 %), 391.2 (M^+, 2.9 %), 249.1 ($[M-C_6H_{12}SCN]^+$, 2.9 %), 222.9 ($[H+(SC_4H_2)(C_6H_{12})(SCN)]^+$, 21.9 %). ^{1}H NMR (500MHz, $CDCl_3$, δ(ppm), J(Hz)): δ 6.90 (d, J = 3.5 Hz, 2H), 6.65 (d, J = 3.5Hz, 2H), 2.95 (t, J_{AC} = 14.5 Hz, J_{AB} = 7 Hz, 2H), 2.80 (m, 4H), 1.85 (m, 2H), 1.72 (m, 4H), 1.55-1.25 (m, 10H), 0.90 (t, J_{AC} = 13 Hz, J_{AB} = 7 Hz, 3H). ^{13}C NMR (500 MHz, $CDCl_3$, δ (ppm), J (Hz)): 144.81 (C, 1C), 143.90 (C, 1C), 135.54 (C, 1C), 135.14 (C, 1C), 124.79 (CH, 1C), 124.58 (CH, 1C), 122.67 (CH, 1C), 122.58 (CH, 1C), 112.36 (CN, 1C), 33.96 (CH_2, 2C), 31.58 (CH_2, 2C), 31.25 (CH_2, 1C), 30.14 (CH_2, 1C), 29.93 (CH_2, 1C), 29.77 (CH_2, 1C), 28.20 (CH_2,1C), 27.68 (CH_2, 1C), 14.09 (CH_3, 1C).

Preparation of 5-hexyl,5'-(6-thiocyanohexyl)-2,2'-bithiophene, ***NCSe-Hx-T$_2$-Hx***

This reaction was adapted from the literature route.[25] Br-Hx-T_2Hx (0.6040 g, 1.46 mmol), 18-crown-6 (0.1373 g, 0.520 mmol), KSCN (0.95 g, 0.66 mmol), and CH_3CN (40 mL) were combined in a 100 mL round bottom flask and reflux condenser was attached. This mixture was refluxed for 16 h under $N_{2\,(g)}$. After this time, the mixture was cooled to room temperature and diluted with Et_2O (100 mL). The

combined organic layers were washed with distilled water and dried over $MgSO_4$. Solvent was removed via rotary evaporation to yield a pale yellow solid (0.5384 g, 84.0 %). IR: 2149.90 cm^{-1} (C≡N stretch) ^1H NMR (500MHz, $CDCl_3$, δ(ppm), J(Hz)): δ 6.90 (d, J = 3.5 Hz, 2H), 6.65 (d, J = 4.5 Hz, 2H), 3.06 (t, J_{AC} = 14.5 Hz, J_{AB} = 7 Hz, 2H), 2.80 (m, 4H), 1.94 (m, 2H), 1.71 (m, 4H), 1.50 – 1.29 (m, 10H), 0.90 (t, J_{AC} = 13.5 Hz, J_{AB} = 6.5 Hz, 3H). ^{13}C NMR (500 MHz, $CDCl_3$, δ (ppm), J (Hz)): 144.82 (C, 1C), 143.94 (C, 1C), 135.53 (C, 1C), 135.15 (C, 1C), 124.79 (C, 1C), 124.58 (C, 1C), 122.67 (C, 1C), 122.59 (C, 1C), 101.54 (CN, 1C), 31.58 (CH_2, 2C), 31.27 (CH_2, 1C), 31.27 (CH_2, 1C), 30.71 (CH_2, 1C), 30.15 (CH_2, 1C), 29.94 (CH_2, 1C), 29.51 (CH_2, 1C), 28.84 (CH_2, 1C), 28.76 (CH_2, 1C), 28.16 (CH_2, 1C), 22.58 (CH_2, 1C), 14.10 (CH_3, 1C).

Preparation of 5-hexyl-2,2'-bithiophene-5'-thiocarbonitrile, ***NCS-T_2-Hx***

This reaction was adapted from the literature route.[25] A 500 mL 3-necked round-bottomed flask was equipped with a rubber septum, gas nozzle, stir bar, and 60 mL constant-pressure dropping funnel. KSCN (4.6523 g, 47.89 mmol) was added and the flask and the apparatus was evacuated and purged with $N_{2\,(g)}$ over several cycles. Dry, distilled methanol (180 mL) and T_2Hx (3.024 g, 12.07 mmol) were added to the flask sequentially via syringe. To the dropping funnel, dry, distilled methanol (40 mL) and $Br_{2\,(l)}$ (4.1 g, 25.66 mmol, 1.3 mL) were added via syringe. The flask was covered with tin foil and all light was extinguished in the area around the reaction apparatus. The flask was cooled on an ice bath under $N_{2\,(g)}$ for 10 minutes. In the dark, the $Br_{2\,(l)}$/methanol solution was added to the flask dropwise through the dropping funnel. The ice bath was removed after the addition was complete and the mixture was allow to stir in the dark, at room temperature, for 2 hours. After this time, the solution was poured into a beaker containing an equal volume of ice and d.w. (~220 mL) and stirred for 1 hour. The mixture was poured into a 1 L separatory funnel and the organic layer was drained off. The aqueous layer was extracted with CH_2Cl_2 (3×100 mL). Combined organic layers were dried over $MgSO_4$ and rotovapped at 30 °C to yield an oil with red and orange phases. The product was purified through column chromatography (SiO_2 gel)

using solvent systems of hexanes and CH_2Cl_2. The product band eluted from the column when hexanes:CH_2Cl_2 ratios of 80:20 and 60:40 were employed. Mp (41.2-44.8 °C) IR: 2156.87cm^{-1} (C≡N stretch). Mass spectrum: m/z 325.2 ($[M+NH_4]^+$, 100 %). ^{1}H NMR (500MHz, $CDCl_3$, δ(ppm), J(Hz)): δ 7.42 (d, J = 4 Hz, 1H), 7.09 (m, 2H), 6.83 (d, J = 3.5 Hz, 1H), 2.84 (m, 2H), 1.68 (m, 2H), 1.39 (m, 6H), 0.90 (s, 3H). ^{13}C NMR (500 MHz, $CDCl_3$, δ (ppm), J (Hz)): 148.06 (C, 1C), 141.24 (C, 1C), 137.84 (C, 1C), 129.43 (C, 1C), 128.99 (CH, 1C), 127.90 (CH, 1C), 125.39 (CH, 1C), 109.71 (CH, 1C), 31.43 (CH_2, 1C), 31.06 (CH_2, 1C), 30.13 (CH_2, 1C), 28.66 (CH_2, 1C), 22.51 (CH_2, 1C), 14.06 (CH_3, 1C).

Preparation of 5-hexyl-2,2'-bithiophene-5'-selenocarbonitrile, ***NCSe-T$_2$-Hx***

This reaction was adapted from the literature route.[25] A 500 mL 3-necked round-bottomed flask was equipped with a rubber septum, gas nozzle, stir bar, and 60 mL constant-pressure dropping funnel. KSeCN (5.05 g, 35.1 mmol) was added and the flask and the apparatus was evacuated and purged with $N_{2(g)}$ over several cycles. Dry, distilled methanol (150 mL) and T_2Hx (2.2 g, 8.8 mmol) were added to the flask sequentially via syringe. To the dropping funnel, dry, distilled methanol (40 mL) and $Br_{2\,(l)}$ (2.75 g, 17.2 mmol, 0.86 mL) were added via syringe. The flask was covered with tin foil and all light was extinguished in the area around the reaction apparatus. The flask was cooled on an ice bath under $N_{2\,(g)}$. In the dark, the $Br_{2\,(l)}$/methanol solution was added to the flask dropwise through the dropping funnel. The ice bath was removed after the addition was complete and the mixture was allow to stir in the dark, at room temperature, for 2 hours. After this time, the solution was poured into a beaker containing an equal volume of ice and d.w. and stirred for 1 hour. The mixture was poured into a 1 L separatory funnel and the organic layer was drained off. The aqueous layer was extracted with CH_2Cl_2 (5×100 mL). Combined organic layers were dried over $MgSO_4$ and rotovapped at 30 °C to yield a red oil. The product was purified through column chromatography (SiO_2 gel) using hexane and CH_2Cl_2 solvent systems of 50:50 and 60:40, respectively. ^{1}H NMR (500MHz, $CDCl_3$, δ(ppm), J(Hz)): δ 7.34 (d, J = 10Hz, 1H), 7.05 (m, 2H), 6.17 (d, J = 3.5, 1H), 2.82 (t, J_{AC} = 15 Hz, J_{AB} = 7.5 Hz, 2H), 1.71 (m, 2H), 1.39 (m, 6H), 0.95 (t, J_{AC}

= 11.5 Hz, J_{AB} = 6 Hz, 3H). IR: 2152 cm^{-1}, 2219 cm^{-1} (C≡N stretch). ^{13}C NMR (500 MHz, $CDCl_3$, δ (ppm), J (Hz)): 147.47 (C, 1C), 147.20 (C, 1C), 139.96 (C, 1C), 132.74 (C, 1C), 125.11 (CH, 1C), 125.02 (CH, 1C), 123.75 (CH, 1C), 109.34 (CH, 1C), 100.89 (CN, 1C), 31.60 (CH_2, 1C), 31.53 (CH_2, 1C), 30.17 (CH_2, 1C), 28.72 (CH_2, 1C), 22.56 (CH_2, 1C), 14.09 (CH_3, 1C).

8.3 Capacitance Measurements

Preparation of thiocyanate and selenocyantes samples for capacitance measurements

In order to conduct the assembly reaction a saturated solution of a thiocyanate or selenocyanate was first prepared. Dry, degassed ethanol (8 mL) was added to a 50 mL round-bottomed flask. The thio- or selenocyante (<30 mg) was added to the flask, which was stirred until no further dissolution was observed. After any remaining solid was allowed to settle to the bottom of the flask, the solution was transferred via Pasteur pipette to a glass vial and capped.

Self-assembly reaction and capacitance measurements

Prior to beginning capacitance measurements, an amorphous gold electrode (Figure 1) was electropolished and flame-annealed. Next, the bare electrode was assembled into an in-house-built electrochemical cell as the working electrode. Its capacitance was measured and checked with literature values. The electrode was then removed from the electrochemical cell and immersed in a prepared saturated solution of one of the thio- or selenocyanates for 24 hours at room temperature. After this time, the electrode was removed from the solution, rinsed with dry, degassed EtOH (~20 mL) and re-assembled into the same electrochemical cell as the working electrode.

In this cell, used for all capacitance measurements, the counter electrode was a platinum coil, which was flame-annealed prior to each experiment. The reference electrode used was a Ag/AgCl (3 M KCl) electrode. The electrolyte medium was 0.05 M $KClO_4$ in pure water and was deaerated with ultra-pure argon (99.99 %). All capacitance experiments were conducted at room temperature (22 ± 2 °C) and

argon was passed over top of the solution during each experiment. In all experiments, a VoltaLab 40 Potentiostat Model PGZ 301 was used with VoltaLab Version 5.1 software. The potential (E/V vs. SCE) was applied from a bias of -0.5 to +0.5 V, using a modulation potential of 10 mV and a frequency of 2.

Figure 30. Electrodes assembled into 'in-house built' electrochemical cell used in capacitance experiments. Left: Ag/AgCl (3M KCl); Center: Platinum Coil; Right: Amorphous Au electrode

8.4 Assembly reactions on sputtered Au substrates

Preparation of Sputtered substrates

To prepare sputtered gold substrates, titanium plates (~1 cm x 1.5 cm) were etched by immersion in HCl (15 %) for 10 minutes. The etched plates were sputtered with an Ernest F. Fullam Inc Sputter Coater using a 99.99 % pure Au target. Bare Ti plates and the resulting sputtered gold substrates are shown in Figure 31.

Figure 31. Titatnium substrates throughout fabrication process. A) Bare Ti substrate. B) Ti substrate after etching in HCL (15 %). C) Ti substrate after sputtering with Au.

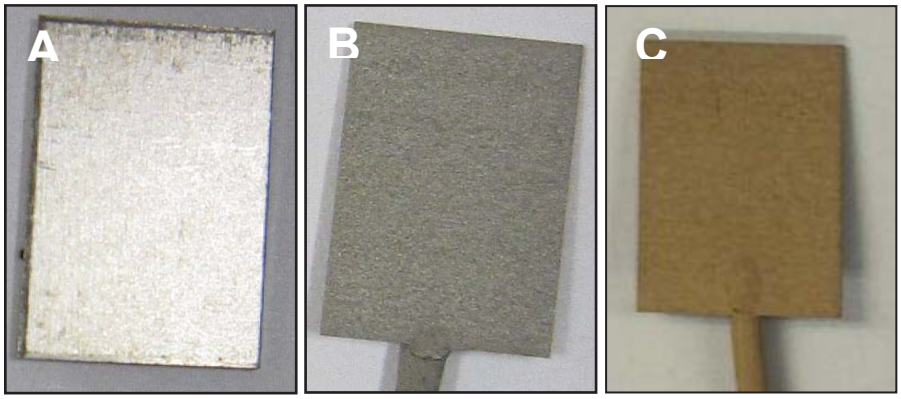

Self-Assembly Reactions on Sputtered Au Substrates

Sputtered gold substrates were immersed in a saturated thio- or selenocyante solution at room temperature for 20 hours. A number of reaction conditions were employed. For substrates A,B and C, the same ethanolic solutions used for 24 h Cp measurements were used for this reaction. Specifically, this means an 'aged' thio-/selenosubstrate solution was used, ie. a solution that had previously had a gold substrate immersed in it. For substrate D, a fresh ethanolic solution was prepared in the same manner as used for 24h Cp experiments. An identical procedure was also used to prepare a fresh solution of substrate E in hexanes. For substrate F, the same procedure was used to prepare a fresh ethanolic solution. However, the solution was transferred to a 25mL round-bottomed flask equipped with a gas nozzle and reflux condenser. The solution was heated under $N_{2\,(g)}$ for 20 hours between 30 and 60 °C using a water bath. After 20 hours, each plate was removed, washed with dry, degassed EtOH (~50 mL) and dried under an $N_{2\,(g)}$ stream for 1h.

8.5 Thin film synthesis on epitaxially grown Au substrates

Synthesis of epitaxially grown Au substrates

A thin film of gold was epitaxially grown on a mica substrate in a vacuum chamber. The thin film was cut into eight individual substrates each was annealed with a butane flame on July 15th, 2014. The existence of Au(111) terraces on the substrates was not confirmed by STM prior to use in self-assembly reactions.

Assembly Reaction

1 mM solutions of NCS-T_2-HX, NCSe-T_2-Hx, NCSe-Hx-T_2-Hx-SeCN, NCS-Hx-T_2-Hx-SCN, NCS-Hx-T_2-Hx, and NCSe-Hx-T_2-Hx in dry hexanes or dry distilled ethanol were prepared in individual round-bottomed flasks. A freshly prepared gold-sputtered Titanium plate was immersed in the solution for 16 hours. After 16 hours, the thiocyanate or selenocyanate solution was pipetted into a clean, dry septum-capped vial. The sealed vials were heated at 50 °C in a drying oven for 24 hours. After this time the substrates were removed from solution, rinsed with dry hexanes or dry distilled ethanol (~20 mL), and dried under a stream of $N_{2\,(g)}$ for several hours.

8.6 Analysis of TFs on epitaxially grown Au

SEM/EDX images and data were collected at Lakehead University using a Hitachi Su-70 Schottky Field Emission microscope equipped with an Oxford Aztec 80 mm/124 eV EDX.

Atomic force microscopy (AFM) at Lakehead University was conducted using a PicoSPM instrument from Aglient Technologies. Images were taken with the tip in contact mode under ambient conditions.

X-ray photoelectron spectroscopy was also used to analyze 6 of the thin films on epitaxially grown gold. Analysis was conducted using a Kratos Axis Ultra X-ray photoelectron spectrometer at the Surface

Western laboratory at the University of Western Ontario. Using this instrument, the surface was probed from a depth of 7 to 10 nanometres. Depending on the element, detection limits of 0.1 to 0.5 atomic percent were obtained. For survey scan analyses, an analysis area of 300 x 700 micron and a pass energy of 160 eV were employed. High resolution scans were carried out using an analysis area of 300 x 700 microns and a pass energy of 20 eV. High resolution spectra were charge corrected to the Au 4f7/2 line set to 83.95 eV.

ToF-SIMs image characteriation was conducted at Surface Science Western by Dr. Heng-Yong Nie using an ION-TOF ToF-SIMS 5 instrument from GmBH. The ion beam generated by the primary ion column was a Bi_3^+ cluster beam that was pulsed at 10 kHz. The ion beam was bombarded onto the surface and generated positive or negative secondary ions which were entrained and detected by a reflection time-of-flight analyzer. Within each 100 μs, this allowed for the detection of ion fragments up to 900 m/z. Sample charging was neutralized through the use of a pulsed, low energy electron flood. Positive and negative ion spectra were collected from a 500 μm^2 area using a raster scan pattern of 128 x 128. From these spectra, chemical maps of HS^-, Se^-, SC_4H^-, Au_3^-, Na^+, K^+, $C_3H_5^+$, and Au_3^+ were generated by plotting the intensity of a selected fragment peak against the pixels.

References

1. Vericat, C.; Vela, M.E.; Benitez, G.; Carro P.; Salvarezza, R.C.; *Chem. Soc. Rev.*, **2010**, *39*, 1805-1834.

2. Ciszek, J.W.; Tour, J.M. *Chem. Mater.* **2005**, *17*, 5684 – 5690.

3. Lamb, B.M.; Barrett, D.G.; Westcott, N.P.; Yousaf, M.N.; *Langmuir*., **2008**, *24*, 8885-8889.

4. Brown, T.T.; Zorabel, M.L.; Liu, K.; Hardin, S.; Li, J.R.; Rupnik, K.; Garno, J.C.; *J. Lab. Autom*. **2011**, *16*, 112-125.

5. Bonanni, B.; Bizzarri, A.R.; Cannistraro, S.; *J. Phys. Chem. B.*, **2006**, *110*, 145774-14580.

6. Ciszek, J.W.; Stewart, M.P.; Tour, J.M.; *J. Am. Chem. Soc*., **2004**, *126*, 13172-13173.

7. Dreesen, L.; Volcke, C.; Sartenager, Y.; Peremans, A.; Thiry, P.A.; Humbert, C.; Grugier, J.; Marchand-Brynaert, J.; *Sur. Sci.*, **2006**, *600*, 4052-4057.

8. Choi, Y.; Jeong, Y.; Chung, H.; Ito, E.; Hara, M.; Noh, J; *Langmuir*, **2008**, *24*, 91-96.

9. Shen, C.; Buck, M.; Wilton-Ely, J.D.E.T.; Weidner, T.; Zharnikov, M.; *Langmuir*, **2008**, *24*, 6609-6615.

10. Lee, S.Y.; Choi, Y.; Ito, E.; Hara, M.; Lee, H.; Noh, J.; *Phys. Chem. Chem. Phys*., **2013**, *15*, 3609-3617.

11. Morgan, I.S.; D'Aleo, D.N.; Hudolin, M.L.; Chen, A.; Assoud, A.; Jenkins, H.A.; MacKinnon, C.D.; *J. Mater. Chem*., **2009**, *19*, 8162-8168.

12. Mishra, M.; Ma, C.Q.; Bäuerle, P.; *Chem. Rev*. **2009**, *109*, 1141-1276.

13. Van Der Heide, P; X-Ray Photoelectron Spectroscopy: An Introduction to Principles and Practices. 2012. John Wiley & Sons, Inc.: Hoboken New Jersey, pg. 3-6.

14. Michler, G.H.; Electron Microscopy of Polymers. 2008. Springer-Verlag: Berlin Heidelberg, pg. 121-143.

15. Hofmockel, R.; Zschieschang, U.; Kraft, U.; Rödel R.; Hansen N.H.; Stolte, M.; Würthner, F.; Takimiya, K.; Kern, K.; Pflaum, J.; Klauk, H.; *Organic Electronics*, **2013**, *14*, 3213-3221.

16. Michler, G.H.; Electron Microscopy of Polymers. 2008. Springer-Verlag: Berlin Heidelberg, pg. 87-120.

17. Wu, G.; MacKenzie, A.; Scanning Electron Microscopy (SEM) Training Manual, GEOL 5155, Course Material, Lakehead University, January 2014.

18. Bejarano-Villafuerte, A.; Van der Meijden, M.W.; Lingerfelder, M.; Wurst, K.; Kellogg, R.M.; Amabilino, D.B.; *Chem. Eur. J.*, **2012**, *18*, 15984-15993.

19. McPail, D.S.; *J. Mater. Sci*. **2006**, *41*, 873-903.

20. Tamao, K.; Kodama, S.I.; Nakajima, I.; Kumada, M.; Minato, A.; Suzuki, K.; *Tetrahedron* **1982**, 38, 3347

21. Barbarella, G.; Favaretto, L.; Sotgiu, G.; Zambiachi, M.; Antolini, L.; Pudova, O.; Bongini, A.; *J. Org. Chem*. **1998**, *63*, 5497-5506.

22. Sears, Wendy. Synthesis and characterization of Donor-Acceptor Oligothiophenes. M. Sc. Thesis, Lakehead University, July 2005.

23. Supplementary Material. Yohann, N.; Blanchard, P.; Levillain, E.; Allain, M.; Mercier, N.; Roncali J. *Org. Lett*. **2004**, 6(2) 273-276.

24. Huang-Minlon, B.Y.; *J. Am. Chem. Soc.* **1946**, 68, 2487

25. Kodomari, M.; Kuzuoka, T.; Yoshitomi, S.; Synthesis, **1983**, 141-142.

26. Inaoka, S.; and Collard, D.M.; *J. Mater. Chem*. **1999**, *9*, 1719-1724.

27. Ciszek, J.W. Thiocyanate monolayers and the synthesis and assembly of transition metal complexes. Doctoral Thesis, Rice University, August 2005.

28. Surface Science Western. http://www.xpsfitting.com/search/ (accessed October 23, 2014).

28. Käfer D. Characterization and optimization of growth and electronic structure of organic thin film for applications in organic electronics. Doctoral Thesis, Ruhr University, November 2008.

30. Waitkins, G.R.; Shutt, R.; *Inorg. Syn*. **1946**, *2*, 186

Appendices

Appendix 1 – Alternate Syntheses

Attempted preparation of 5-hexyl-2,2'-bithiophene T_2Hx via lithiation with nBuLi

T_2 (0.99 g, 5.95 mmol) was added to a 250 mL 3-necked round-bottomed flask equipped with a gas nozzle, rubber septum, thermometer, and stir bar. The flask was evacuated and purged with $N_{2\,(g)}$ over three cycles. Dry THF (40 mL) was added to the flask via syringe. The solution was cooled to -50 ˚C with a $N_{2\,(l)}$/acetone bath. At this temperature, nBuLi (10 mL,0.6 M, 6 mmol) was added dropwise via syringe. The solution was stirred at -50 ˚C for 30 minutes, after which, 1-bromohexane (1.2 mL, 1.41 g, 8.5 mmol) was added dropwise via syringe. The mixture was allowed to warm to room temperature and stirred overnight. After this time, the reaction mixture was poured into a saturated solution of NH_4Cl (100 mL) and stirred for 20 minutes. The mixture was poured into a 1 L separatory funnel and extracted with CH_2Cl_2 (3×50 mL). Combined organic fractions were dried over $MgSO_4$ and solvent was removed via rotary evaporation at 35 ˚C to yield a green oil. ^{1}H NMR spectrum was observed to contain mostly starting material with a small amount of T_2Hx product.

Attempted preparation of T_2Hx via lithiation with tBuLi

T_2 (1.004 g, 6.25 mmol) was added to a 500 mL 3-necked round-bottomed flask equipped with a gas nozzle, rubber septum, thermometer adapter, and stir bar. The oven-dried apparatus was evacuated and purged with $N_{2\,(g)}$ over five cycles. Dry THF (35 mL) was added via syringe. The resulting solution was cooled to -50 ˚C with a $N_{2(l)}$/acetone bath. At this temperature, tBuLi (1.7 M, 3.6 mL, 6.12 mmmol) was added dropwise via syringe. The solution was stirred at -50 ˚C for 30 minutes, after which 1-bromohexane (0.86 mL,1.01 g, 6.08 mmol) was added dropwise via syringe. The solution was allowed to warm to room temperature and stirred overnight. After this time, the mixture was poured into a saturated solution of NH_4Cl (200mL) and stirred for 20 minutes. Next, the mixture was poured into a separatory funnel and the aqueous layer was extracted with CH_2Cl_2 (4×50 mL). Combined organic fractions were

dried over $MgSO_4$ and solvent was removed via rotary evaporation at 30 ˚C to obtain a blue oil. The oil was further purified through column chromatography (SiO_2 gel) using hexanes as eluent. ^{1}H NMR spectrum was observed to contain mostly starting material with a small amount of T_2Hx product.

Attempted preparation of T_2Hx via Grignard #1

A 250 mL 3-necked round-bottomed flask was equipped with a gas nozzle, rubber septum, stir bar and 125 mL equal-pressure dropping funnel. $Mg_{(s)}$ turnings (0.5989 g, 24.64 mmol) were added to the flask and it was heated with a heat gun to drive off water. The assembled apparatus was allowed to cool to room-temperature and dry Et_2O (5 mL) was added to the flask via syringe. To the dropping funnel, dry Et_2O (25 mL) and 2-bromothiophene (3.39 g, 20.79 mmol) were added sequentially via syringe. A crystal of I_2 was added to the flask as an initiator and the 2-bromothiophene solution added to the flask in portions of several millilitres to initiate reflux and then dropwise. An ice water bath was used to maintain a controlled reflux during the addition. After completion of the addition, the mixture was stirred under $N_{2\,(g)}$ at room temperature for 3 hours. A second 250 mL 3-necked round-bottomed flask equipped with a gas nozzle, stir bar, rubber septum and glass stopper $Ni(dppp)Cl_2$ (0.17 g, 0.3136 mmol, 1.54 mol%) was added the flask, which was then evacuated and purged with $N_{2(g)}$ over three cycles. After the flask cooled to room temperature, dry Et_2O (25 mL) and 5-hexyl-2-bromothiophene (5.04 g, 20.39 mmol) were added sequentially to the flask via syringe. Both 3-necked flasks were cooled on an ice bath for 10 minutes. After this time, the Grignard reagent mixture was cannulated into the catalyst solution, while both solutions were on ice baths. The resulting mixture was allowed to stir overnight at room temperature. The reaction mixture was poured into a saturated solution of NH_4Cl and stirred for 20 minutes. The aqueous layer was extracted with CH_2Cl_2 (3×80 mL). The combined organic layers were dried over $MgSO_4$ and rotovapped at 30 ˚C to obtain a dark brown, opaque oil. Only starting material was observed in the ^{1}H NMR spectrum of the product.

Attempted preparation of T_2Hx via Grignard #2

A 100 mL 3-necked round-bottomed flask was equipped with a gas nozzle, rubber septum, stir bar and 125 mL equal-pressure dropping funnel. $Mg_{(s)}$ turnings (0.46 g, 18.9 mmol) were added to the flask and it was heated with a heat gun under vacuum to drive off water. The assembled apparatus was allowed to cool to room-temperature and dry Et_2O (5 mL) was added to the flask via syringe. Dry Et_2O (30 mL) and 2-bromothiophene (2.14 g, 13.1 mmol) were added to the dropping funnel sequentially via syringe. Immediately before addition of the 2-bromothiophene, 1 crystal of I_2 was added to the flask as an initiator. The 2-bromothiophene solution was added to the flask in portions of several millilitres to initiate reflux and then dropwise. An ice water bath was used to maintain a controlled reflux during the addition. After completion of the addition, the mixture was stirred at room temperature for 3 hours. A 500 mL 3-necked round-bottomed flask equipped with a gas nozzle, stir bar, rubber septum and glass stopper. $Ni(dppp)Cl_2$ (0.2 g 0.369 mmol, 2.8 mol%) was added the flask, which was then evacuated and purged with $N_{2(g)}$ over three cycles. Dry Et_2O (50 mL), dry toluene (50 mL), and 5-hexyl-2-bromothiophene (3.25 g, 13.1 mmol) were added sequentially to the flask via syringe. Both 3-necked flasks were cooled on an ice bath for 10 minutes. After this time, the Grignard reagent mixture was cannulated into the catalyst solution, with both on ice baths. The resulting mixture was stirred under $N_{2(g)}$ overnight at room temperature. The reaction mixture was poured into a saturated solution of NH_4Cl and stirred for 20 minutes. The aqueous layer was extracted with Et_2O (2×80 mL). The combined organic layers were dried over $MgSO_4$ and rotovapped at 30 ˚C to obtain a dark brown, opaque oil. Only starting material was observed in the ^1H NMR spectrum of the product

Appendix 2 - Starting Materials

A.2.1 Chemicals obtained commercially and used as received

Acetone	Aldrich
Acetonitrile	Caledon
Ammonium chloride	Baker
Ammonium thiocyanate	Caledon
Benzene	EMD Science
[1,3-Bis(diphenylphosphino)propane]dichloronickel(II)	Aldrich
Bromine	Anachemia
1-bromohexane	Aldrich
2-bromothiophene	Aldrich
N-butyllithium solution (1.6M in hexanes)	Aldrich
Tert-butyllithium solution (1.7M in pentane)	Aldrich
1,6-dibromohexane	Aldrich
Diethylene glycol	Fischer
Diethyl ether	Caledon
D-chloroform	Cambridge Isotopic Laboratories
Ethanol	Commercial Alcohols
Hexanes	Caledon
Hexanoyl chloride	Aldrich
Hydrazine monohydrate	Aldrich
Hydrochloric acid	Caledon
Iodine	Anachemia
Magnesium sulphate	Caledon
Magnesium turnings	Aldrich
Malononitrile	Aldrich
Methyl iodide	Aldrich
Methanol	Caledon
Molecular sieves, Davison Type 4A	Fischer

N-bromosuccinimide	Aldrich
N,N-dimethylformamide	Aldrich
Potassium hydroxide	Caledon
Potassium thiocyanate	BDH
Selenium dioxide	Aldrich
Sodium bicarbonate	Malinckrodt
Sodium chloride	BDH
Thiophene	Aldrich
Tin (IV) tetrachloride	Aldrich
Tetramethylethylenediamine	Aldrich
Toluene	

A.2.2 Chemicals obtained commercially and further purified

Dimethyl sulfoxide – Distilled under $N_{2(g)}$ and stored over molecular sieves

Ethanol – Dried over Mg turnings and distilled under $N_{2(g)}$

Methanol – Dried over Mg turnings and distilled under $N_{2(g)}$

Potassium thiocyanate – Stored over self-indicating silica gel in a desiccator

A.2.3 Chemical synthesized in house

Potassium selenocyanate[30]

Appendix 3 – Map sum spectra from EDX mapping

Figure 32. Map sum spectrum of Spectrum from EDX mapping shown in Figure 13.

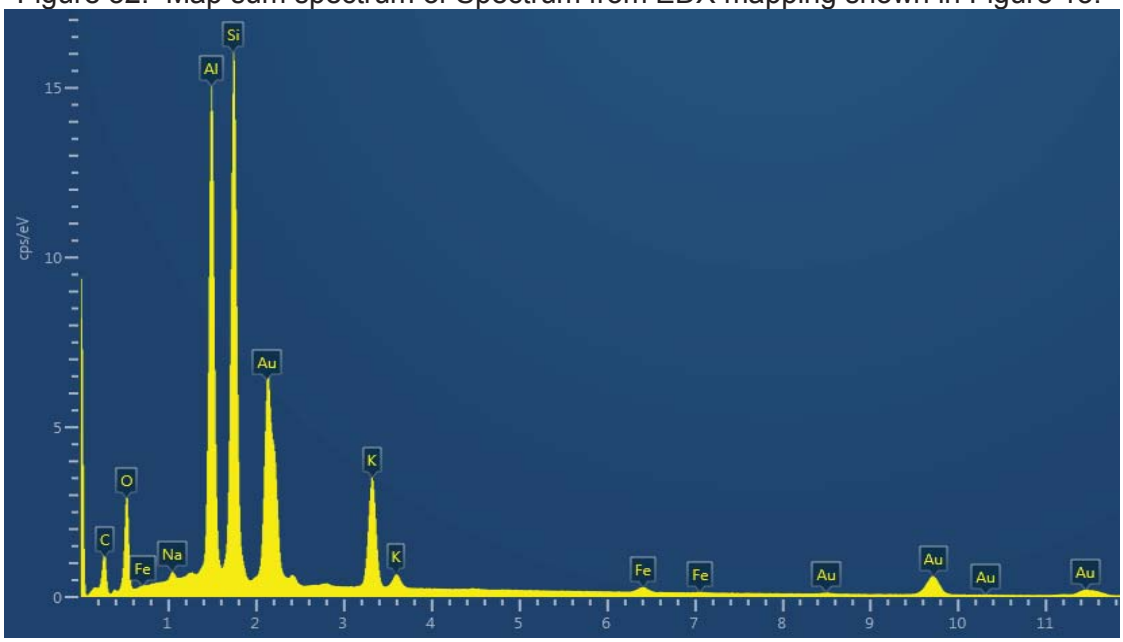

Figure 33. Map sum spectrum of Spectrum from EDX mapping shown in Figure 14.

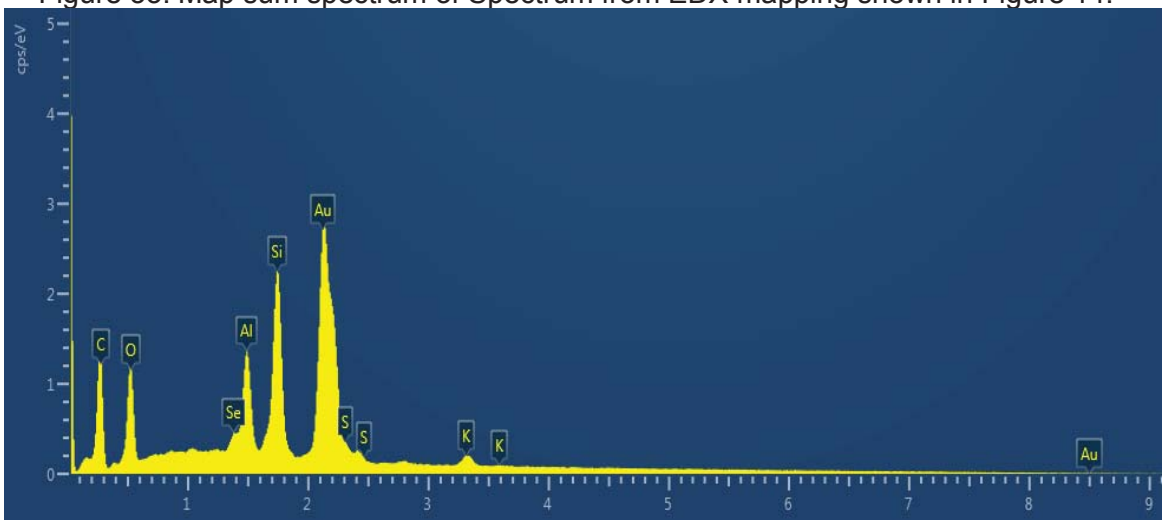

Figure 34. Map sum spectrum of Spectrum from EDX mapping shown in Figure 15.

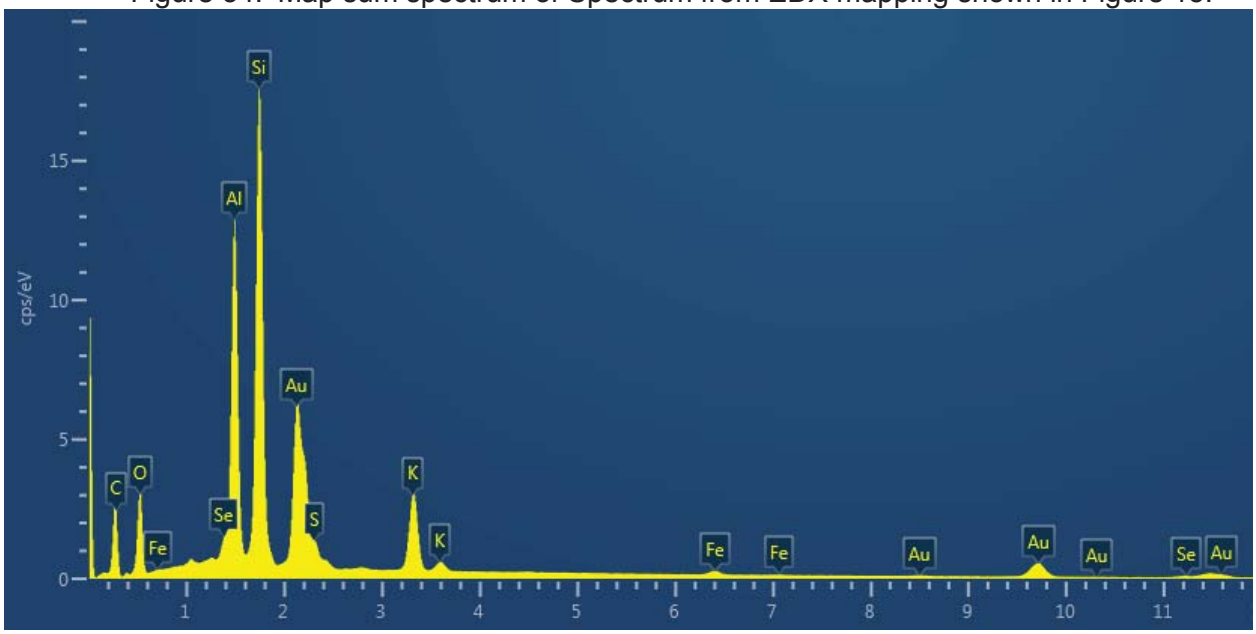

Appendix 4 – High Resolution XPS Spectra

Figure 35. High resolution XPS spectra for TF-N (Au-S-T_2-Hx from hexanes as solvent). A) N 1s spectrum. B) S 2p spectrum.

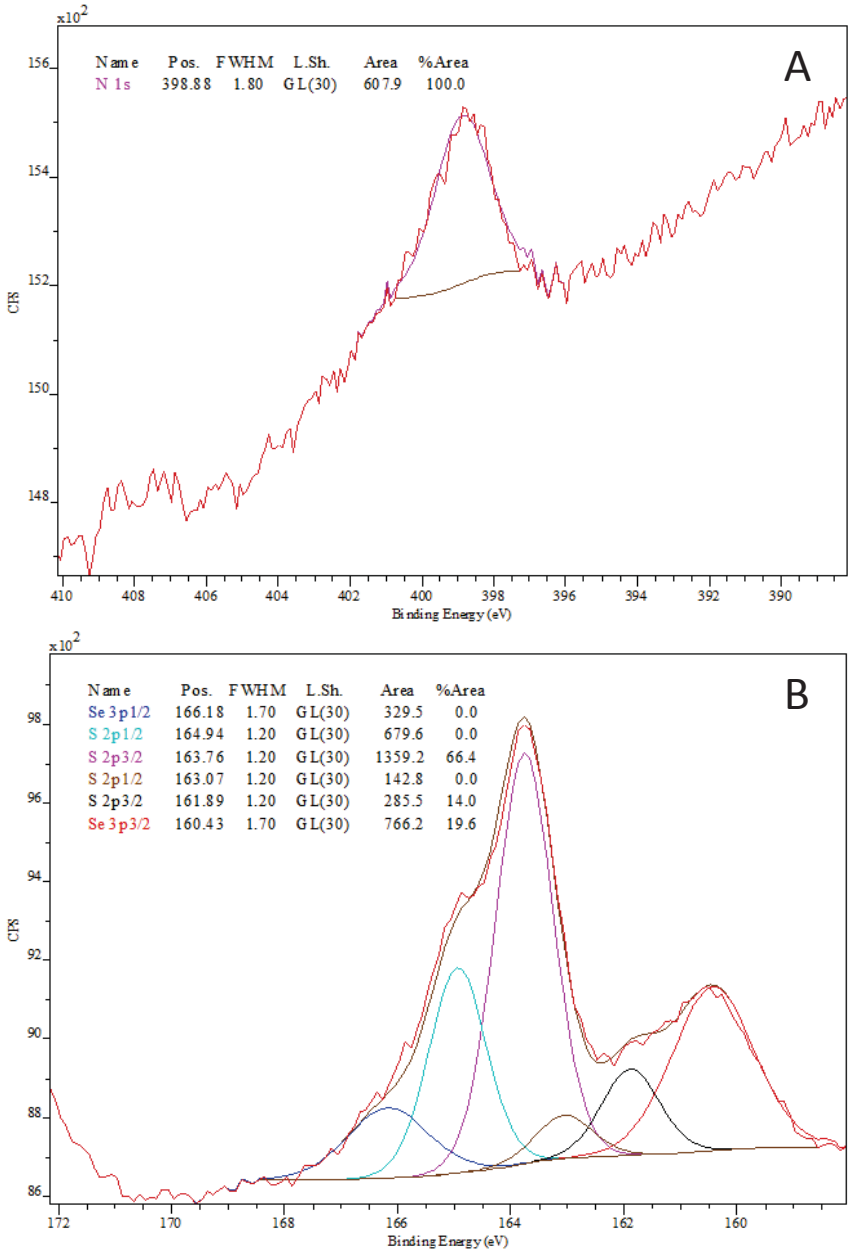

Figure 36. High Resolution XPS spectra for TF-N (Au-S-T_2-Hx from hexanes solvent). A) C 1s spectrum. B) Au 4f spectrum

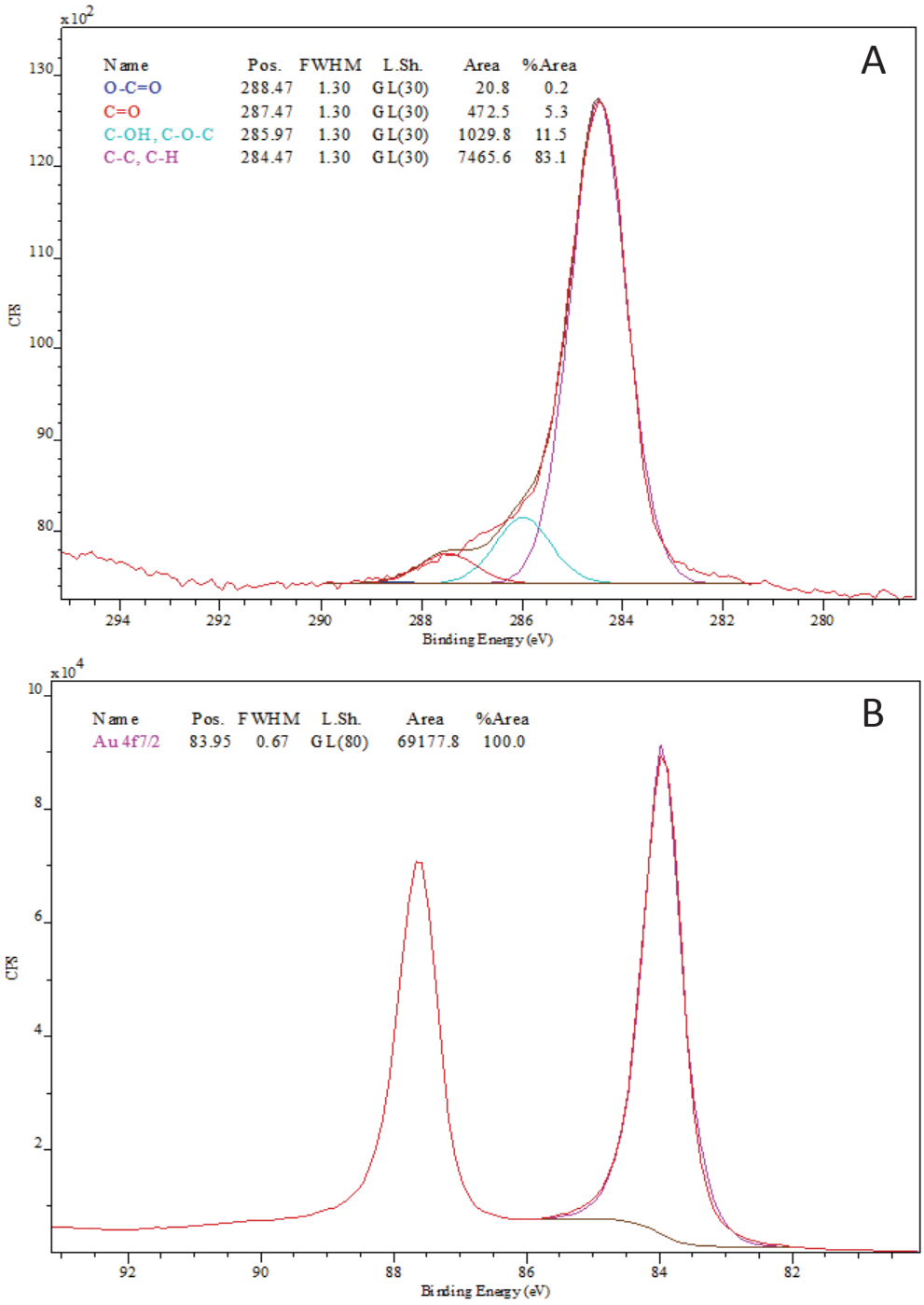

Figure 37. High Resolution XPS Spectra for TF-M (Au-S-T_2-Hx from ethanol solvent). A) N 1s spectrum. B) S 2p spectrum

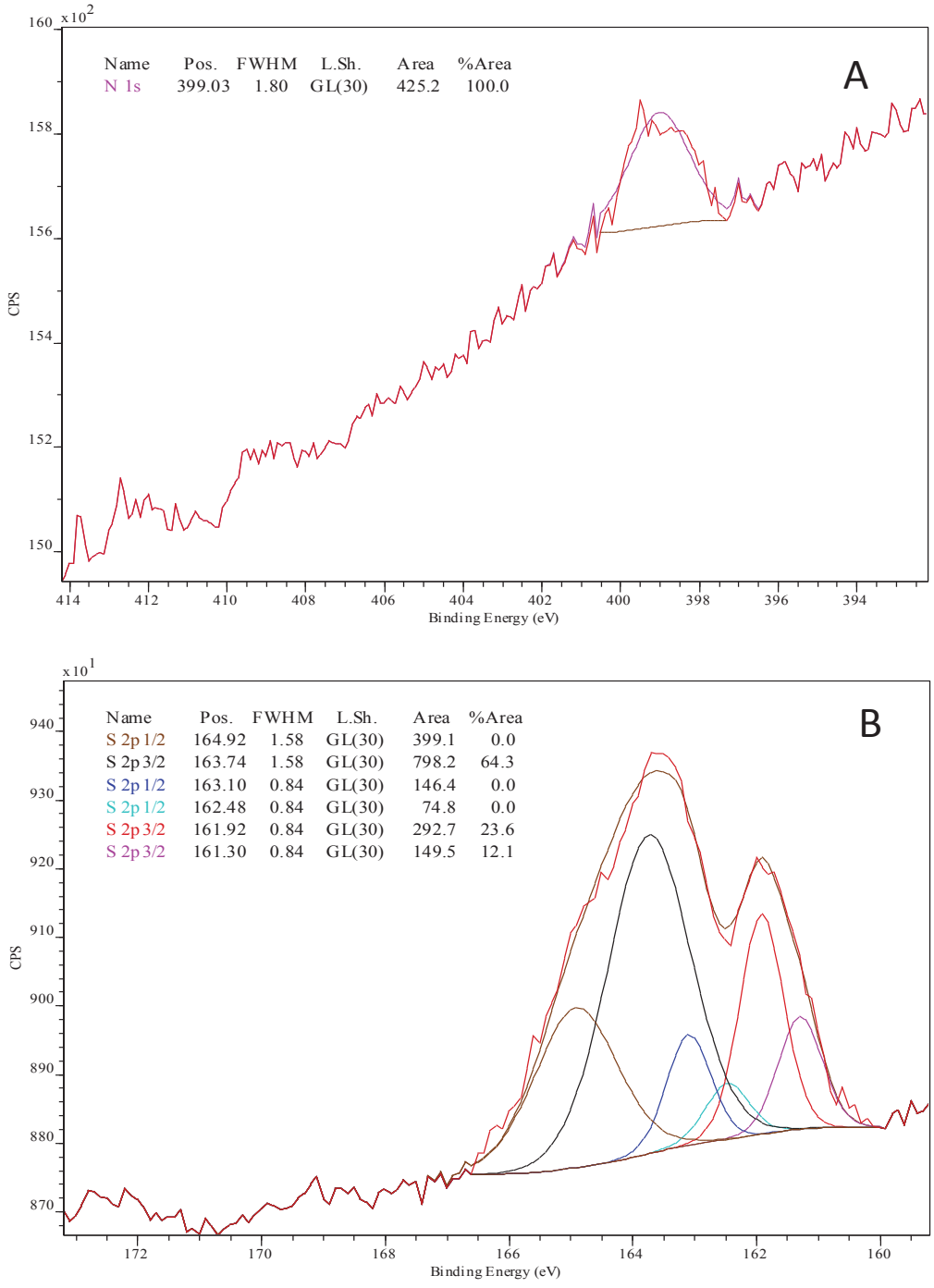

Figure 38. High resolution XPS spectra for TF-M (Au-S-T_2-Hx in ethanol). A) C 1s spectrum. B) Au 4f spectrum.

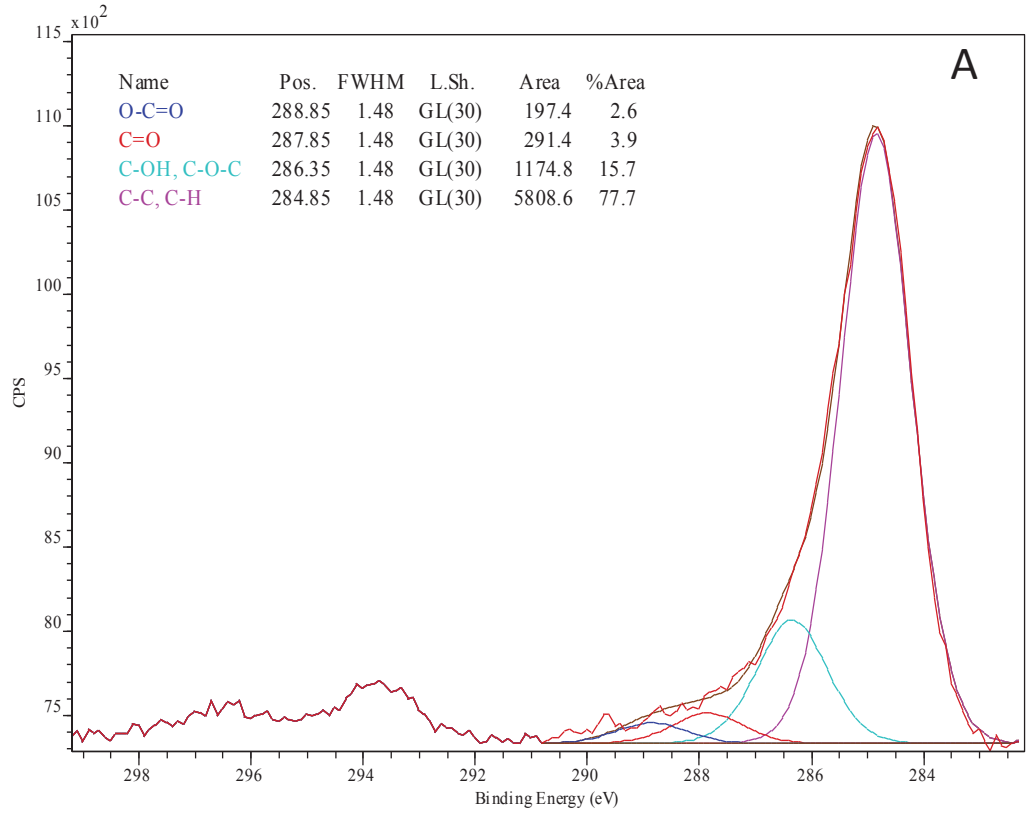

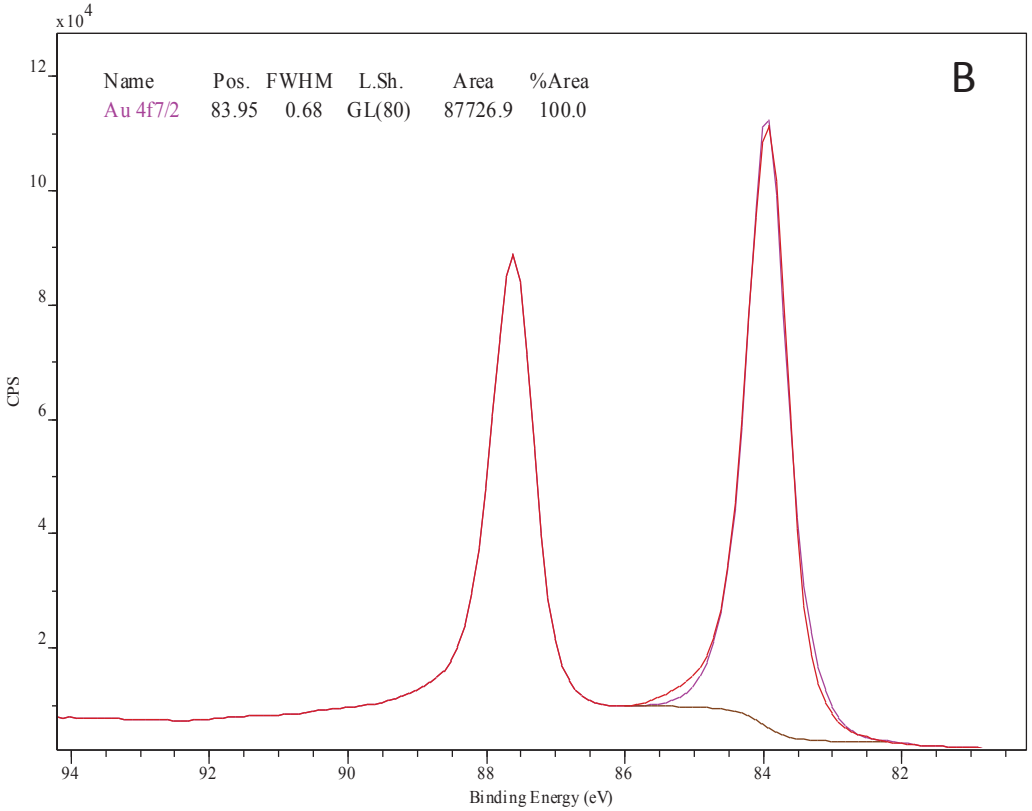

Figure 39. High Resolution XPS spectra for TF-J (Au-S-Hx-T_2-Hx from ethanol solvent). A) N1s spectrum. B) S 2p spectrum.

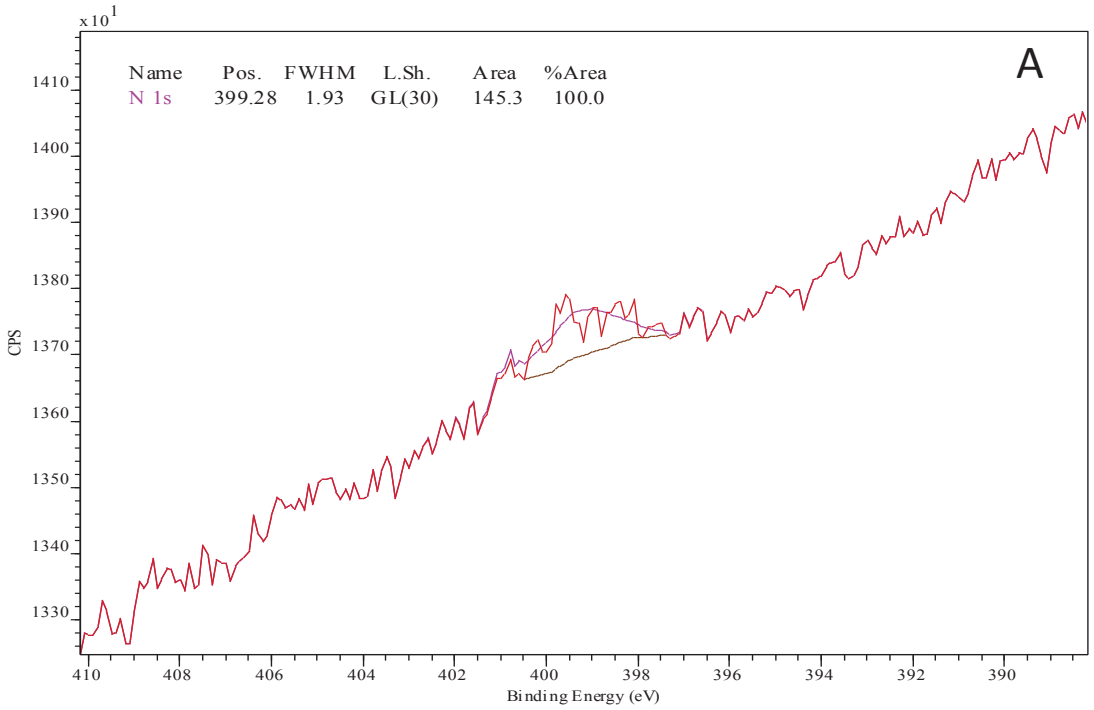

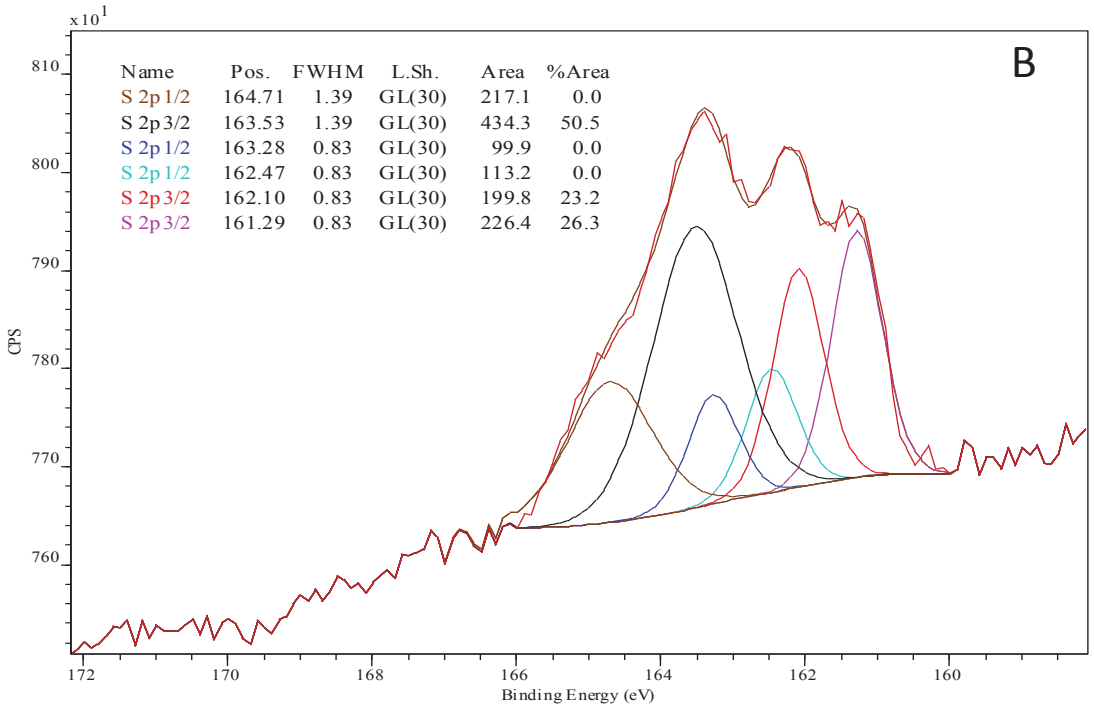

Figure 40. High Resolution XPS spectra for TF-J (Au-S-Hx-T_2-Hx from ethanol solvent). A) C 1s spectrum. B) Au 4f spectrum

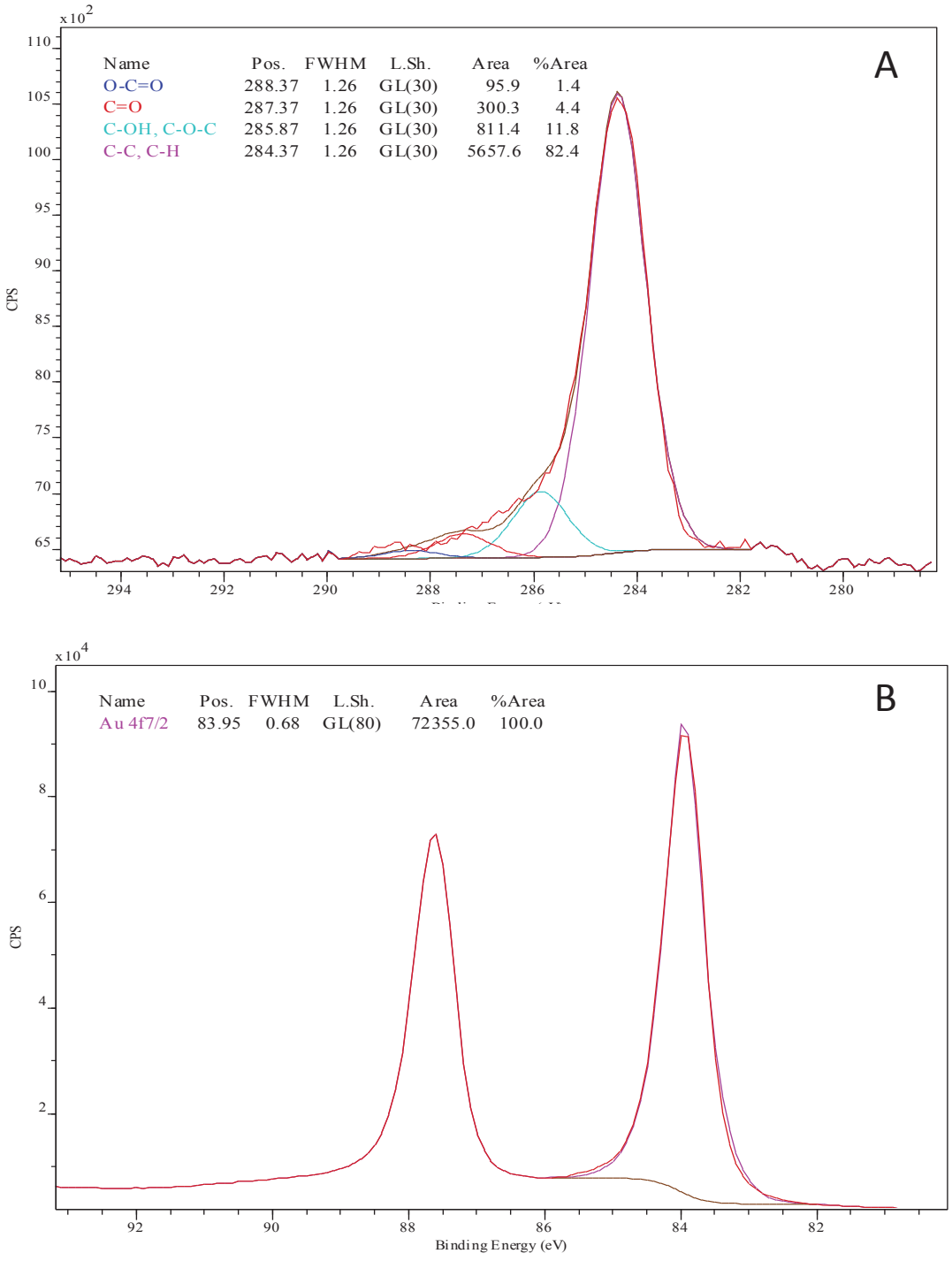

Figure 41. High Resolution XPS spectra for TF-K (Au-Se-Hx-T_2-Hx from ethanol solvent). A) N 1s spectrum. B) S 2p spectrum

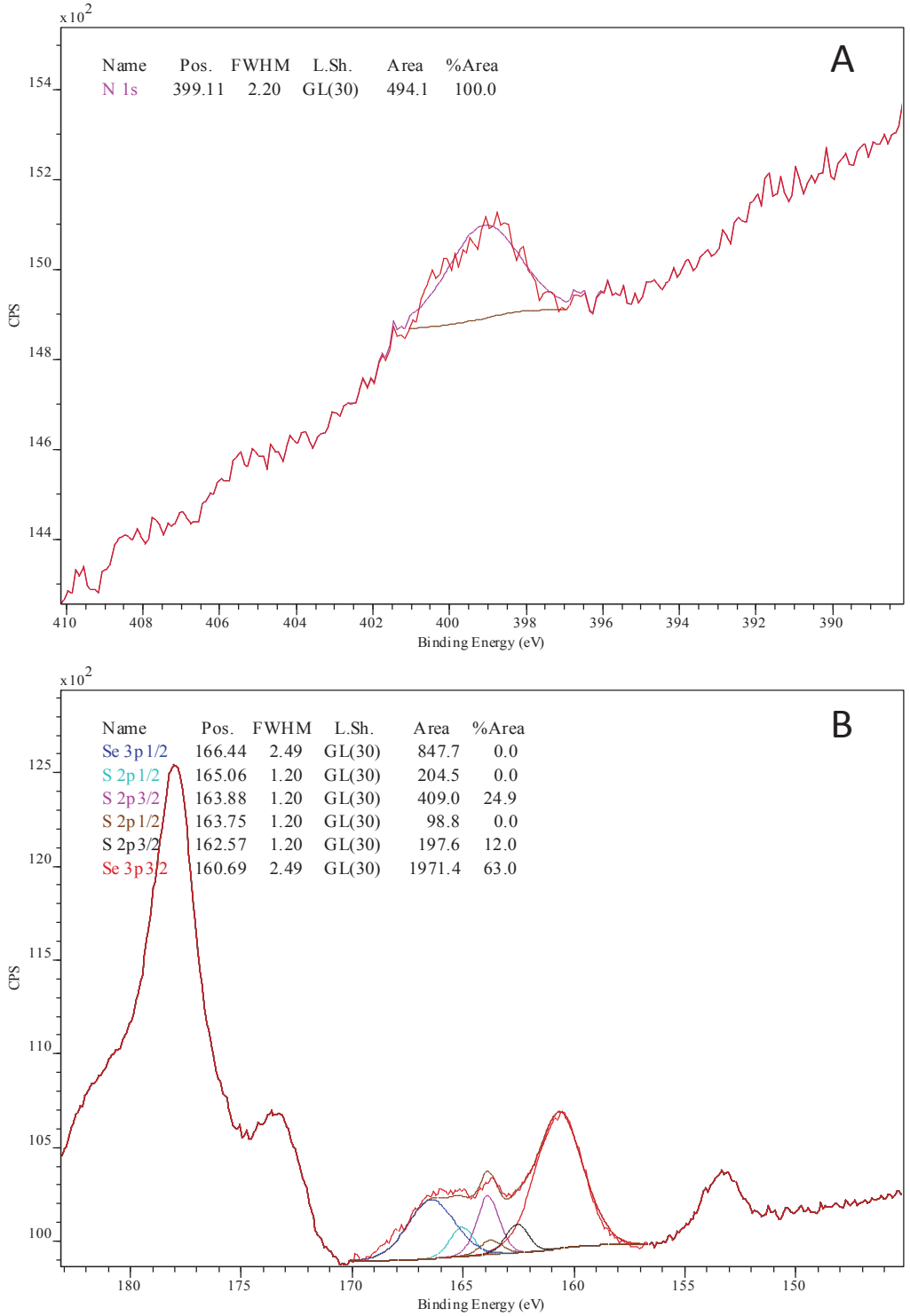

Figure 42. High Resolution XPS spectra for TF-K (Au-Se-Hx-T_2-Hx). A) C 1s spectrum B) Au 4f spectrum

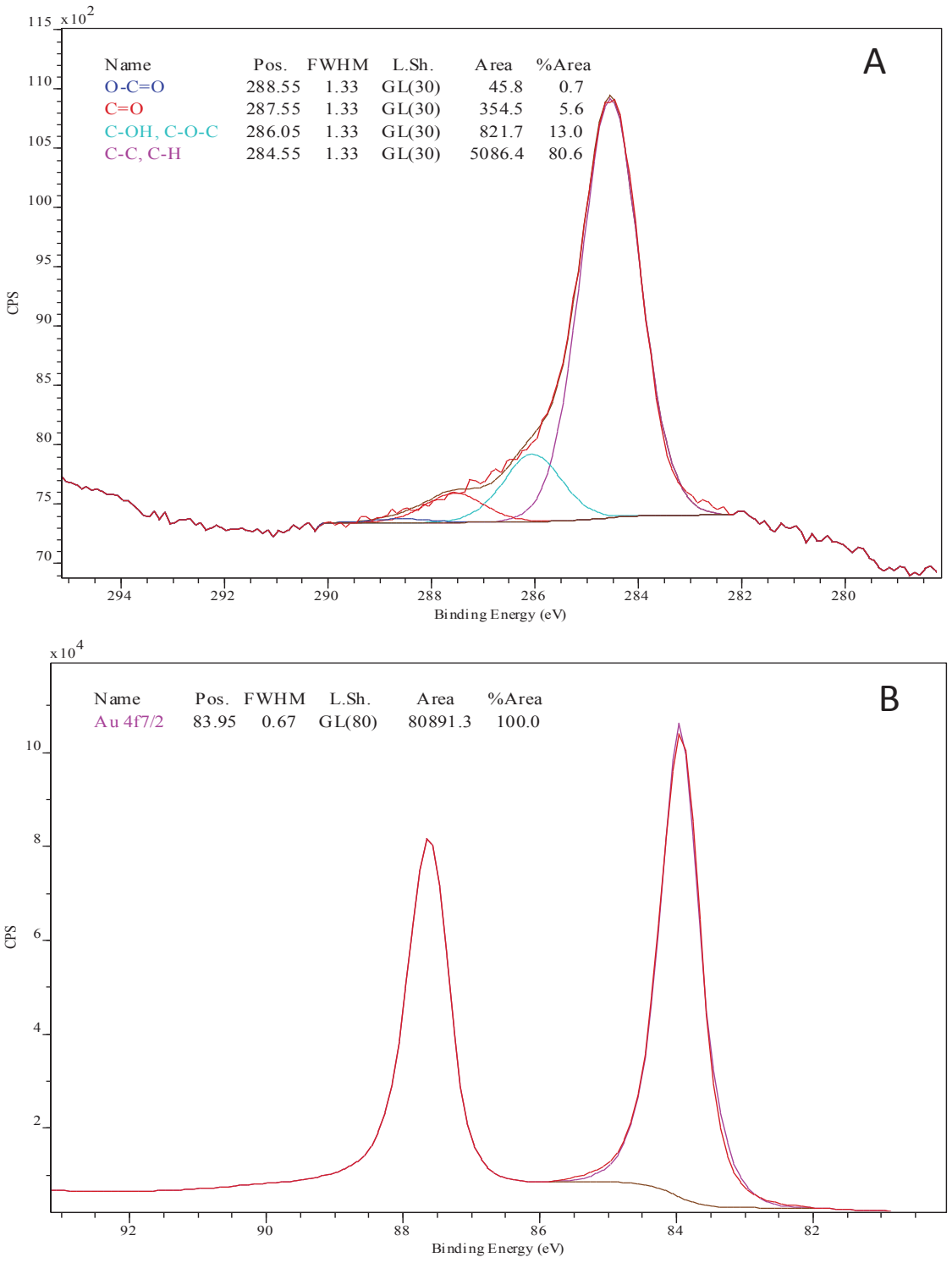

Figure 43. High Resolution XPS spectra for TF-K (Au-Se-Hx-T_2-Hx) of Se 3d peak.

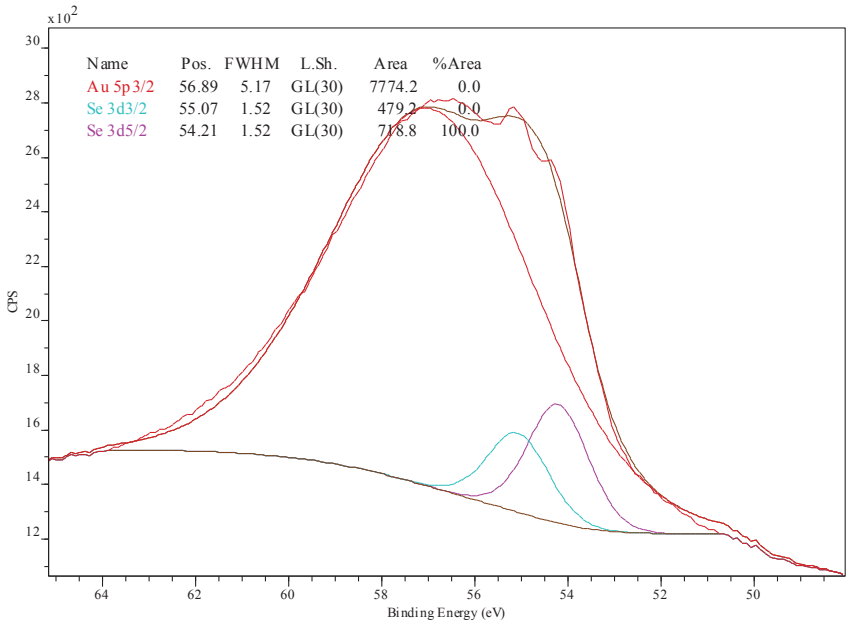

Figure 44. High resolution XPS spectra for TF-L (Au-Se-T_2-Hx from ethanol solvent). A) N 1s spectrum. B) S 2p spectrum

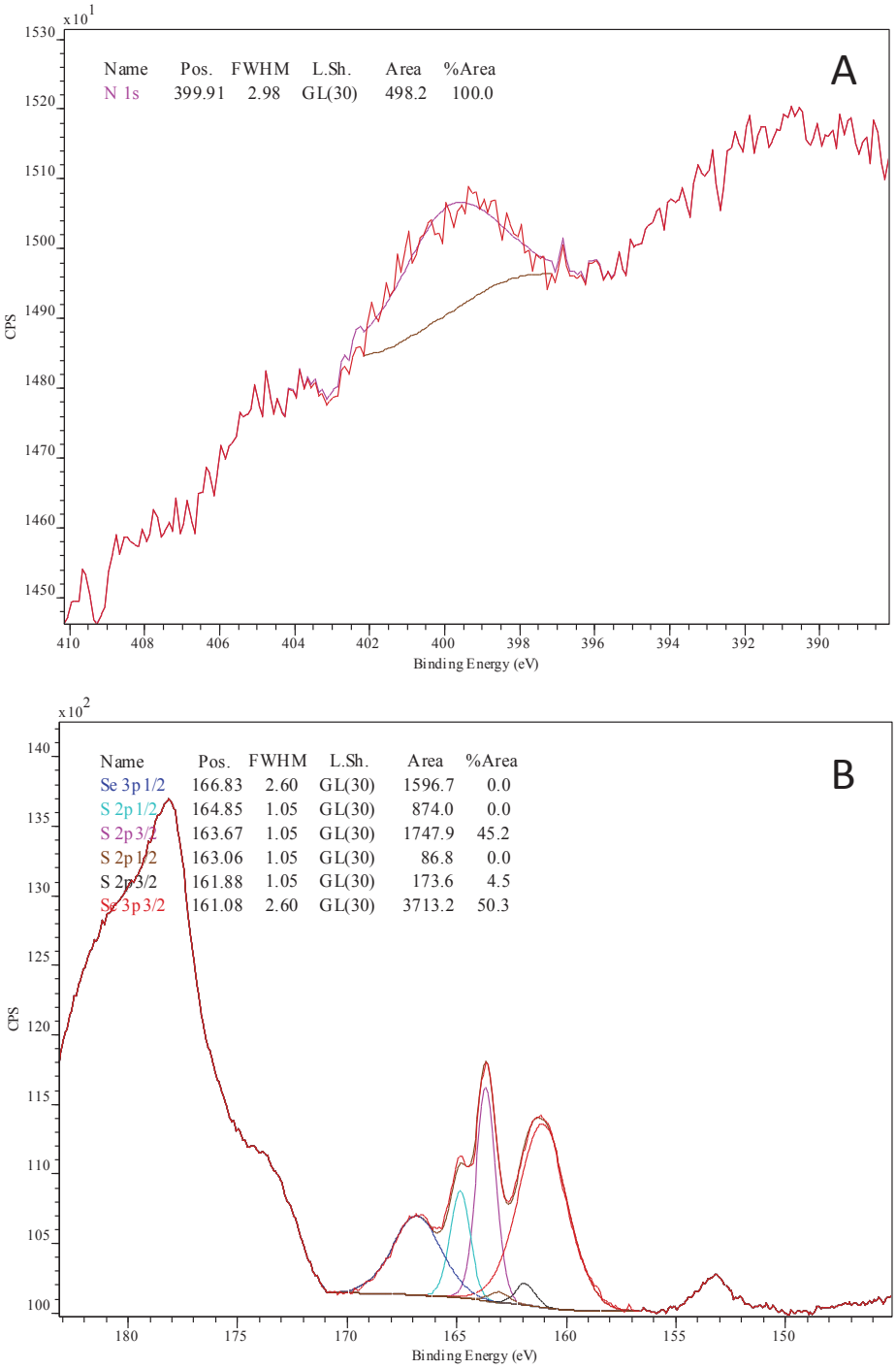

Figure 45. High Resolution XPS spectra of TF-L (Au-Se-T_2-Hx from ethanol solvent). A) C 1s spectrum. B) Au 4f spectrum

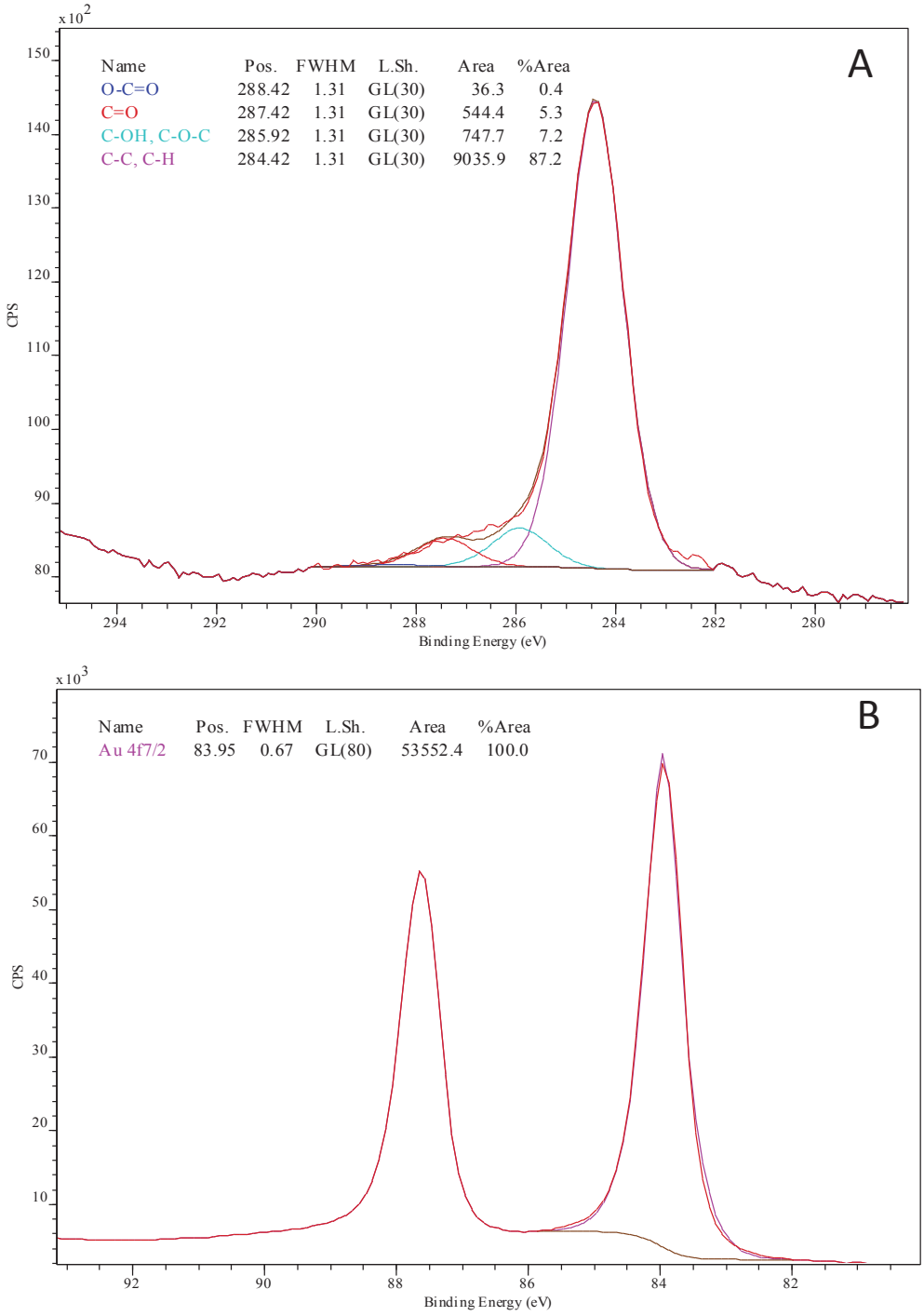

Figure 46. High Resolution XPS spectra of TF- L (Au-Se-T_2-Hx from ethanol solvent) of Se 3d peak

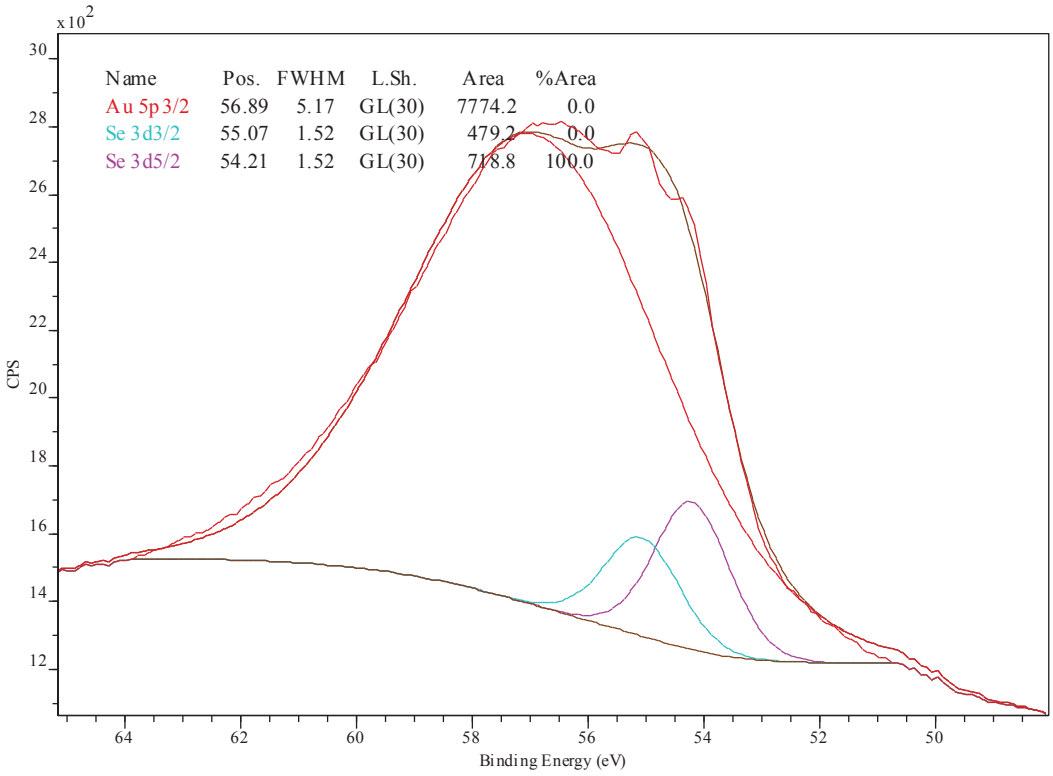

Figure 47. High resolution XPS spectra of TF-I(Au-S-Hx-T_2-Hx-SCN). A) N 1s spectra. B) S 2p spectrum

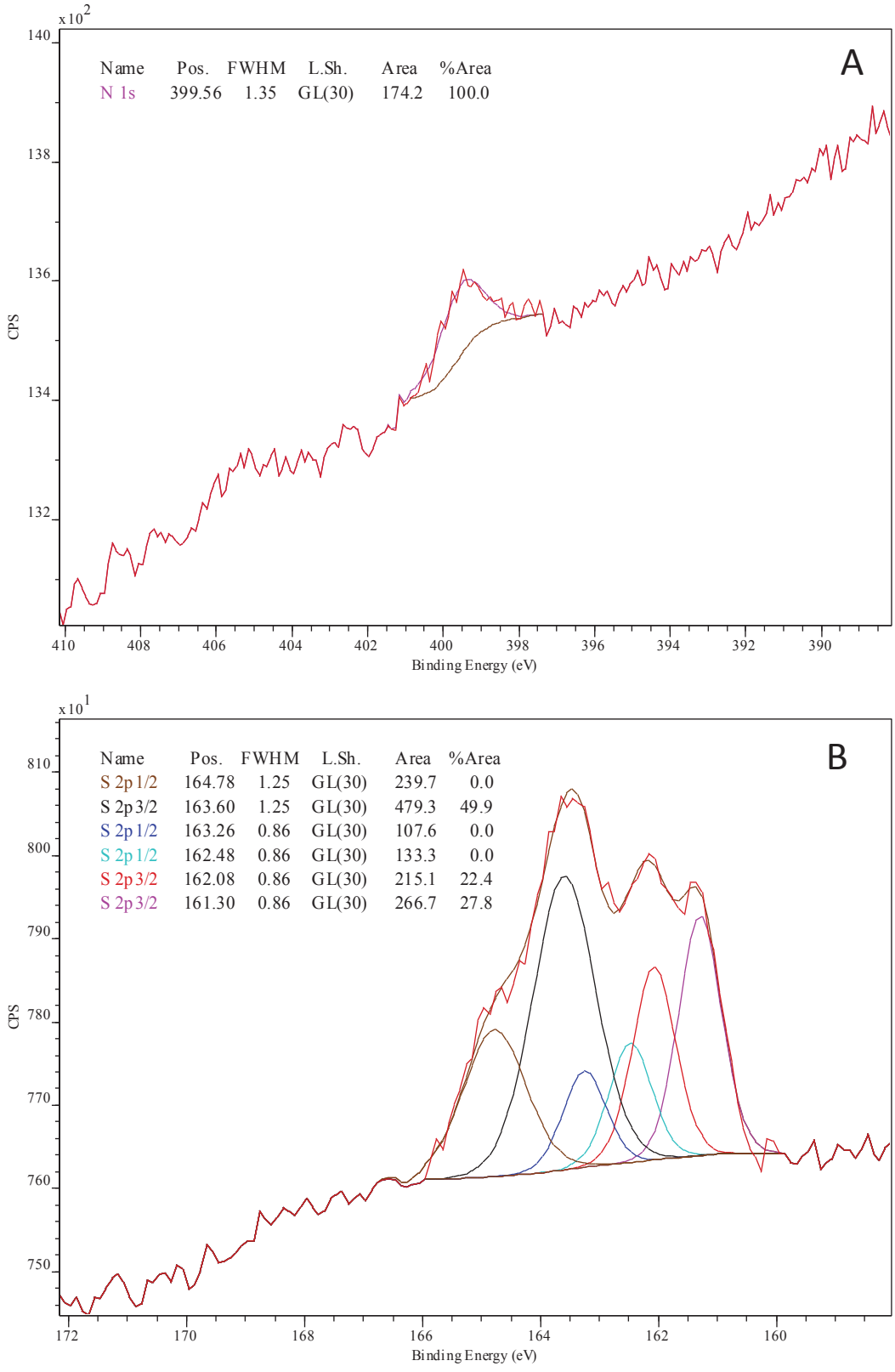

Figure 48. High Resolution XPS spectra of TF-I (Au-S-Hx-T_2-Hx-SCN). A) C 1s. B) Au 4f.